

PL-TR-91-2134

AD-A239 199



2

**ADVANCED WAVEFORM RESEARCH METHODS  
FOR GERESS RECORDINGS**

H.P. Harjes  
N. Gestermann  
M. Jost  
J. Schweitzer  
J. Wuster

Ruhr-University-Bochum  
D-4630 Bochum  
FEDERAL REPUBLIC OF GERMANY

15 April 1991

DTIC  
ELECTE  
JUL 31 1991  
S B D

Scientific Report No. 1

APPROVED FOR PUBLIC RELEASE; DISTRIBUTION UNLIMITED



PHILLIPS LABORATORY  
AIR FORCE SYSTEMS COMMAND  
HANSCOM AIR FORCE BASE, MASSACHUSETTS 01731-5000

91-06424



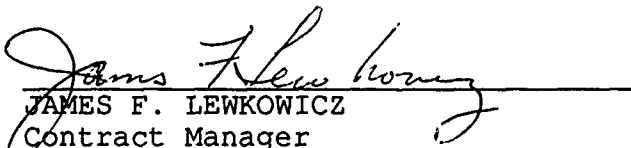
91 7 29 126

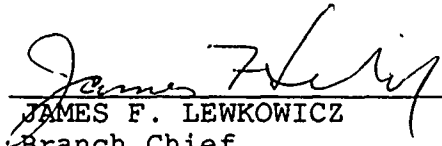
SPONSORED BY  
Defense Advanced Research Projects Agency  
Nuclear Monitoring Research Office  
ARPA ORDER NO. 5307

MONITORED BY  
Phillips Laboratory  
Contract AFOSR-90-0189

The views and conclusions contained in this document are those of the authors and should not be interpreted as representing the official policies, either expressed or implied, of the Defense Advanced Research Projects Agency or the U.S. Government.

This technical report has been reviewed and is approved for publication.

  
JAMES F. LEWKOWICZ  
Contract Manager  
Solid Earth Geophysics Branch  
Earth Sciences Division

  
JAMES F. LEWKOWICZ  
Branch Chief  
Solid Earth Geophysics Branch  
Earth Sciences Division

  
DONALD H. ECKHARDT, Director  
Earth Sciences Division

This report has been reviewed by the ESD Public Affairs Office (PA) and is releasable to the National Technical Information Service (NTIS).

Qualified requestors may obtain additional copies from the Defense Technical Information Center. All others should apply to the National Technical Information Service.

If your address has changed, or if you wish to be removed from the mailing list, or if the addressee is no longer employed by your organization, please notify PL/IMA, Hanscom AFB, MA 01731-5000. This will assist us in maintaining a current mailing list.

Do not return copies of this report unless contractual obligations or notices on a specific document requires that it be returned.

Unclassified

SECURITY CLASSIFICATION OF THIS PAGE

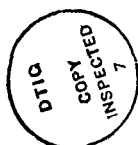
REPORT DOCUMENTATION PAGE				Form Approved OMB No. 0704-0188	
1a. REPORT SECURITY CLASSIFICATION Unclassified			1b. RESTRICTIVE MARKINGS		
2a. SECURITY CLASSIFICATION AUTHORITY			3. DISTRIBUTION/AVAILABILITY OF REPORT Approved for public release; Distribution unlimited		
2b. DECLASSIFICATION/DOWNGRADING SCHEDULE					
4. PERFORMING ORGANIZATION REPORT NUMBER(S)  RUB-91-100			5. MONITORING ORGANIZATION REPORT NUMBER(S)  PL-TR-91-2134		
6a. NAME OF PERFORMING ORGANIZATION  Ruhr-University-Bochum		6b. OFFICE SYMBOL (If applicable)	7a. NAME OF MONITORING ORGANIZATION  Phillips Laboratory		
6c. ADDRESS (City, State, and ZIP Code)  D-4630 Bochum FEDERAL REPUBLIC OF GERMANY			7b. ADDRESS (City, State, and ZIP Code)  Hanscom AFB Massachusetts 01731-5000		
NAME OF FUNDING / SPONSORING ORGANIZATION  DARPA		8b. OFFICE SYMBOL (If applicable)  NMRO	9. PROCUREMENT INSTRUMENT IDENTIFICATION NUMBER  AFOSR-90-0189		
8c. ADDRESS (City, State, and ZIP Code)  1400 Wilson Blvd Arlington, VA 22209			10. SOURCE OF FUNDING NUMBERS		
			PROGRAM ELEMENT NO. 62714E	PROJECT NO. 0A10	TASK NO. DA
					WORK UNIT ACCESSION NO. AE
11. TITLE (Include Security Classification)  Advanced Waveform Research Methods for GERESS Recordings					
12. PERSONAL AUTHOR(S) H.-P. Harjes, N. Gestermann, M. Jost, J. Schweitzer, J. Wüster					
13a. TYPE OF REPORT Scientific #1		13b. TIME COVERED FROM 2/15/90 TO 2/14/91		14. DATE OF REPORT (Year, Month, Day) 1991/04/15	
				15. PAGE COUNT 120	
16. SUPPLEMENTARY NOTATION					
17. COSATI CODES			18. SUBJECT TERMS (Continue on reverse if necessary and identify by block number)		
FIELD	GROUP	SUB-GROUP	Seismic array		
			Nuclear test detection		
			GERESS		
19. A. ABSTRACT (Continue on reverse if necessary and identify by block number)					
<p>The German Experimental Seismic Array System (GERESS) array project is a cooperative research program, jointly undertaken by Southern Methodist University Dallas, USA, and Ruhr-University Bochum in Germany. It is part of a multi-array network which includes NORESS, ARCESS, and FINESA in Scandinavia. This report summarizes research activities carried out at the array data centre in the Institute of Geophysics in Bochum.</p> <p>The inner ring of the array elements began recording in March 1990 and since then the number of active channels has gradually increased. Since August 1990, all 25 vertical short-period channels have been operational. The first chapter of this report contains a detailed description of GERESS including geographical coordinates, geological setting, and basic noise figures according to rules set up in the Sourcebook of the Group of Scientific Experts (GSE) in Geneva.</p> <p>The second chapter describes the instrumentation of the array, especially the system transfer function of the sensors installed at GERESS.</p> <p>Chapter 3 gives an overview of the status of the array as seen from the data centre in Bochum and documented in monthly status reports by our institute.</p> <p style="text-align: right;">( continued )</p>					
20. DISTRIBUTION / AVAILABILITY OF ABSTRACT <input type="checkbox"/> UNCLASSIFIED/UNLIMITED <input type="checkbox"/> SAME AS RPT <input type="checkbox"/> OTIC USERS			21. ABSTRACT SECURITY CLASSIFICATION Unclassified		
22a. NAME OF RESPONSIBLE INDIVIDUAL James Lewkowicz			22b. TELEPHONE (Include Area Code)		22c. OFFICE SYMBOL PL/LWH

To facilitate easy access to the GERESS data for remote users, an on-line Display Manager has been developed as described in chapter 4. The Display Manager not only allows to look at the results of the Bochum on-line processing, i.e. event bulletins, but also includes a module to display waveforms using a Tektronix emulation.

The development of the GERESS data centre in Bochum aimed at participating in the second Technical Test (GSETT-2) of the GSE planned for the time period from 22 April to 2 June 1991. The final preparatory test for this large-scale data exchange experiment took place from 26 November to 2 December 1990. We took this occasion and fully analyzed GERESS data for the first time. The results reported in chapter 5, clearly demonstrate that the new array is the most sensitive and capable seismic installation in Central Europe.

Seismic waves of most of the presumed or announced underground nuclear explosions which were detonated in 1990 were detected at GERESS. The evaluation of these waveforms is described in chapter 6. Most remarkable is the low detection threshold for the French test site in the Pacific. Although this area is by far the most distant test site from GERESS, the array records very clear signals due to the focusing effect of the Earth's core. We derive a detection threshold of  $mb(PKP) = 3.9$  for the Tuomoto Archipelago events.

In the final chapter 7 first results of advanced waveform research methods for regional events are reported. Using a continuous f-k analysis and calculating synthetic seismograms with the reflectivity method, it is shown that a full waveform analysis reveals details of the crust/mantle structure which are difficult to identify otherwise. Taking into account the excellent location capability of GERESS within 500 km to 1000 km distance, this study will be continued to derive source-receiver specific models of the European lithosphere for different azimuths.



Accession For	
NTIS GRA&I	<input checked="" type="checkbox"/>
DTIC TAB	<input type="checkbox"/>
Unannounced	<input type="checkbox"/>
Justification	
By	
Distribution/	
Availability Codes	
Dist	Avail and/or Special
A-1	

## TABLE OF CONTENTS

	page
1 Description of a New Regional Array - GERESS German Experimental Seismic System	1
2 Signal Transfer Functions and Sensitivities for GERESS Seismometers	11
3 GERESS Status Report January 1990 - March 1991	28
4 The Bochum On-line Processing Display Manager	38
5 Evaluation of GERESS for Phase 3 of GSETT-2 November 26 - December 2, 1990	44
6 Nuclear Tests Observed with the GERESS Array in 1990	56
7 Regional Waveform Analysis with GERESS Data	79
8 Acknowledgements	101

# **1. DESCRIPTION OF A NEW REGIONAL ARRAY**

## **GERESS**

### **GERMAN EXPERIMENTAL SEISMIC SYSTEM**

**GEC2 (the key station of the array)**

Latitude	:	48.84511 N
Longitude	:	13.70156 E
Elevation	:	1132 m

#### **1.1 General**

The German Experimental Seismic System (GERESS) array project is a cooperative research program, jointly undertaken by Southern Methodist University in Dallas, Texas, and Ruhr-University Bochum, Germany. It is part of a multi-array network which includes NORESS, ARCESS and FINESA in Scandinavia. The GERESS array is located in the Bavarian Forest area at the southeastern part of Germany near the border to Austria and Czechoslovakia (Figure 1-1). The array consists of 25 stations with vertical-component short-period (1 Hz) Teledyne Geotech GS-13 type instruments sampled at 40 Hz. In addition, four of the sites include horizontal component instruments. At the key station of the array, GEC2, there is a supplemental three-component set of GS-13's sampled at 120 Hz (high-frequency element) and a three-component set of broad-band seismometers (Teledyne Geotech BB-13) sampled at 10 Hz.

The geometry of the array is based on concentric rings spaced at log-periodic intervals in radius  $R$  with 3, 5, 7, and 9 elements in each ring, plus one in the center (Figure 1-2). The radii of the rings are 200, 430, 925, and 1988 m, respectively, providing an overall aperture of about 4 km. The spacings between stations extend from 161 m to 3925 m. The location of each of the sites is given in Table 1-1.

The array became fully operational in January 1991. The inner ring of the array elements started data recording in March 1990 and since then the number of active channels has increased gradually. Since August 1990, all 25 vertical short-period channels have been operational. Seismic data from the array instruments are continuously archived on exabyte tapes at the Institute of Geophysics, Ruhr-University Bochum.

In addition to the seismic data, meteorological data from the array center near GEC2, including temperature and wind velocity, are available almost in real time. However, at present, these data are not permanently archived.

## 1.2 Geology

The Bavarian Forest area, as part of the Bohemian Massive, represents the largest outcropping crystalline block in Germany. In the array area, there is outcropping crystalline rock at the mountain top, while in the valleys, soil covers the basement rock. Most of the instruments are placed directly on granite or gneiss. However, because of the fixed concentric ring geometry, some stations had to be placed on weathered crystalline rock.

## 1.3 Sensitivities

The GS-13 instruments employ velocity transducers. The resulting channel sensitivity as a function of frequency is plotted in Figure 1-3. It displays a plateau of 26.5 counts/(nm/s) between 1.0 and 16.5 Hz (3 dB points).

The BB-13 instruments are acceleration transducers. The resulting channel sensitivity as a function of frequency is plotted in Figure 1-4. It displays a plateau of 0.428 counts/(nm/s<sup>2</sup>) between 0.01 and 4 Hz (3 dB points).

All channels have been adjusted to the same sensitivity by the manufacturer.

## 1.4 Noise

Background noise spectra from station GEC2 are shown in Figure 1-5 (day) and Figure 1-6 (night). The spectra are derived from 6 time-windows at day and night on December 13, 1990. The day spectrum is dominated by a noise maximum at 4-5 Hz, which is assumed to originate from a saw mill at a distance of a few kilometers. Apart from this peak the noise spectrum shows a smooth decay proportional to about  $f^{-4}$  from 1 Hz to 20 Hz.

## 1.5 Data Acquisition

Seismometer output signals are digitized with a sampling rate of up to 120 Hz by microprocessor-based equipment (RDAS-200 of Teledyne Geotech) at each array site. The RDAS-200 automatically accommodates a signal amplitude over a range of  $2^{24}$  (144 dB). The digital data are encoded into a Teledyne Geotech internal 24-bit integer format. Data are sent from each array site via fiber optic communications equipment to the array controller at the HUB near the key station GEC2. From this site, the data are transmitted to the Institute of Geophysics in Bochum and to the NORSAR data processing center, Kjeller Norway, by telephone lines. At the Institute of Geophysics in Bochum, the data are converted to CSS 2.8 format and are stored continuously on exabyte tapes. At the same time, the data are available almost in real time for bulletin preparation.

## 1.6 Data Processing

Data processing includes detection, phase identification, and location. NOR-SAR kindly supplied the RONAPP signal analysis software package. The detection algorithm is based on a conventional short-term average (STA)/ long-term average (LTA) technique. The STA/LTA detector works on a set of filtered beams deployed at typical velocities of teleseismic and regional seismic phases. When a detection is found, data within a certain time window around the detection time are used for estimates of arrival-time and signal frequency. The subsequent frequency-wavenumber analysis gives estimates of phase velocity, azimuth, and polarization for each detection. The automatic event location for local and regional events is based on azimuth and S-P travel times. If a detection is identified by its phase velocity as an S-type wave, and a preceding P-wave has been detected from about the same direction, an estimate of the event epicenter is calculated. All these determined values are printed into log files which can be remotely accessed by scientists via WIN.

Nicolai Gestermann  
Hans-Peter Harjes



Table 1.1: Location of the GERESS sites

Station Code	Longitude [degree]	Latitude [degree]	Elevation [m]
GEA0	13 42'06.780''	48 50'12.497''	1022.36
GEA1	13 42'14.117''	48 50'10.597''	1004.12
GEA2 *	13 42'06.543''	48 50'19.025''	1055.55
GEA3	13 42'00.122''	48 50'06.038''	1011.87
GEB1	13 42'27.116''	48 50'19.996''	1009.86
GEB2	13 41'54.998''	48 50'22.345''	1088.73
GEB3	13 41'45.536''	48 50'13.027''	1053.56
GEB4	13 41'55.882''	48 49'57.848''	1000.85
GEB5	13 42'21.397''	48 50'04.450''	971.73
GEC1	13 42'35.704''	48 50'28.428''	1022.55
GEC2 o	13 42'05.613''	48 50'42.382''	1132.46
GEC3	13 41'30.070''	48 50'32.535''	1070.47
GEC4	13 41'14.983''	48 50'06.718''	1098.09
GEC5	13 41'44.503''	48 49'46.568''	1004.20
GEC6	13 42'32.558''	48 49'36.372''	937.11
GEC7	13 42'52.134''	48 50'07.599''	980.78
GED1 *	13 42'53.188''	48 51'06.512''	1056.74
GED2	13 41'47.157''	48 51'11.600''	994.10
GED3	13 40'54.463''	48 50'47.402''	944.70
GED4 *	13 40'46.702''	48 50'18.871''	1034.69
GED5	13 40'50.471''	48 49'28.612''	1080.40
GED6	13 41'47.914''	48 49'09.856''	1079.35
GED7 *	13 42'57.329''	48 49'15.318''	955.41
GED8	13 43'33.916''	48 49'59.402''	933.03
GED9	13 43'25.644''	48 50'36.346''	981.79

\* 3-component short-period  
o 3-component broad-band  
3-component high-frequency  
vertical short-period

elevation : bottom of vaults  
coordinates : geographical (UTM) coordinates defined  
in the meridional zone #33

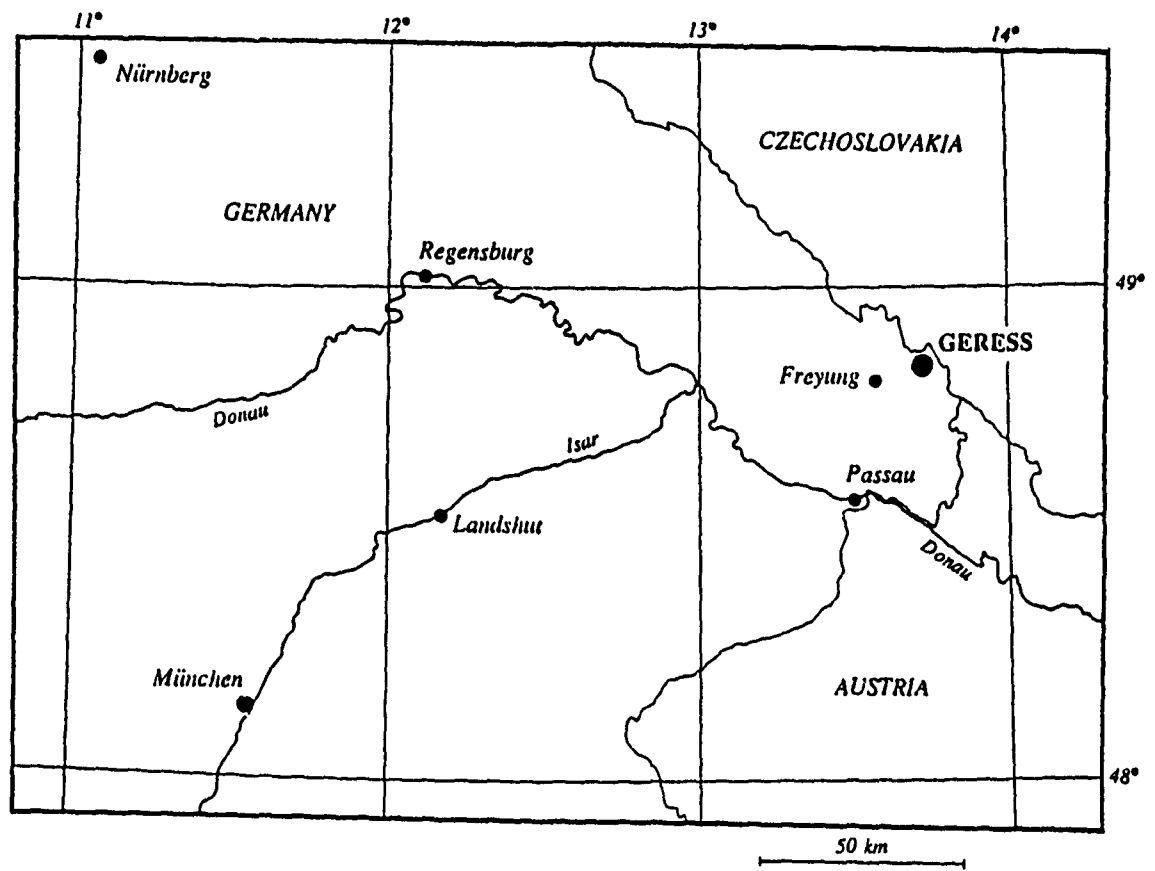


Figure 1-1      Geographical location of the GERESS array.

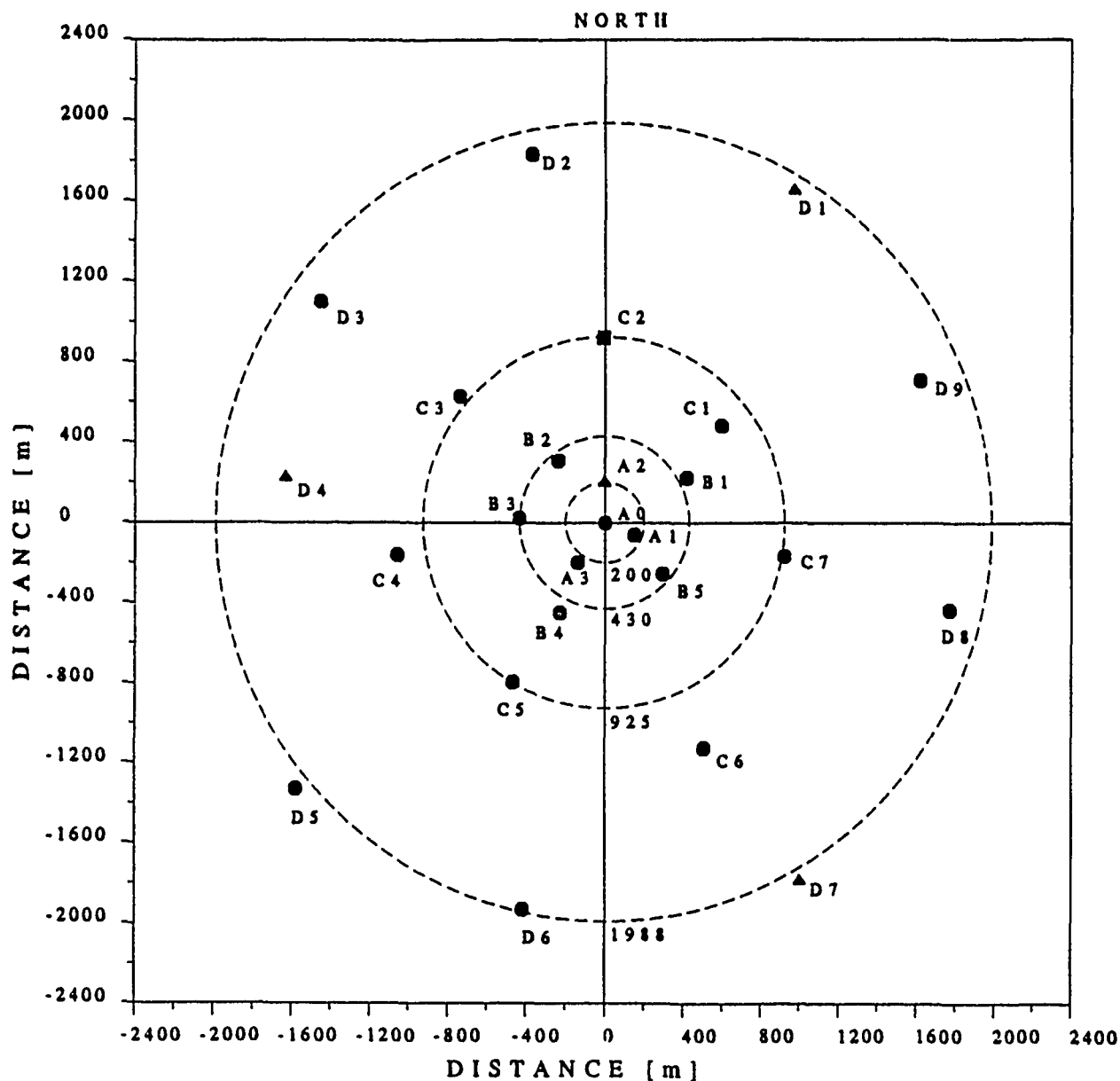


Figure 1-2 Configuration of the GERESS array.

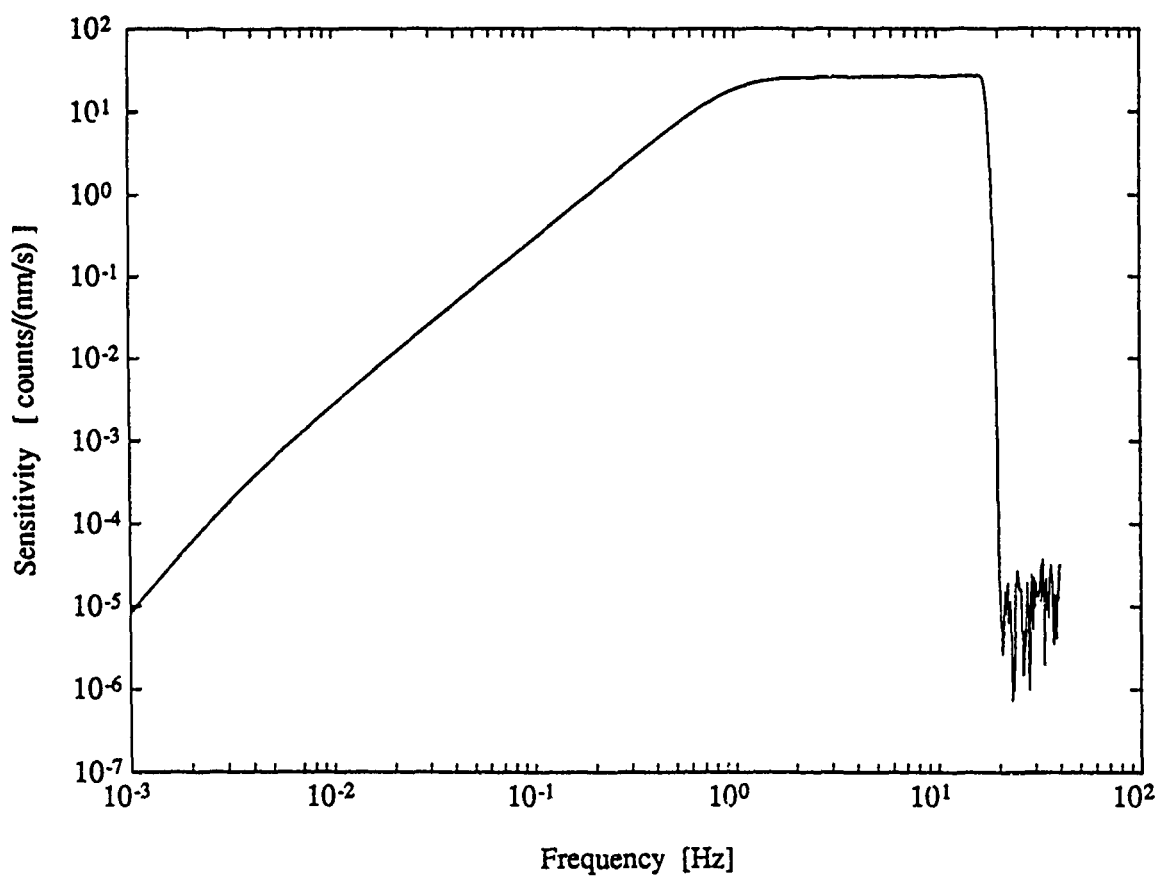


Figure 1-3 GERESS GS13 velocity response, sampling frequency 40 Hz.

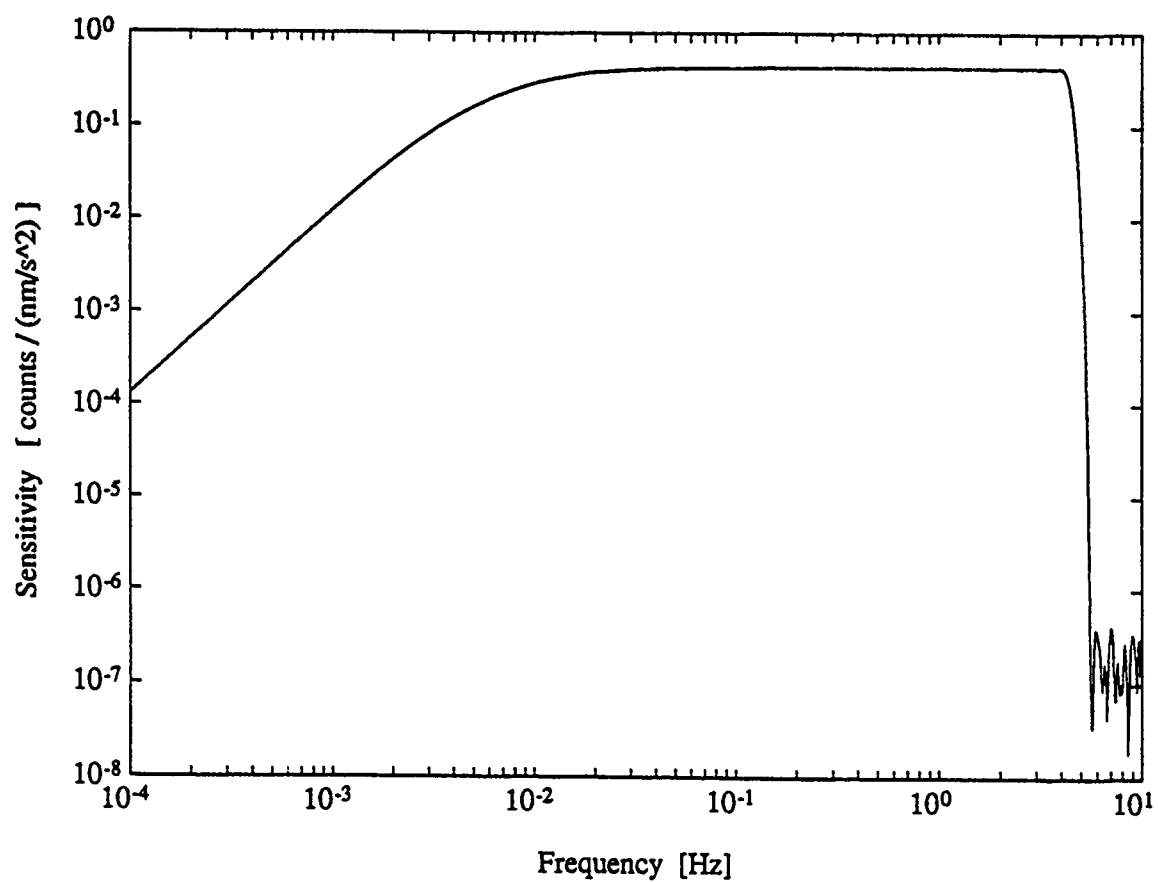


Figure 1-4 GERESS BB13 acceleration response, sampling frequency 10 Hz.

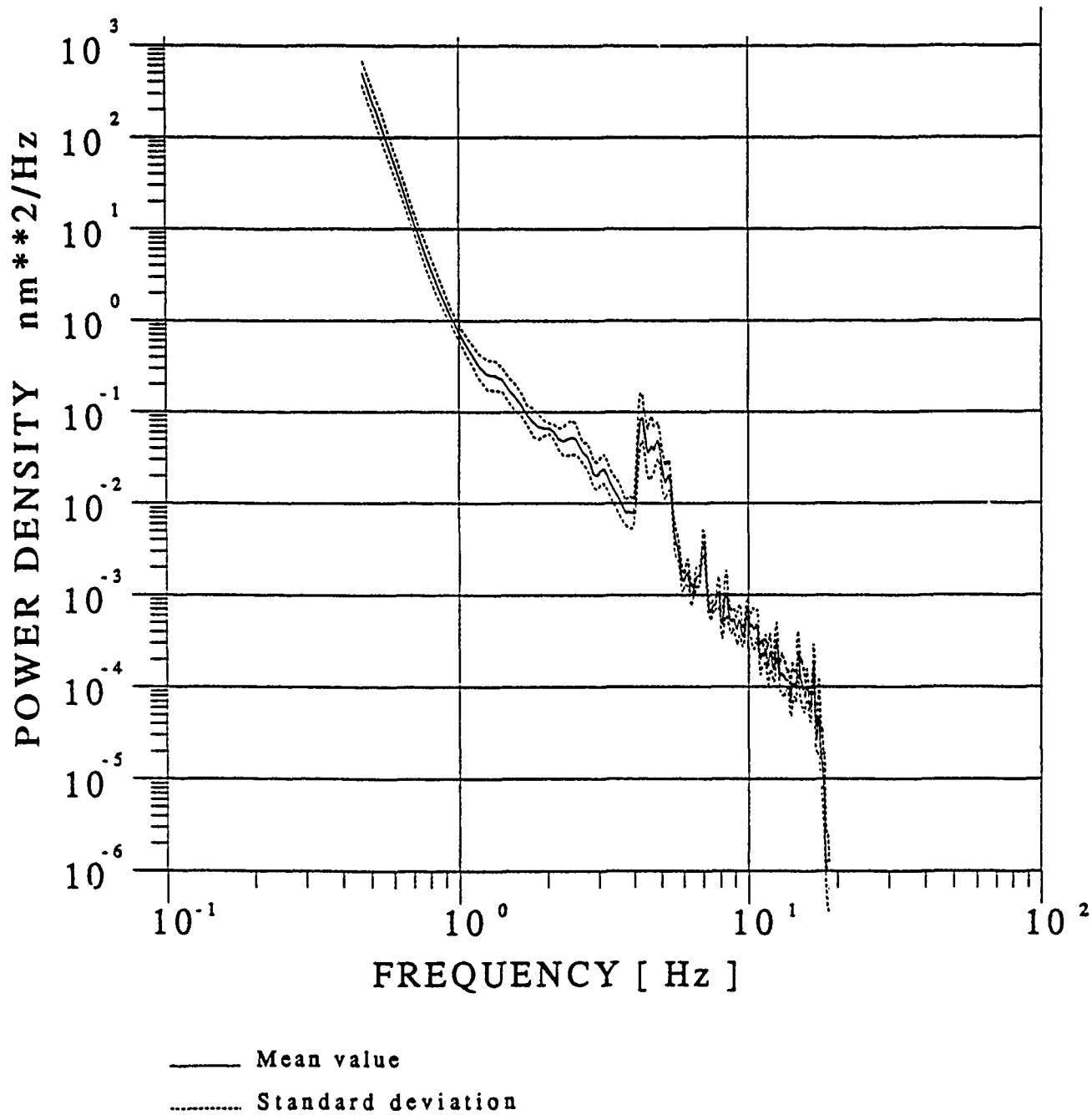


Figure 1-5 Short-period vertical component displacement power spectrum of noise at the key station GEC2 for day time. The solid line represents an average spectrum of 6 different time-windows. Each sample was 40 seconds in length and was divided into 11 analysis sections with a length of 6.4 seconds each.

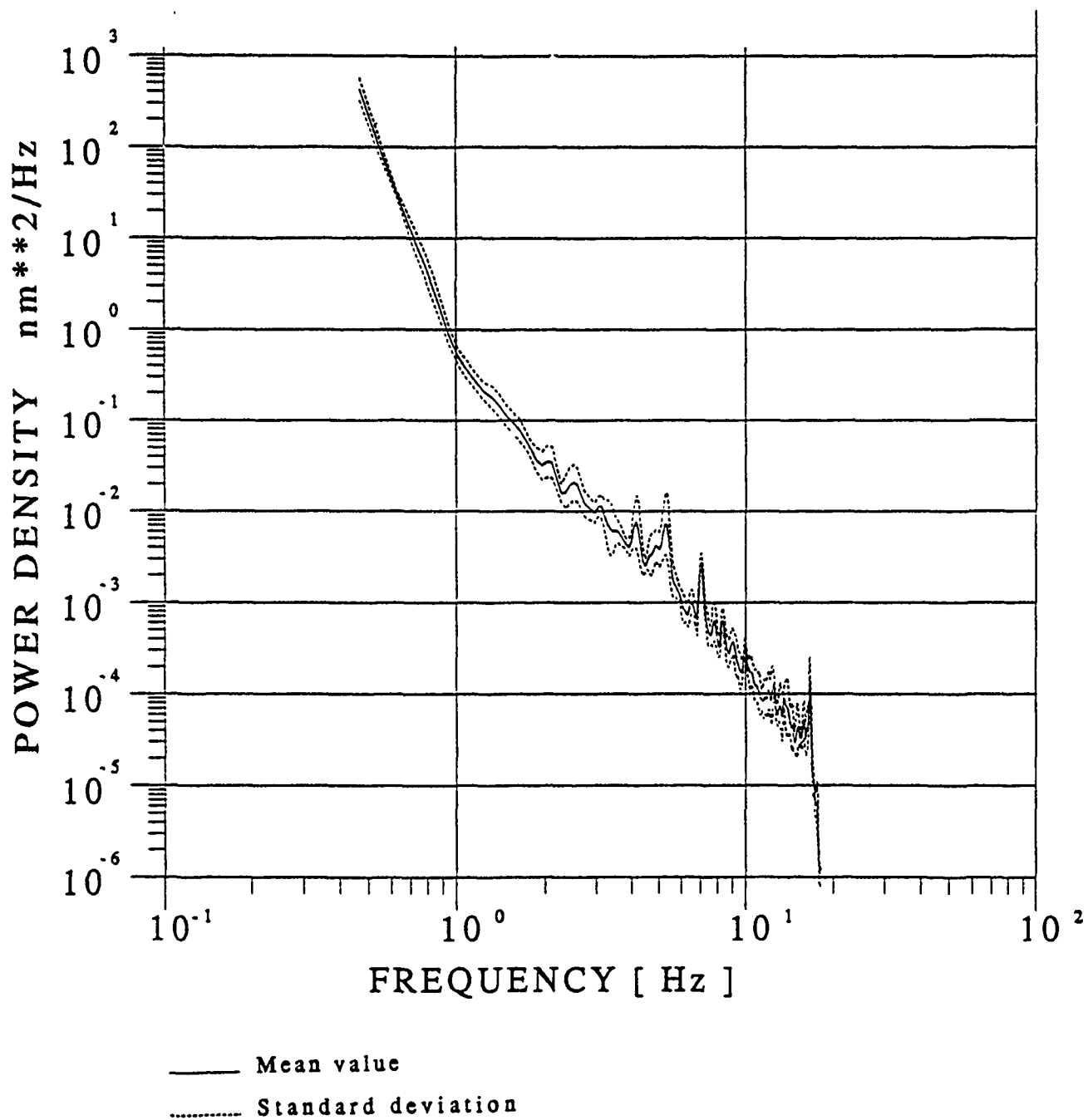


Figure 1-6

Short-period vertical component displacement power spectrum of noise at the key station GEC2 for night time. The solid line represents an average spectrum of 6 different time-windows. Each sample was 40 seconds in length and was divided into 11 analysis sections with a length of 6.4 seconds each.

## 2. Signal Transfer Functions and Sensitivities for GERESS Seismometers

### 2.1 Introduction

The GERESS regional seismic array is equipped with seismometers of GS13 (short period) and BB13 (broad band) types. They are described in Tele-dyne's Operation and Maintenance Manuals M-55400 and M-57760 respectively.

As indicated in fig. 2.1, the complete signal acquisition system consists of 4 stages:

1. the mechanical suspension system,
2. several analog stages including the transducer, amplifiers and, in the case of BB13, a feedback loop,
3. the analog/digital converter,
4. digital filtering and resampling stages.

If true ground movement is to be restituted from the recorded signals, the performance of each of these stages must be known precisely.

### 2.2 Transfer Functions

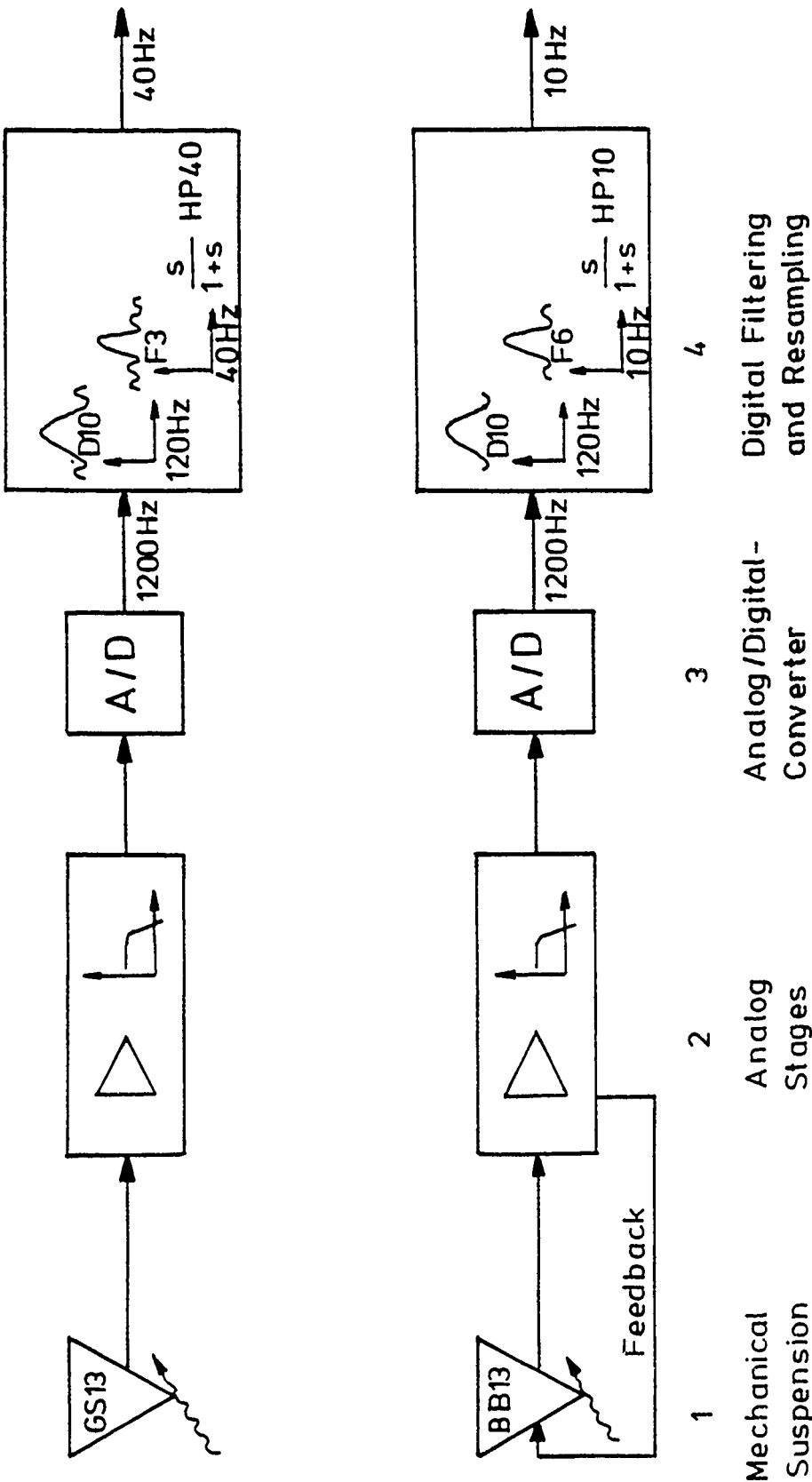
The analog stages (1. and 2.) can be described in terms of transfer function  $H(s)$  in the  $s$ -plane, ( $s \in \mathbb{C}$ ), such that

$$Y(s) = H(s) \cdot X(s) ,$$

where  $X(s)$  is the Laplace-transform of the ground displacement  $x(t)$ , velocity  $v(t)$  or acceleration  $a(t)$  at the location of the seismometer and  $Y(s)$  is the



Figure 2.1: GERESS signal acquisition system



Laplace-transform of the output signal. The one-sided Laplace-transform is defined as

$$\mathcal{L} \{f(t)\} = F(s) = \int_0^{\infty} f(t)e^{-st} dt.$$

Both mechanical and analog electronic systems are governed by general differential equations with constant coefficients. Theory (e.g. Doetsch, 1967)<sup>1</sup> proves that  $H(s)$  is the quotient of two polynomials in this case:

$$H(s) = \frac{A(s)}{B(s)} = \frac{\sum_{k=0}^M a_k s^k}{\sum_{l=0}^N b_l s^k},$$

and since every polynomial of degree  $M$  can be factored into  $M$  roots over the complex space  $\mathbb{C}$ ,

$$A(s) = \prod_{k=1}^M (s - r_k) \quad , \quad r_k \in \mathbb{C}$$

is an entirely equivalent formulation of the numerator. Roots of the numerator polynomial are called zeroes, those of the denominator polynomial are called poles. Thus, a transfer function can be given in terms of its poles and zeros

$$H(s) = V_0 \cdot \frac{\prod_{k=1}^M (s - z_k)}{\sum_{l=1}^N (s - p_l)}.$$

The gain factor  $V_0$  is often added for convenience, but could be included into the numerator or denominator term if required.

For quick reference, poles and zeroes of GERESS analog channels are tabulated in appendix C.

Poles and zeroes for a given system can either be calculated from system parameters such as natural frequency and damping, together with theoretical assumptions about the nature of the system, or they can be determined experimentally via RMS-approximation by measuring phase and amplitude response over a wide range of frequencies with a signal analyzer. The former method has been used at SMU for the GS13. Assuming that the analog stages beyond the transducer do not greatly change amplitude nor phase

---

<sup>1</sup>Doetsch, Gustav: Anleitung zum praktischen Gebrauch der Laplace-Transformation und der Z-Transformation. München, Wien 1967<sup>3</sup>

characteristics apart from uniform amplification, and assuming zero coupling between the electronic and the mechanical system, the well-known Laplace-transform of the seismometer-equation is used

$$H(s) = G \cdot \frac{s^2}{s^2 + 2\lambda\omega_0 s + \omega_0^2}$$

where  $G$  is the generator constant,

$\lambda$  is the effective damping factor = 0.775, and

$\omega_0$  is the free circular frequency =  $2\pi/T = 2\pi$   
(free period  $T = 1$  sec)

to find the two zeroes at zero and the two poles at

$$\begin{aligned} p_{1/2} &= -\lambda\omega_0 \pm \omega_0 \cdot \sqrt{\lambda^2 - 1} \\ &= -4.869 \pm i \cdot 3.971 . \end{aligned}$$

In case of considerable coupling, as with the BB13 feedback loop, the above formula cannot be used.

By means of an HP-3582 Signal Analyzer Teledyne derived transfer functions with 8 poles and 1 zero for the GS13 and with 10 poles and 4 zeroes for the BB13 (see figs. 2.2 and 2.3.) In order to compare GS13 transfer functions from Teledyne and from SMU, the Teledyne function must be subjected to the following transformations:

- (a) add one zero at zero to obtain velocity-proportionality,
- (b) multiply each pole and zero value supplied by Teledyne by  $2\pi$  and
- (c) adjust the gain factor according to  $V = V_{Teledyne} \cdot (2\pi)^{N-M}$ ,  
where  $N = \#$  of poles and  $M = \#$  of zeroes.

Proofs for this procedure can be found in appendices A and B.

To facilitate visual comparison of the different transfer functions, their amplitudes and phases

$$\begin{aligned} \text{amp}(s) &= |H(s)| \\ \text{phase}(s) &= [\arg(H(s)) \pm n \cdot 2\pi] \cdot 180/\pi \end{aligned}$$

were plotted against frequency with  $s = 2\pi \cdot i \cdot \nu$ . Fig. 2.4 shows that Teledyne and SMU transfer functions are generally in good agreement in the frequency range considered (Nyquist-frequency is 20 Hz.) The linear plot

Figure 2.2: Information from Teledyne on GS13 transfer function

Synthesis			
<u>Poles And Zeros</u>			
POLES		8	ZEROS 1
1	-697.818m±j	665.463m	0.0
2	-19.4449 ±j	62.7201	
3	-96.651		
4	-211.642		
5	-3.97887M		
6	-27.6311M		
Time delay= 0.0 S Gain=38.E+30 Scale= 1.0			

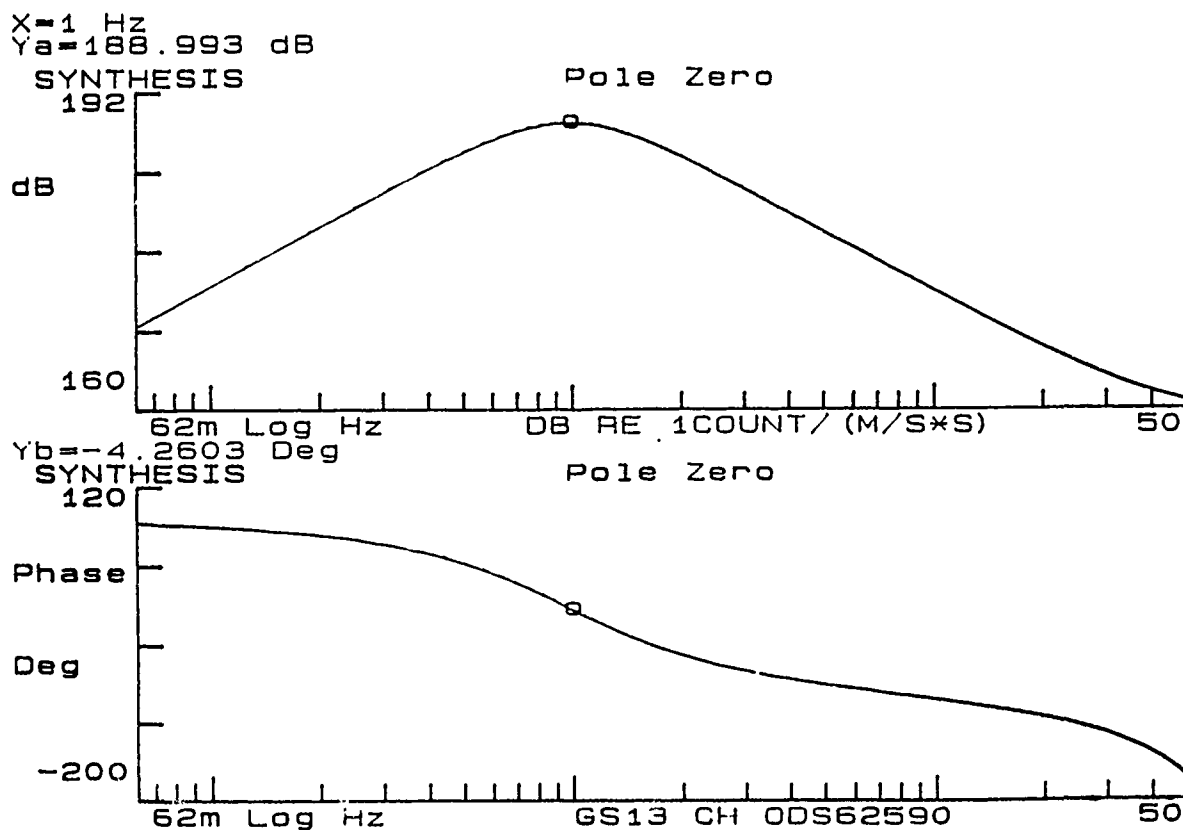


Figure 2.3: Information from Teledyne on BB13 transfer function

Synthesis		
Poles And Zeros		
POLES		ZEROS
	10	4
1	-482.88	-5.09537k
2	-193.706	-193.978
3	-97.0394	-9.7389 $\mu$
4	-9.9311m	-203.601
5	-16.5294	
6	-7.28119 $\pm j$ 19.6113	
7	-211.642	
8	-3.97887M	
9	-27.6311M	

Time delay= 30.58 $\mu$ S Gain=3.2E+27 Scale= 1.0

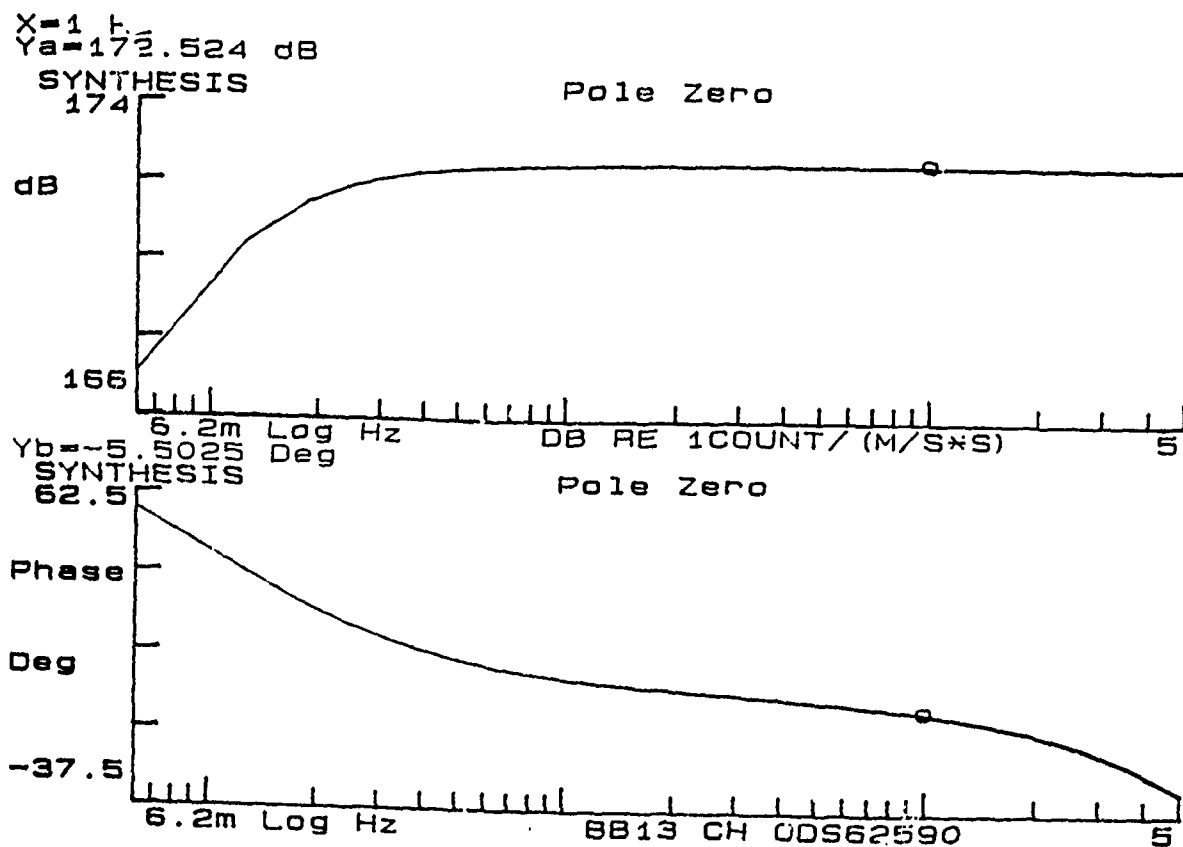
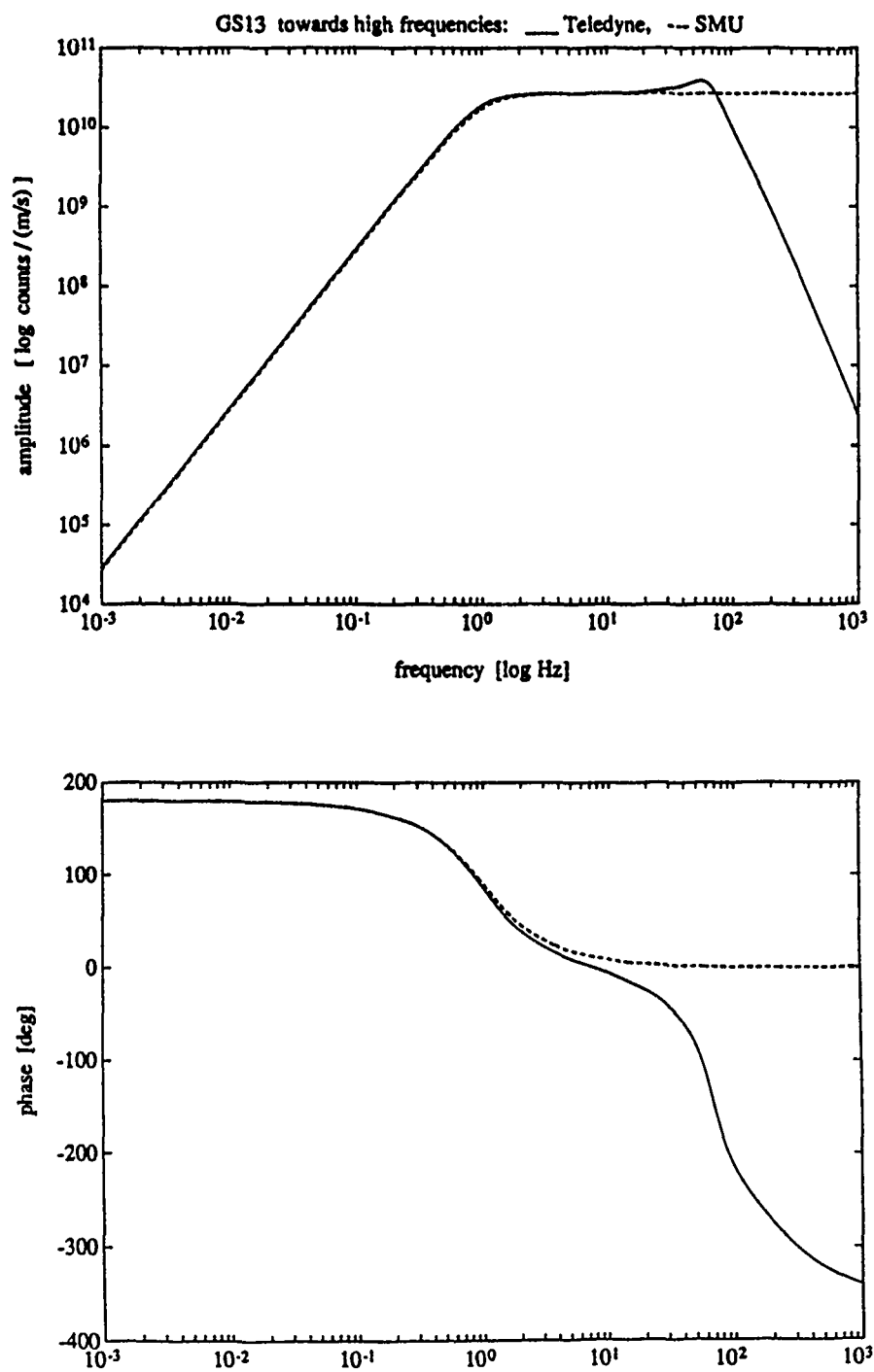


Figure 2.4: Comparison of measured (Teledyne) and theoretically derived (SMU) transfer function for GS13



(fig. 2.5) shows the slight deviation in amplitude. Thus it appears justified to use SMU's conveniently simpler transfer function for the GS13. This is no longer true for the GS13 high frequency element (60 Hz Nyquist-frequency.) Both amplitude curves have been normalized to a value of 26.53 counts per  $nm/sec$  at 5 Hz (see below under Sensitivity.)

Fig. 2.6 is a plot of the BB13 transfer function from poles and zeroes supplied by Teledyne.

## 2.3 Sensitivities

The total sensitivity of a channel is determined by the generator constant of the seismometer, the total amplification of the analog system, the conversion ratio of the A/D-converter and the amplification of any digital filters employed. Its dimension is digital counts per  $m/sec$  for the velocity transducer GS13 and digital counts per  $m/sec^2$  for the acceleration transducer BB13. If ground-displacement amplitude is to be calculated from velocity or acceleration data, one or two zeroes at zero can be added to the transfer function, respectively, before the analog amplification is calculated. This amounts to a multiplication of analog amplification by  $\omega$  or  $\omega^2$ . The resulting sensitivity then has the dimension counts per  $m$ . Note, however, that this manipulation does not make the system a displacement transducer (to that end the output signal would have to be integrated) and that the derived displacement sensitivity is strictly speaking valid for monochromatic signals only.

Within their passbands, the digital filters employed have unit gain (see below) and therefore need no consideration.

Thus, channel sensitivity is

$$\frac{G \cdot P}{LSB},$$

where  $G$  is the generator constant,  $P$  is the preamplification factor and  $LSB$  is the least significant bit of the A/D-converter. The 24-bit A/D-converter has an input range of 40 Volts peak to peak, so its  $LSB = 2.3841857 \mu V$ .

For the GS13, Teledyne adjusted the generator constants to  $2000 V/(m/s)$ . Pre-amplification is 30dB (factor 31.6228). With these values the GS13 total sensitivity is 26.53 counts per  $nm/sec$  in the plateau-region around 5 Hz.

For the BB13 the "generator constant" (i.e. the sensitivity of the seismometer unit including the feedback loop) is  $102 V/(m/s^2)$  on its plateau.

Figure 2.5: Linear plot comparing measured (Teledyne) and theoretically derived (SMU) transfer function for GS13. Both curves were normalized to 26.53 counts per  $\mu\text{m/s}$  at 5 Hz.

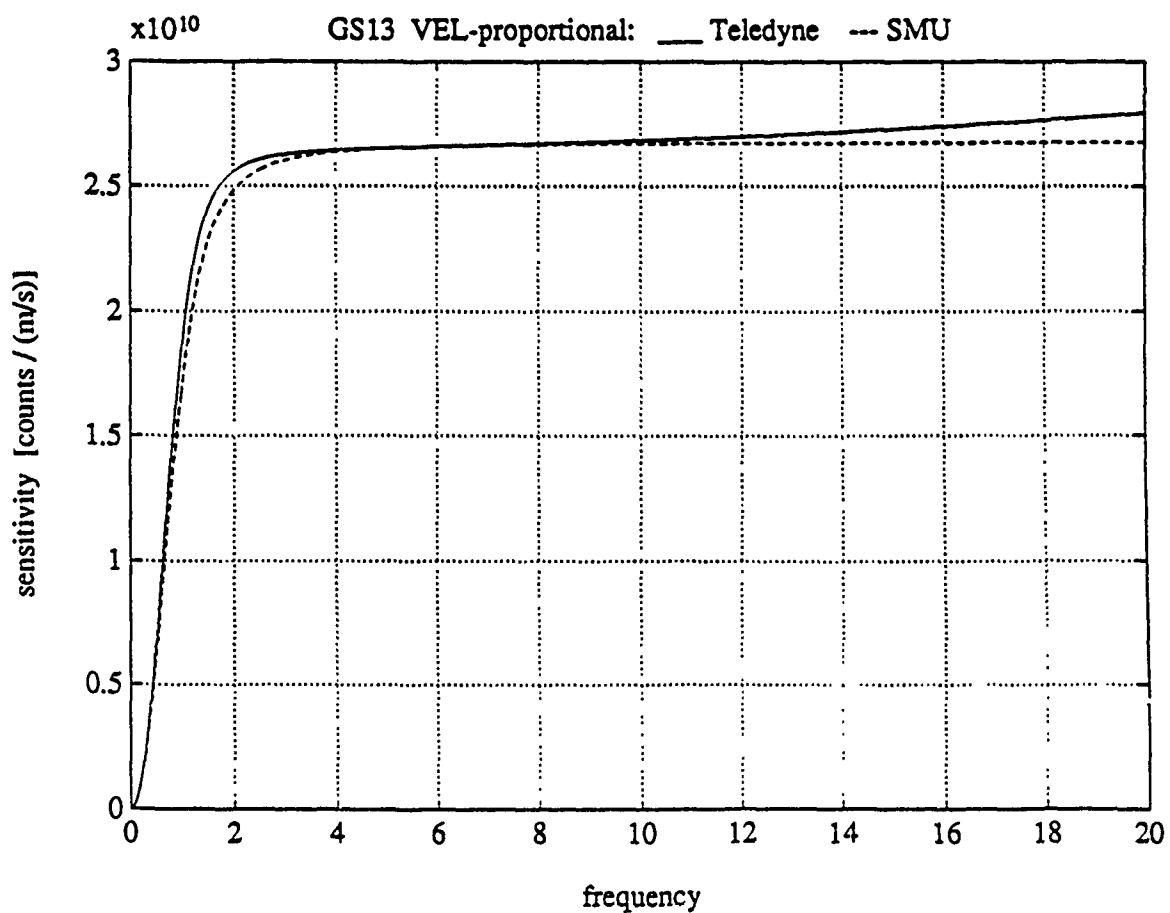
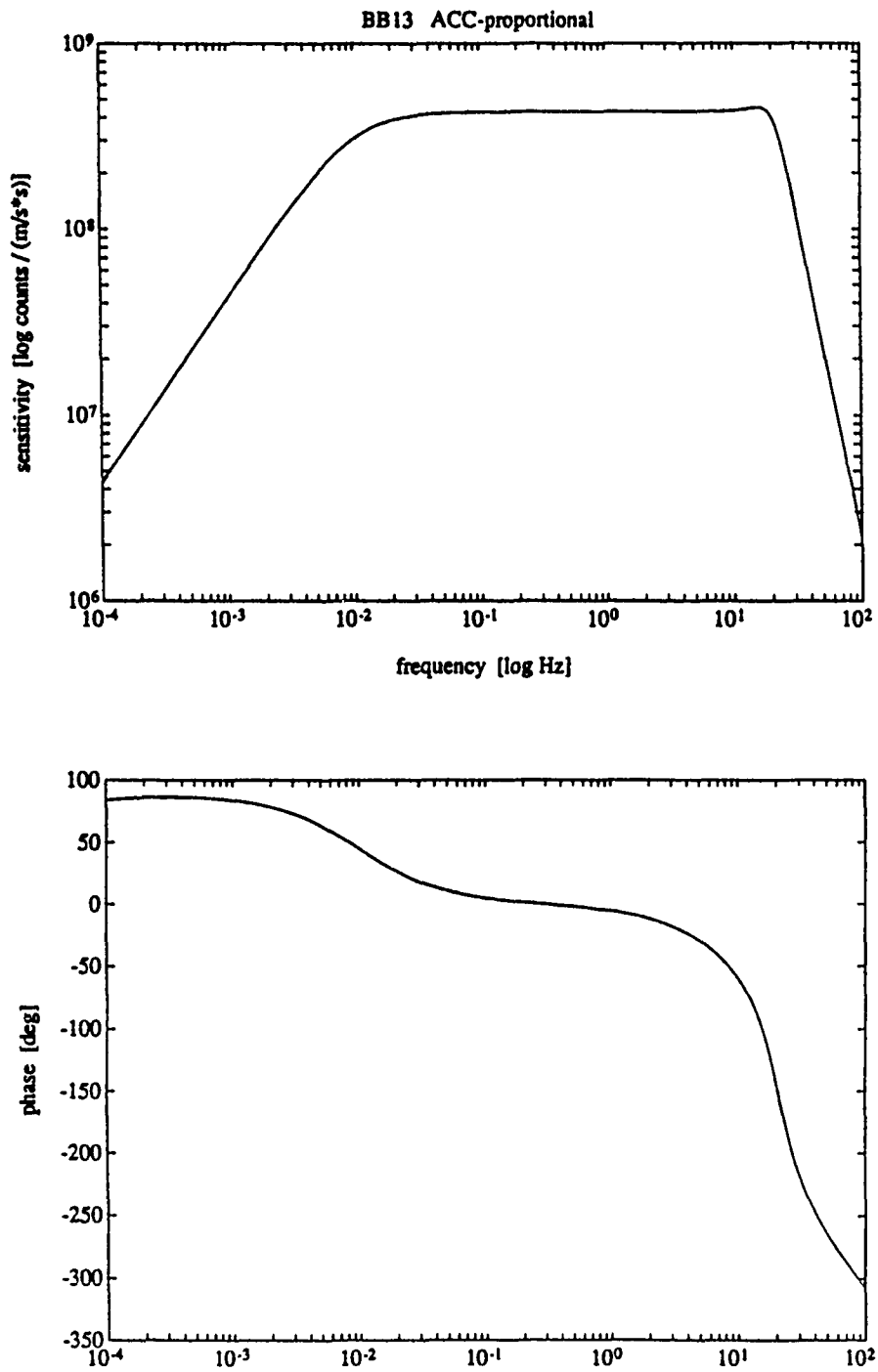




Figure 2.6: Transfer function for BB13 (measured)



Gain factors for the transfer functions supplied by Teledyne need to be slightly adjusted, so that total sensitivities reach their theoretical values at 5 Hz (GS13) and 0.75 Hz (BB13.) Both original and adjusted values are listed in appendix C.

Teledyne has conducted measurements to verify the theoretically derived sensitivities, but the results have not been released yet. Another way to test the assumptions would be the evaluation of the calibration pulses, which are available for each channel daily.

## 2.4 Digitization and digital filters

At the A/D-converter, data are sampled at 1200 Hz. It is evident from figs. 2.4 and 2.6, that the transfer functions of both GS13 and BB13 have low pass properties towards high frequencies, so that aliasing is prevented. Both types of channels are then cascaded down to 40 Hz and 10 Hz sampling frequency, respectively, through two stages of low-pass filters and re-sampling algorithms. Finally a digital high-pass filter (1st order Butterworth, 3dB-point at 300 sec) is employed to remove dc-offset. Fig. 2.7 shows the cascade.

The digital filters are FIR filters, applied in the time domain. As an example, figs. 2.8 and 2.9 show filter coefficients in the time domain and amplitude characteristics of filter F6. The low-pass filters cannot be conveniently expressed in terms of poles and zeroes. Within their passbands they have unit gain, cut-off is very sharp and attenuation is 120dB per stage. The final figs. 2.10 and 2.11 show the overall (analog plus digital) amplitude characteristics for GS13 and BB13 channels.

Jan Wüster

Figure 2.7: Cascade of digital low-pass and resampling stages for GS13 and BB13 channels

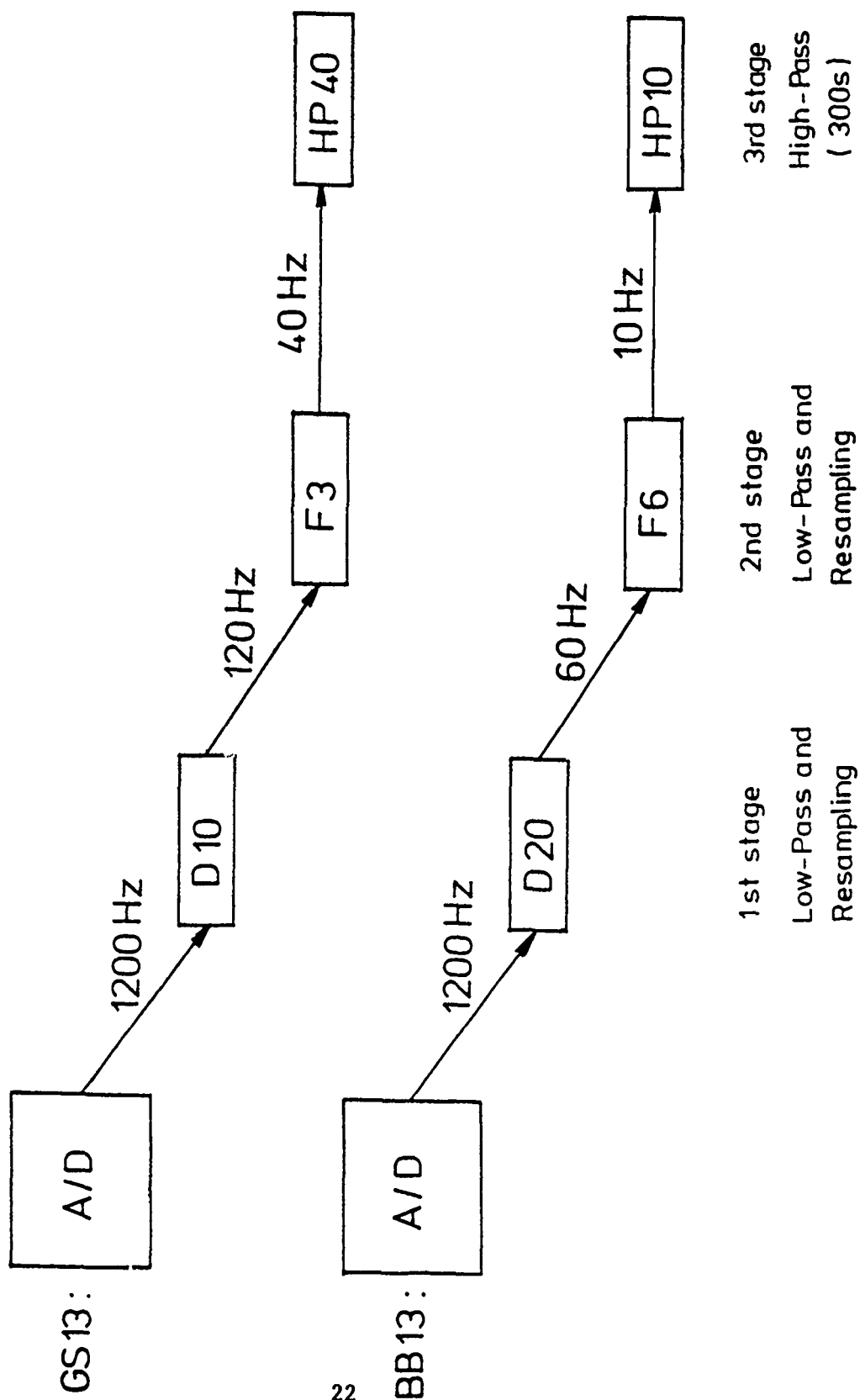


Figure 2.8: Digital filter F6 in time domain

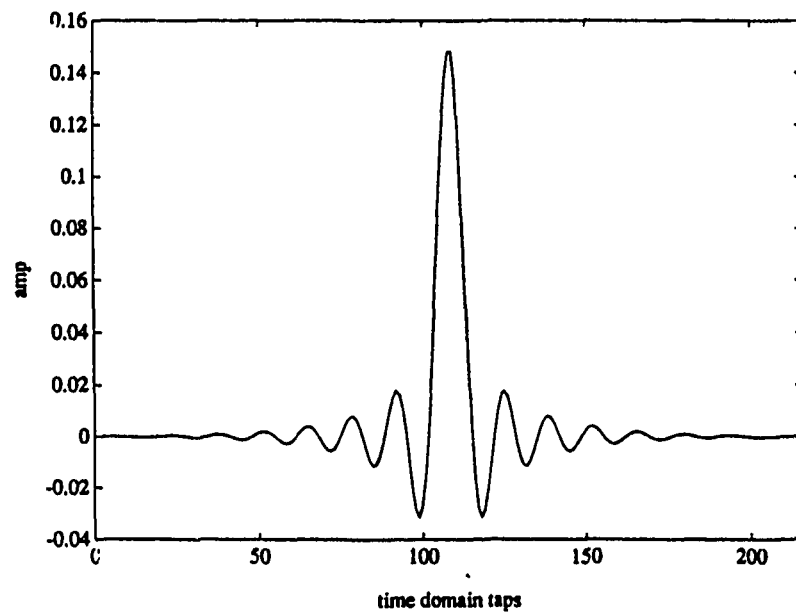


Figure 2.9: Digital filter F6 in frequency domain

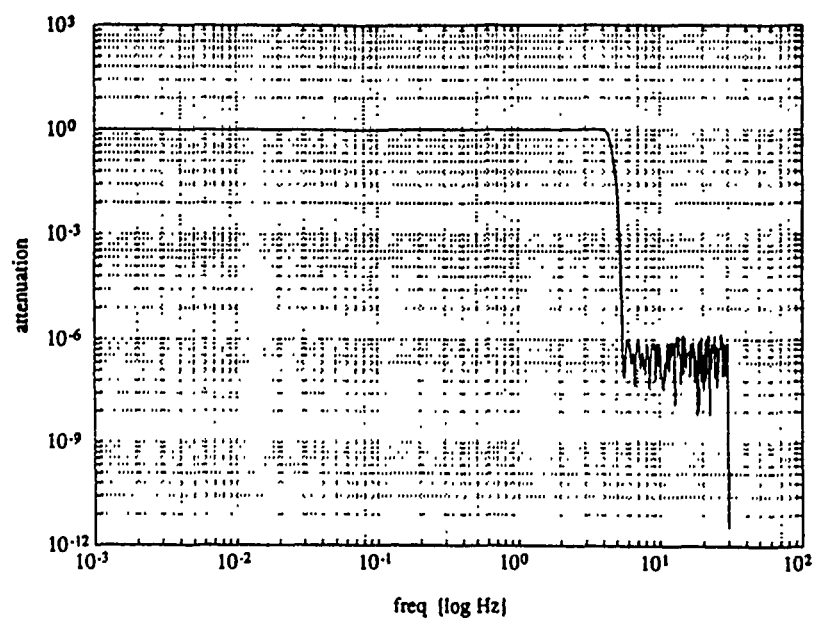


Figure 2.10: Overall amplitude characteristics of GS13 channel, calculated by multiplication in the frequency domain of analog and digital stages

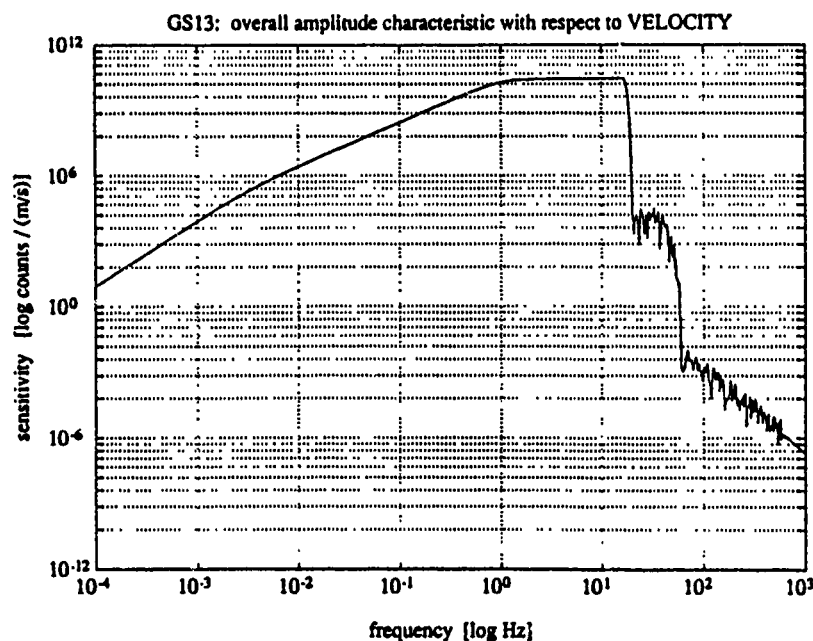
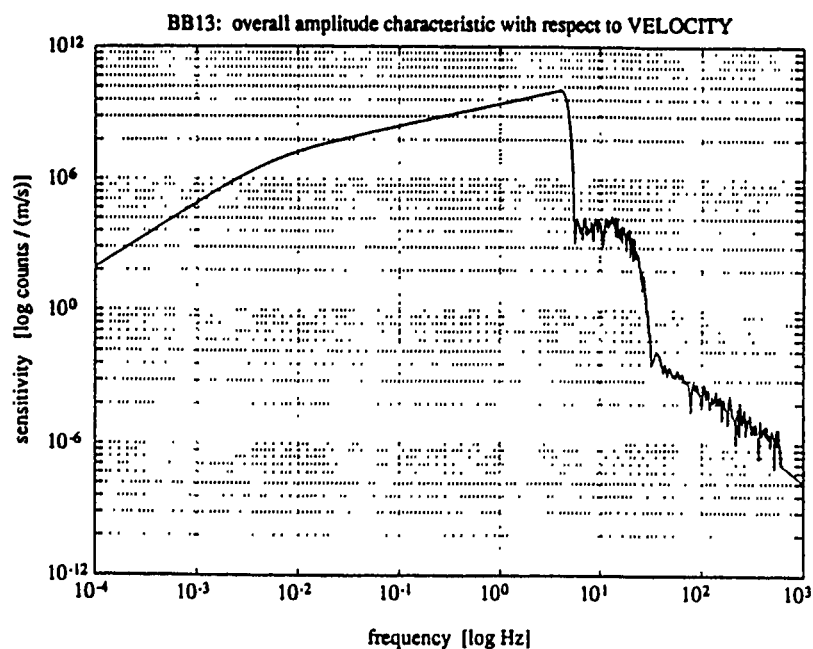


Figure 2.11: Overall amplitude characteristic of BB13 channel, calculated by multiplication in the frequency domain of analog and digital stages



## 2.5 Appendix A: proof of conjecture (a)

Be  $H^{ACC}(s)$  a transfer function assuming ground-acceleration  $a(t)$  as input.

We have the transfer equation in the  $s$ -plane

$$Y(s) = A(s) \cdot H^{ACC}(s) , \quad (2.1)$$

$A(s)$  being the Laplace-transform of the input signal

$$A(s) = \mathcal{L} \{a(t)\} . \quad (2.2)$$

From (2) we get with  $a = \frac{dv}{dt}$

$$A(s) = \mathcal{L} \{a(t)\} = \mathcal{L} \{\dot{v}\} , \quad (2.3)$$

and with the differentiation theorem for the Laplace-transform

$$A(s) = s \cdot \mathcal{L} \{v(t)\} = s \cdot V(s) . \quad (2.4)$$

Substituting (4) into (1)

$$\begin{aligned} Y(s) &= V(s) \cdot \underbrace{s \cdot H^{ACC}(s)} \\ Y(s) &= V(s) \cdot H^{VEL}(s) \end{aligned} \quad (2.5)$$

we identify

$$H^{VEL}(s) = H^{ACC}(s) \cdot s . \quad (2.6)$$

This proves, that  $H^{VEL}(s)$ , the transfer function assuming ground velocity  $v(t)$  as input is obtained from  $H^{ACC}(s)$  by adding one zero at zero frequency.

## 2.6 Appendix B: Proof of conjectures (b) and (c)

Let  $s = i\omega = i2\pi\nu$  and  $t = i\nu$  be the two conventions for mapping the frequency axis onto the complex plane.

A transfer function supplied by Teledyne using the  $t$ -convention is

$$H(t) = V_t \cdot \frac{\prod_{k=1}^M (t - z_k^{(t)})}{\prod_{l=1}^N (t - p_l^{(t)})} . \quad (2.1)$$

Expanding (7) by a suitable number of  $2\pi$ -factors makes it

$$H(t) = V_t \cdot \frac{(2\pi)^N}{(2\pi)^M} \cdot \frac{\prod_{k=1}^M (2\pi t - 2\pi z_k^{(t)})}{\prod_{l=1}^N (2\pi t - 2\pi p_l^{(t)})} , \quad (2.2)$$

and the transformation  $t \longrightarrow s = 2\pi t$  gives

$$H(s) = V_0 \cdot \frac{\prod_{k=1}^M (s - z_k)}{\prod_{l=1}^N (s - p_k)} . \quad (2.3)$$

Comparing (9) to (8) we find that "our" poles, zeroes and gain factors are related to Teledyne's via

$$\begin{aligned} z_k &= 2\pi \cdot z_k^{(t)} \\ p_l &= 2\pi \cdot p_l^{(t)} \\ V_0 &= V_t \cdot (2\pi)^{M-N} \end{aligned} \quad (2.4)$$

## 2.7 Appendix C

Poles and zeroes of GERESS analog channels, as supplied by Teledyne.

The transfer-functions are acceleration-proportional as given [counts/(m/s<sup>2</sup>)],  
 add one zero at 0 to obtain velocity-proportionality [counts/(m/s)],  
 add two zeroes at 0 to obtain displacement-proportionality [counts/m].

Values have been transformed to the convention  $s = i * w = i * 2\pi * \text{freq[Hz]}$ ,  
 as opposed to the convention used by Teledyne  $s = i * \text{freq[Hz]}$ .

This implies multiplication of each pole and zero with factor  $2\pi$ , and  
 a corresponding adjustment in the gain factor

$\text{our\_gain} = \text{their\_gain} * (2\pi)^{(1-k)}$   
 where  $k$  = number of zeroes and  
 $l$  = number of poles.

The number of significant digits is 6 for poles & zeroes and only 2 for  
 gainfactors. JW/RUB/25.01.91

### A) Broad-band channels BB13 .....

BB13poles =     -3.034025e+03  
                   -1.217091e+03  
                   -6.097165e+02  
                   -6.239894e-02  
                   -1.038573e+02  
                   -4.574907e+01 + 1.232214e+02i  
                   -4.574907e+01 - 1.232214e+02i  
                   -1.329786e+03  
                   -2.499998e+07  
                   -1.736113e+08

BB13zeroes =    -3.201515e+04  
                   -1.218800e+03  
                   -6.119131e-05  
                   -1.279263e+03

BB13gain =       1.97e+32  
                   (1.9991e+32 to obtain 0.4279 counts/(nm/s<sup>2</sup>) at 0.75 Hz)

### B) Short-period channels GS13 .....

GS13poles =     -4.384520e+00 + 4.181227e+00i  
                   -4.384520e+00 - 4.181227e+00i  
                   -1.221759e+02 + 3.940820e+02i  
                   -1.221759e+02 - 3.940820e+02i  
                   -6.072761e+02  
                   -1.329786e+03  
                   -2.499998e+07  
                   -1.736113e+08

GS13zeroes =     0

GS13gain =       1.47e+37  
                   (1.5818e+37 to obtain 26.530 counts/(nm/s) at 5 Hz)



### 3. GERESS STATUS REPORT

JANUARY 1990 - MARCH 1991

In 1990, the hardware installation at the GERESS array-site progressed to completion. All stations were on-line in August (Figure 3-1). However, technical problems hindered the operation of the high frequency station C2B until literally the last day of 1990 when the array started full operation. But even in the first few months of 1991, the array cannot be considered fully operational. Various problems still remain unsolved: Channels consistently are desynchronized by a fraction of a second (e.g., Figure 3-2). The array-controller has a tendency to become unstable (e.g., Figure 3-3). There are more gaps in the data stream than expected from the quality of the communication line (e.g., November 1990 GERESS Status Report). The number of gaps per data channel were found to form 4 groups. These 4 groups correspond to the 4 communication boards on the array-controller. In addition, the number of gaps per communications board correlates to the number of channels connected to the communications board of the array-controller. Data are sent with time stamps far in the future (e.g., Figure 3-4).

In 1990, the GERESS recording site at Ruhr University Bochum was set up. At Bochum, first the data acquisition system was installed. In spite of various hardware problems at the array site, first priority was assigned to data archiving starting in April 1990. Due to a massive malfunction of SCIENCE HORIZONS equipment, data archival had to be done manually from the beginning of April to the beginning of October: an operator had to be present every day for at least 1 hour (most of the time 2 hours) to write data to tape. On the other hand, GERESS data are now available as continuously as possible from the beginning of April 1990. Some data recordings exist even for February 1990 and March 1990. In October, an automatic tape archiver was developed and implemented after a hardware change by Bochum's system engineer. A spooler was developed, holding the latest 2 1/2 days of GERESS data in CSS-2.8 format on disk for off-line data processing. In February 1991, SCIENCE HORIZONS installed a SPARC based replacement of the data acquisition hardware at Bochum.

With the help from NORSAR, the RONAPP software package was installed at Bochum. In June 1990, an on-line STA/LTA detector was implemented. However, due to limitations of performance and disk space, an effective work using the NORSAR package on-line was not possible for the first 10 months of 1990. The same is also true for interactive data analysis: A single fk-transformation took 5 minutes at best. However, this dramatically changed after a SUN SPARC computer system was installed at Bochum in early October 1990. A STA/LTA detector, fk-analyzer, and location routine were implemented for on-line data analysis. A detailed description of the on-line data analysis is given in *The Bochum On-line Processing Display Manager*

in this volume. Figure 3-5 shows the present hardware and data-flow at Bochum station. The powerful NORSAR package is also used for off-line data analysis.

Tasks completed at the Bochum Data Center included (Appendix 3-1): Installation, adaptation, and debugging (in cooperation with SCIENCE HORIZONS) of the on-line data acquisition software (4 software reviews implemented). Installation and adaptation of the NORSAR on-line data analysis package (4 different updates installed). Purchase and installation of a SUN 4/330 server (96 MB in core, 6 GB disks), 4/65 SPARC station (40 MB in core), and two 4/20 (8 MB in core). Integration of acquisition workstation SUN 3E and monitoring workstation SUN 3/50 into the ethernet of the SUN 4s. Installation of system software (2 versions of X11 window system, 2 versions of a FORTRAN compiler, MATLAB). Establishment of a seismological observatory routine at Bochum: An automatic data archiver was developed and implemented. Monthly GERESS status reports are published (available upon request). Interesting events are analyzed and written to event tapes. Since June 1990, GERESS data are processed on-line. Since October 1990, a downtime list for Bochum is available (see monthly GERESS Status Reports). Data distribution has started, e.g. to BGR (Bundesanstalt für Geowissenschaften und Rohstoffe) and NORSAR.

In conclusion: during 1990 and the first few months of 1991, a seismic observatory was established at Bochum for the GERESS array. Since April 1990, the GERESS project team at Bochum archives GERESS data continuously; since June 1990, a detector is on-line; since October 1990, a fk-analysis routine is on-line and data are automatically archived. A powerful off-line analysis package is available: for the test-week of 26.11.-2.12. 1990 (GSETT-2, phase-3), 218 events were located by the GERESS project team in Bochum. Since January 1991, an automatic location routine is in operation; since February 1991, scientists can remotely access the results of the Bochum on-line processing via X25 (WIN); since March 1991, a stable, powerful acquisition workstation is on-line freeing scientific personnel from unnecessary routine work. For April, the first routine bulletin for GERESS is in preparation.

Michael L. Jost

### Appendix 3-1: Chronological Status List

- Jan. 1990: Data acquisition software and hardware by SCIENCE HORIZONS was analyzed. Preparation of data transfer to BGR. Visit of BGR for analyzing GERESS data with a frequency-wavenumber transformation algorithm. Implementation of the fk-analysis module of the XAP (experimental array processor) software package. Various fk-analyses of data from the GERESS TEST array.
- Feb. 1990: GERESS sites on-line: 8. On Feb 7, first successful run of on-line data acquisition, first data archival tape on acquisition workstation. First off-line data analysis using VISTA (SCIENCE HORIZONS). Visit of technicians from SCIENCE HORIZONS from 26.-28.: hardware change, new operating system and acquisition software installed. Training on the new software release.
- Mar. 1990: GERESS sites on-line: 9. Documentation of acquisition start without losing data. Test of data segmenter successful (data segments have to be sufficiently short to be suitable for the fk-analysis module of XAP). Transformation of GERESS data to XAP data format, and adaptation of XAP's fk-analysis module. Various fk-analyses of data from the GERESS array. Acquisition system crashed due to a blown fuse. Reinstallation of system and data acquisition software. Software development of an automatic tape archiver. Installation of X11 window system on data acquisition machine (For X11, at least 8 MB were required in core. Acquisition workstation has 16 MB in core, the only other available workstation (SUN 3/50) had 4 MB in core where a memory upgrade failed). Visit of J. Fyen (NORSAR). Installation of NORSAR software on data acquisition workstation since X11 was installed there. Acquisition workstation has severe problems staying on-line when running the NORSAR detector together with the data acquisition. Furthermore, a standard fk-analysis took more than 10 minutes.
- Apr. 1990: GERESS sites on-line: 14. Start of routine data archival. Analysis and documentation of EXABYTE problems: It is not possible to archive data on acquisition workstation unattended. Therefore, the previously developed automatic tape archiver is obsolete. Development and documentation of manual data archival procedure: Due to a malfunction on SCIENCE HORIZONS data acquisition workstation, every day (including weekends and holidays) an operator had to be present for at least one hour (very often 2) to archive data manually. SCIENCE HORIZONS promised a solution to this hardware problem. Implementation of reviewed on-line data acquisition software from SCIENCE HORIZONS.

May 1990: GERESS sites on-line: 16. Work with NORSAR package. Due to space problems on disk (for manual data archiving, disk space is needed for at least 24 hours of CSS-2.8 data), NOKSAR software and X11 window system removed from disk. Future date on data, restart of data acquisition documented which included a reinstallation of diskloop. Visit of M. L. Jost to NORSAR (training on NORSAR software, i.e., on-line detector, fk-analyzer, and locating routine RONAPP). SCIENCE HORIZONS postponed the promised solution to the EXABYTE problem.

June 1990: GERESS sites on-line: 20. Reinstallation of X11 and NORSAR software on acquisition workstation. Installation of STA/LTA on-line detector. Detector ran only with very few beams due to overload problems on acquisition workstation. Other packages such as on-line fk or RONAPP were not implemented due to overload problems on data acquisition workstation. Installation of a new on-line acquisition software release (structure of disk-loop changed). SCIENCE HORIZONS again postponed the solution to the EXABYTE problem.

July 1990: GERESS sites on-line: 23. Visit by J. Fyen (NORSAR). First compilation of detector software at Bochum. Restructuring disk space on acquisition workstation. Status of acquisition workstation changed: machine runs as root to allow using all possible disk space (24 hours of CSS data needed to be held on disk due to the inability of the acquisition workstation to archive data). SCIENCE HORIZONS again postponed the solution to the EXABYTE problem. Test of detector. Preparation of computer purchase. Computer ordered by university administration.

Aug. 1990: All 25 GERESS sites on-line. However C2B is sampled at 40 Hz instead of 120 Hz. Synchronization errors between traces reported. Visit of E. Herrin and P. Golden (SMU). August 22 marks the first time that all stations of GERESS (in their proper configuration) were on-line for 15 minutes. SCIENCE HORIZONS again postponed the solution to the EXABYTE problem.

Sep. 1990: Since SCIENCE HORIZONS did not deliver the promised solution to the EXABYTE problem, Bochum's system engineer disassembled the acquisition workstation to take out the EXABYTES and connect them to a workstation of the department. Data transfer via ethernet turned out to be stable. However, a workstation (3/50) of the department dedicated to other projects became fully occupied with data archiving and array monitoring.

Oct. 1990: An automatic array downtime routine was developed and implemented. Development and implementation of an automatic tape

archival routine. Installation of a SUN 4/330 server (96 MB in core, 6 GB disks), 4/65 SPARC station (40 MB in core), and two 4/20 (8 MB in core): Formatting additional disks and installation of kernel patches. Optimization of system kernels. Integration of acquisition workstation SUN 3E and monitoring workstation SUN 3/50 into the ethernet of the SUN 4s. Installation of system software (X11 window system, FORTRAN compiler version 1.3.1). Installation of NORSAR software and recompilation.

Nov. 1990: Compilation of NORSAR software on SPARC systems. Problem: library modules compiled with different FORTRAN compiler versions are incompatible. Installation of MATLAB software package on SPARC server. Installation of on-line detector and on-line fk-analyzer on SPARC server. Training of GERESS project team on NORSAR software. A module correcting for instrument responses was developed and included into the NORSAR package. Extensive GERESS data analysis in connection with the GSETT-2, phase 3:

Dec. 1990: Extensive GERESS data analysis in connection with the GSETT-2, phase 3. Upgrading the automatic data archiver (about 7 days of data can be archived without manual interference). Implementation of remote (using a PC and a modem) status testing and problem solving of data acquisition. Installing another FORTRAN compiler version (1.2). Testing RONAPP (automatic location routine of the NORSAR package).

Jan. 1991: Disk reformatting on acquisition workstation after frequent crashes due to disk failures. Due to those crashes, station uptime below 80 %. Complete recompilation of the NORSAR software and implementation of RONAPP (automatic location routine).

Feb. 1991: Frequent crashes of acquisition workstation reappeared. Station uptime at 81 %. Visit by technician of SCIENCE HORIZONS and installation of replacement of the acquisition system at Bochum (CIM with SCSI; workstation: SUN 4/65 with 40 MB in core and 1.3 GB disk; 4 EXABYTE drives). Customizing acquisition software. Adaptation of data spooler and automatic data archiving routine. Correction of calculation of ML magnitudes in RONAPP. Development of an on-line processing display manager.

Mar. 1991: The new acquisition system at Bochum turned out to be very stable. Uptime reached 96 %. Customizing acquisition software and debugging in cooperation with SCIENCE HORIZONS. Cooperation with NORSAR on further adaptation and debugging RONAPP. Evaluation of Vogtland (Germany) earthquake swarm. Upgrading the on-line processing display manager.

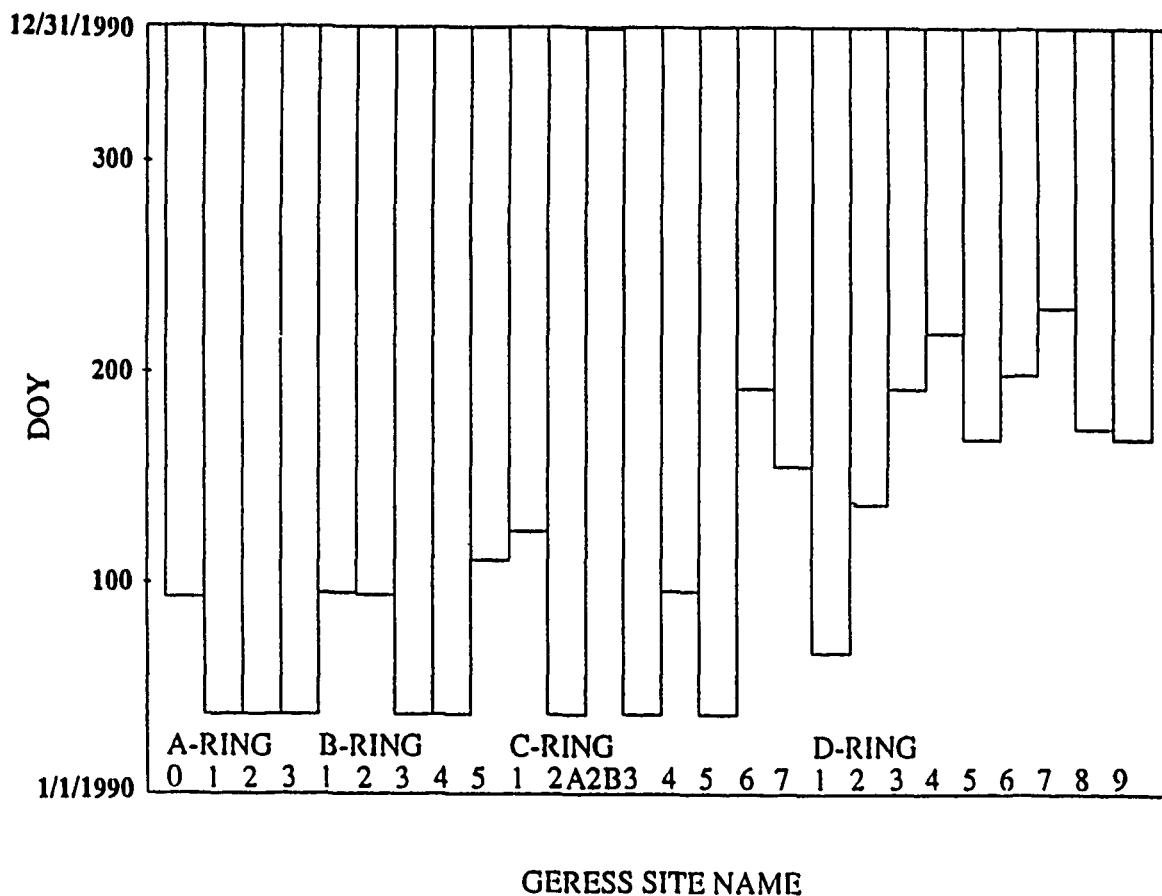
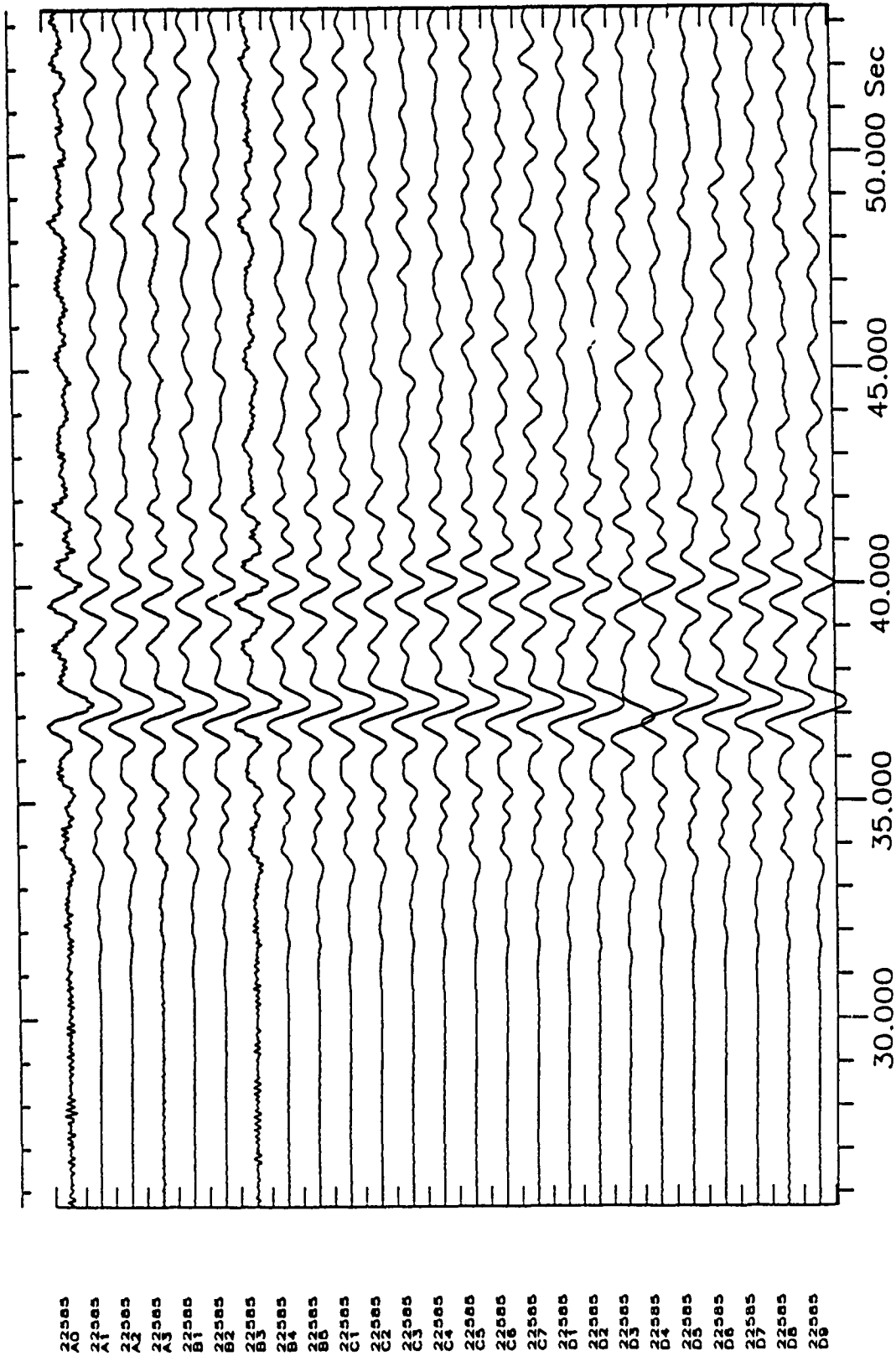


Figure 3-1: Startup of GERESS SITES. Time increases in days of year from bottom (Jan. 1, 1990) to top (Dec. 31, 1990).



1991-067:11.47.00.000 GER.sz

Figure 3-2: Onset of a teleseismic event (Mar. 8, 1991, 11:36:31.0, 60.8 N, 167.1 E, 33 km,  $m_b = 6.3$ ,  $M_s = 6.7$ , E. Siberia). Note the desynchronization on D3.







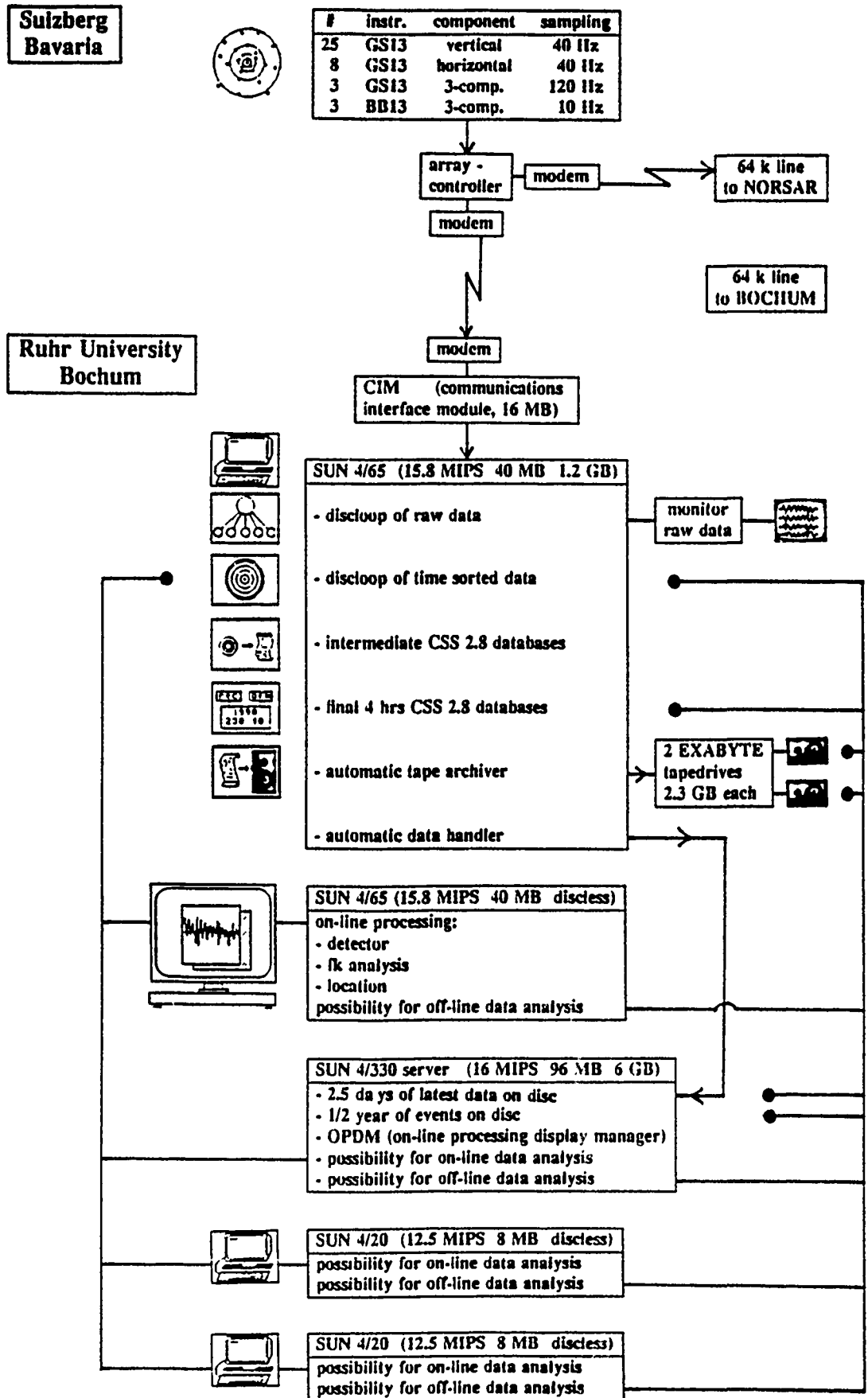


Figure 3-5: Bochum station hardware and data-flow.

#### 4. THE BOCHUM ON-LINE PROCESSING DISPLAY MANAGER

The Department of Geophysics of Ruhr-University Bochum operates an experimental on-line processing system for GERESS data. This system uses software developed at NORSAR and modified at Bochum. The on-line processing consists of 3 steps: detection, fk-analysis, and location. Consequently 3 consecutive lists exist for each day. The purpose of the ON-LINE PROCESSING DISPLAY MANAGER is to make these three lists available for interested scientists.

The GERESS data are transmitted to Bochum via a 64 kbit land-link. The acquisition processing results in CSS-2.8 databases used for archiving. For the seismological on-line processing, the circular buffer of 24 bit time sorted real-time data is used.

The first stage of the on-line processing accesses data in 30 second segments and runs a STA/LTA detector. The detector presently recognizes an onset if the STA/LTA ratio for a filtered trial-beam exceeds a threshold of 4. The present beam set for the detector is given in option *deti* of the display manager. As a result of the detection processing, a daily list is updated to present a detection beam identifier, day of year, detection time, values for STA, LTA, and the STA/LTA ratio. This list is displayed in option *det* of the display manager.

The next step of the on-line processing is the transformation of a 3 second filtered data segment at each onset time (derived from the detection time) into the frequency-wavenumber domain. As a result, the slowness and back-azimuth of the phase is determined. From the slowness information, seismic phases are identified. Consequently, the daily list of the fk processing includes an identification number, day of year, onset time of the phase, time difference between onset time and detection time, a beam identifier, signal noise ratio (i.e., the STA/LTA ratio), phase velocity in km/sec, a phase identifier, back-azimuth in degrees from north, and a coherency value describing the quality of the fk-result (1.0 being excellent, 0.0 being very poor). These lists are available in option *fk* of the display manager.

The final step of the on-line data processing is the location of events. The seismic phases as identified in the fk-analysis are associated to events in this step. From the arrival time difference of regional phases, the distance to the epicenter can be determined from standard travel time tables. Together with a mean back-azimuth, the epicenter locations of local and regional events are determined. Only these epicenter locations are displayed in the third list: after a line specifying the Flinn Engdahl region, the next line shows origin time, latitude and longitude, ML magnitude, epicentral distance in km, back-azimuth in degrees, and depth in km, where "F" means that the depth was fixed in the location algorithm. These automatically calculated epicenter locations are displayed in option *epi* and some location statistics are available under option *err* of the display manager.

After describing the processing stages, the term "on-line processing" needs some specification. All processing is done on hardware that has the ability to perform the processing much faster than real-time. The detector accesses real-time data. After it catches up to real-time, it stops for 5 minutes and restarts again. The same procedure holds for the fk-analysis and the location routine, where the sleep-times are 3 minutes, however. Generally, the results of the detector and fk-analysis should be available 10 minutes after real-time.

Waveforms of the raw data can be displayed using a TEKTRONIX terminal emulation (option *plot* of the display manager).

The caveat of using results of the ON-LINE PROCESSING DISPLAY MANAGER are obvious: Results of the on-line processing system, e.g. the locations, are calculated completely automatic and have NOT been reviewed by an analyst (Reviewed epicenter locations will be available shortly under option *loc*). Algorithms of the processing (e.g., beam set and filters in the detector, phase association rules) have changed with time. The implemented on-line processing system is experimental and the quality of results varies. The option *down* of the display manager informs about array downtimes.

This ON-LINE PROCESSING DISPLAY MANAGER is subject to updates. An on-line information is available under option *info*. Option *mess* enables a one-line message to the system manager. For more extensive remarks, please contact Mike Jost at

TEL.: 49 234 - 700 3277

FAX: 49 234 700 2442

E-MAIL: c=de; a=dbp; p=ruhr-uni-bochum; ou=geophysik; s=jost

In Appendix 4-1, a brief sample session is given.

Michael L. Jost

# Appendix 4-1: Sample Session

login via x25 (WIN) # 45050310818

login >>> gress

passwd >>> bochum

TODAYs DATE: 91083

Commands:	det	detection lists	deti	info on current detector
	fk	fk lists	down	info on array downtimes
	epi	unreviewed location lists	err	info on location errors
	loc	reviewed location lists	doy	info on days in year
	plot	TEKTRONIX plot module	info	info on display manager
	exit	logout, end session	mess	message to manager

Enter command>det

Commands: <CR> next screen, continue

q abort, stop

Detection lists available since : 90150

ENTER DATE in the format: yyddd (yy = year; ddd = day of year) >>>91083

BEAM	DOY:DETECTION	TIME	STA	LTA
GF777	083:00.11.38.6 - 11.39.1	241.47	48.83	4.946
GF104	083:01.28.29.8 - 28.30.8	54.83	10.43	5.256
GF103	083:03.10.01.1 - 10.03.1	127.83	10.95	11.668
GF103	083:03.10.12.1 - 10.12.8	86.94	19.17	4.534
GRP	083:03.13.34.6 - 13.42.8	474.74	10.37	45.774
GF619	083:03.13.35.6 - 13.41.1	474.74	10.37	45.774
GF621	083:03.13.40.8 - 13.44.1	74.79	13.35	5.604
GRP	083:03.14.02.8 - 14.08.8	181.26	18.07	10.029
GF612	083:03.14.03.6 - 14.08.1	181.26	18.07	10.029
GF999	083:03.43.49.6 - 43.51.6	94.98	20.17	4.710
GF619	083:04.34.00.8 - 34.02.3	67.30	9.10	7.393
GF888	083:05.05.30.3 - 05.34.1	304.60	45.83	6.646
GF724	083:05.05.36.6 - 05.46.3	716.31	10.33	69.373
GRP	083:05.05.36.6 - 05.50.3	716.31	10.33	69.373
GF713	083:05.05.45.8 - 05.49.8	331.88	50.94	6.515
GF777	083:05.05.50.8 - 05.51.8	1023.89	203.50	5.031
GRP	083:05.06.00.7 - 06.08.1	855.09	32.43	26.365
GF106	083:05.06.00.8 - 06.06.6	855.09	32.43	26.365
GF104	083:05.06.07.3 - 06.08.8	395.64	60.12	6.581
GF724	083:05.35.53.6 - 36.00.8	131.91	10.56	12.492
GF623	083:05.36.00.6 - 36.01.6	73.97	15.85	4.668
GRP	083:05.36.16.2 - 36.23.1	187.25	13.10	14.290
GF608	083:05.36.16.6 - 36.22.3	187.25	13.10	14.290
GVI1	083:06.21.30.7 - 21.32.7	380.06	53.52	7.101

q

Commands:	det	detection lists	deti	info on current detector
	fk	fk lists	down	info on array downtimes
	epi	unreviewed location lists	err	info on location errors
	loc	reviewed location lists	doy	info on days in year
	plot	TEKTRONIX plot module	info	info on display manager
	exit	logout, end session	mess	message to manager

Enter command>fk

Commands: <CR> next screen, continue

q abort, stop

FK lists available since : 90311

ENTER DATE in the format: yyddd (yy = year; ddd = day of year) >>>91083

#	DOY	T <sub>on</sub>	T <sub>on</sub> -T <sub>d</sub>	BEAM	SNR	VEL	PHASE	BAZ	COH
1427	083:00.11.38.406	0.19	GF777	4.9	1.9	nois	46.9	0.08	
1428	083:01.28.28.500	1.30	GF104	5.3	21.5	P	56.3	0.28	
1429	083:03.09.59.925	1.18	GF103	11.7	40.8	P	94.3	0.71	
1430	083:03.10.10.475	1.62	GF103	4.5	70.2	P	344.5	0.52	
1431	083:03.13.34.413	1.19	GF619	45.8	6.6	PG	185.7	0.17	
1432	083:03.13.40.538	0.26	GF621	5.6	2.0	nois	38.8	0.08	
1433	083:03.14.01.850	1.75	GF612	10.0	3.9	LG	182.1	0.33	
1434	083:03.43.47.673	1.93	GF999	4.7	30.0	P	214.3	0.79	
1435	083:04.34.00.463	0.34	GF619	7.4	3.2	RG	63.2	0.08	
1436	083:05.05.30.131	0.17	GF888	6.6	3.4	RG	21.3	0.08	
1437	083:05.05.35.862	0.74	GF724	69.4	9.1	PN	325.0	0.21	
1438	083:05.05.45.538	0.26	GF713	6.5	6.7	PG	327.0	0.07	
1439	083:05.05.50.631	0.17	GF777	5.0	2.0	nois	228.2	0.09	
1440	083:05.05.59.450	1.35	GF106	26.4	3.9	LG	324.7	0.48	
1441	083:05.06.06.775	0.52	GF104	6.6	4.2	LG	317.5	0.27	
1442	083:05.35.52.588	1.01	GF724	12.5	8.2	PN	314.6	0.11	
1443	083:05.36.00.338	0.26	GF623	4.7	6.7	PG	329.3	0.07	
1444	083:05.36.14.800	1.80	GF608	14.3	4.0	LG	323.7	0.35	
1445	083:06.21.30.175	0.52	GVI1	7.1	11.4	P	33.0	0.18	

q

Commands:	det	detection lists	deti	info on current detector
	fk	fk lists	down	info on array downtimes
	epi	unreviewed location lists	err	info on location errors
	loc	reviewed location lists	doy	info on days in year
	plot	TEKTRONIX plot module	info	info on display manager
	exit	logout, end session	mess	message to manager

Enter command>epd

Commands: <CR> next screen, continue      q abort, stop

Unreviewed location lists available since : 91021

ENTER DATE in the format: yyddd (yy = year; ddd = day of year) >>>91083

	DOY	OT	HYP	Fl-Eng	REGION	ML	D[km]	BAZ	DP
8000			EPX	LAT	LONG				
			HYP	546	AUSTRIA				
8000	083:03.12.58.8		EPX	46.866	13.485	1.40	220.5	184.3	0F
8010			HYP	543	GERMANY				
8010	083:05.05.11.2		EPX	50.124	12.333	1.84	173.1	325.7	0F
8020			HYP	543	GERMANY				
8020	083:05.35.26.9		EPX	50.072	12.305	1.27	169.6	324.0	0F

q

Commands:	det	detection lists	deti	info on current detector
	fk	fk lists	down	info on array downtimes
	epi	unreviewed location lists	err	info on location errors
	loc	reviewed location lists	doy	info on days in year
	plot	TEKTRONIX plot module	info	info on display manager
	exit	logout, end session	mess	message to manager

Enter command>plot

YOUR SCREEN SHOULD BE IN TEKTRONIX MODE NOW

EXIT PLOT ROUTINE	(0)
Display map of GERESS stations	(1)
Plot waveforms of the 25 vertical channels	40 Hz (2)
Plot waveforms of the four 3-component stations	40 Hz (3)
Plot waveforms of the high frequency channels	120 Hz (4)
Plot waveforms of the broad-band channels	10 Hz (5)
Plot waveforms of the 3 verticals at C2	120,40,10 Hz (6)

Enter option>2

ENTER DATE yyddd (yy=year;ddd=day of year) [0] >>>91083  
 ENTER HOUR hh (hh = hour) [0] >>>05  
 ENTER MINUTE mm (mm = minute) [0] >>>05  
 ENTER SECOND ss (ss = second) [0] >>>32  
 ENTER DURATION ssss (ssss second) [0] >>>60  
 ENTER DECIMATION dd (plot every dd-th point) [0] >>>1  
 ENTER AMPLIFICATION a.a (largest amplitude = a.a cm)[0] >>>1.0  
 ENTER VIEWING DURATION sss (sss = seconds) [0] >>>20  
 Reading data of channel GEA0sz  
 Reading data of channel GED9sz

Here comes the plot

Commands:	det	detection lists	deti	info on current detector
	fk	fk lists	down	info on array downtimes
	epi	unreviewed location lists	err	info on location errors
	loc	reviewed location lists	doy	info on days in year
	plot	TEKTRONIX plot module	info	info on display manager
	exit	logout, end session	mess	message to manager

Enter command>exit



## **5. EVALUATION OF GERESS FOR PHASE 3 of GSETT-2**

**NOVEMBER 26 - DECEMBER 2, 1990**

### **5.1 Introduction**

In 1991, the Group of Scientific Experts (GSE) of the Conference of Disarmament in Geneva is planning a second Technical Test (GSETT-2) to contribute to the further elaboration of a modern seismic monitoring system.

The overall purposes of GSETT-2 are

- testing of methods and procedures developed by the GSE to expeditiously extract and transmit data from stations to experimental international data centers (EIDCs), to process these data at EIDCs, and to transmit the results back to the participants.

Prior to the main experiment which is scheduled for the time period April 22 - June 2, 1991 several preparatory tests were performed by the GSE. The final preparatory experiment testing all elements and procedures of the envisaged system took place from November 26 - December 2, 1990 and involved data exchange for 7 consecutive days. We took this occasion and fully analyzed GERESS data for the first time.

### **5.2 GERESS Data Analysis**

During this time period, the array uptime was 99.5 % but due to problems with the acquisition system in Bochum, 12 hours of data were lost on December 1. Therefore, the period of analysis covered only 92.1%.

In Bochum, an automatic on-line processing was implemented which included beamforming, detector, and f-k analysis.

Beams were computed for 30 degree azimuth intervals and 3 velocities (3.5 km/s, 7.0 km/s, and 11 km/s), and in addition for teleseismic events (999.9 km/s) and for air-coupled disturbances (0.3 km/s). The last beam was necessary to discriminate events which originated from practice firing at a tank training area which is located about 20 km NW of the array site.

At a STA/LTA ratio of 4, 1007 detections were triggered, 611 of which could be confirmed as seismic phases by inspection. On the other hand, the analysts found 201 additional seismic onsets by looking at the raw traces in a time window around the automatic detections. From these numbers, it seems to be justified to conclude that the false alarm rate as well as the missed event rate is about 40%.

The location process was performed interactively by reading each onset time and reanalyzing the f-k results in different frequency bands. In this way,

219 local and regional events were found comprising 621 seismic phases. Additionally 79 phases were associated with 43 teleseismic events by using PDE (weekly listing) and EIDC reports. In summary, only 112 phases (14%) were left unassociated.

At NORSAR, a completely automatic RONAPP analysis was carried out using the same GERESS data. With possibly different parameter setting, the detector triggered 1171 times (91 detections were found in the 12 hours data gap at Bochum), which is very similar to the number of detections in Bochum. But RONAPP located only 95 events, which is 40% of the events located interactively in Bochum.

The GRF broad-band array is located about 150 km north of GERESS, a comparison of the performance is interesting. The GRF detector found 107 phases which is only 10% of the GERESS detections. Since GRF has no location capabilities at regional distances, no epicenters were reported. But if these detections are associated in hindsight, GRF found 68 events which corresponds to one third of the GERESS events. A further analysis shows that GERESS is also superior to GRF in the teleseismic range where GRF found 9 events compared to 43 at GERESS.

In conclusion, this one week experiment already demonstrated that a teleseismic broad-band array like GRF is of limited value in the context of a CTB or low-yield treaty monitoring system.

Figure 5-1 summarizes the number of detections and locations for GERESS determined interactively (Bochum) and determined automatically (RONAPP) and the equivalent numbers for GRF. Figure 5-2 shows a map of all GERESS (Bochum) locations. Most of these events originate from quarry blasts within 200 km distance from the array. In addition, the earthquake sequence in Yugoslavia can be recognized and also the two mining areas in Poland are visible.

A further comparison of interactive and automatic locations for the GERESS data shows that there is not only a quantitative but also a qualitative difference. For that purpose, the common events are plotted separately in Figure 5-3 and Figure 5-4. In general, a larger scatter in the RONAPP locations is obvious. Moreover, some remarkable outliers on the RONAPP map were further investigated (event nos. 17, 18, 24, 50).

Figure 5-5 shows the waveform segment from one GERESS vertical channel for a Polish mining event (no. 17). A comparison between the RONAPP and interactive analysis yields that RONAPP misidentified a secondary phase as Sn instead of Sg. A similar misidentification happened for the second example which is shown in Figure 5-6 (no. 18). Again a secondary phase is labeled as Lg which is recognized as Sn by the analyst. A third example shows a Yugoslavian earthquake mislocated by RONAPP (Figure 5-7). This event (no. 24) is a mixed event where a second event for which no Pn-phase was found is associated as Lg by RONAPP to the first event. Similarly, the last example (Figure 5-8) shows a mixed event situation where a local quarry blast is interpreted as a regional event by RONAPP due to a very noisy situation which is typical for

midday time in this part of Europe.

In all cases the f-k analysis and consequently the azimuth determination is quite acceptable but the phase association and consequently the distance of the events is wrongly determined by the automatic processing.

These results should not be misinterpreted. Overall RONAPP performed amazingly well taking into account that no special tuning for the specific GERESS situation was undertaken. On the other hand, much work remains to be done to achieve satisfactory results for an automatic bulletin.

Finally a very preliminary comparison between the GERESS locations and those of international data centers was tried. Only a few larger events were located by data centers which are shown in Figure 5-9. In general, GERESS achieved excellent locations whereas the EIDC locations exhibit some scatter compared to PDE. An explanation might be the fact that PDE uses more routinely reporting stations than participated in the GSE experiment.

### 5.3 Conclusion

Regional arrays like GERESS can make significant contributions to a global seismic monitoring system in terms of lowering its worldwide detection threshold and yielding excellent locations even for small events at regional distances. In this way, the number of unassociated phases which are inherent in every network of single 3 component stations can drastically be reduced.

Nicolai Gestermann  
Hans-Peter Harjes  
Michael L. Jost  
Johannes Schweitzer

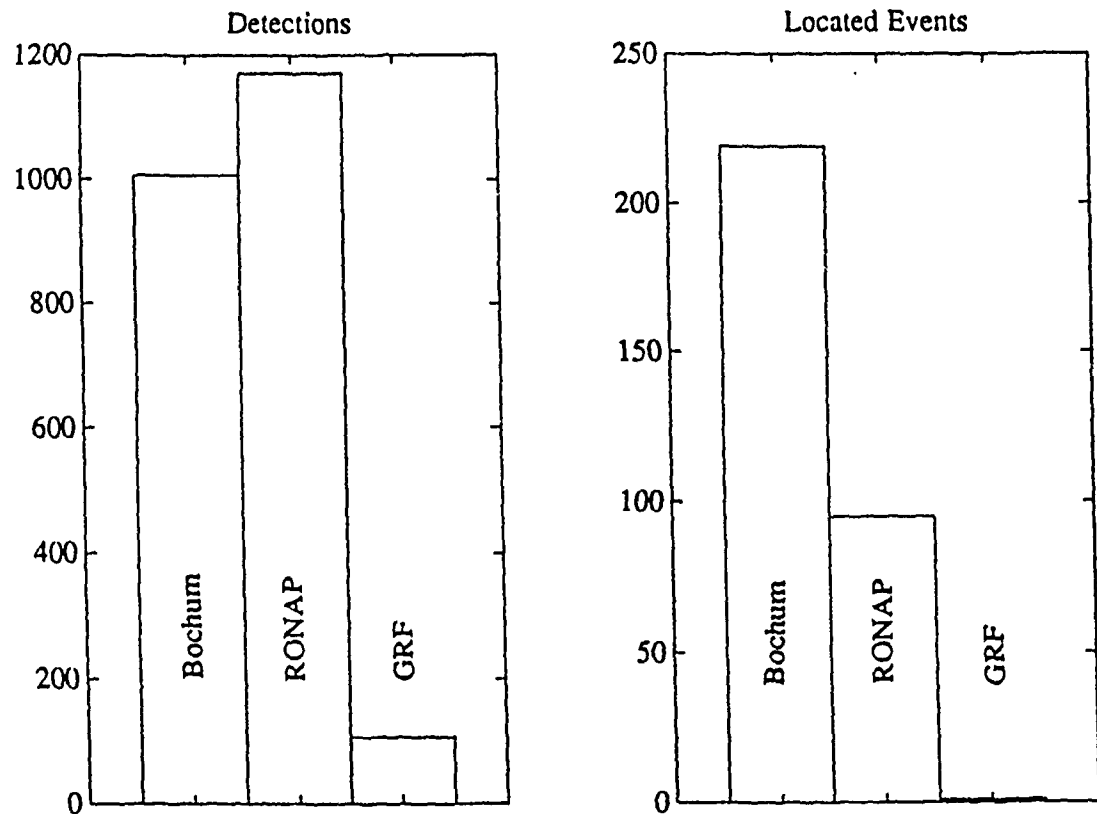


Figure 5-1: Number of detections and locations from GERESS (Bochum and RONAPP) and GRF array.

GERESS: Located Events Nov 26 - Dec 2 1990

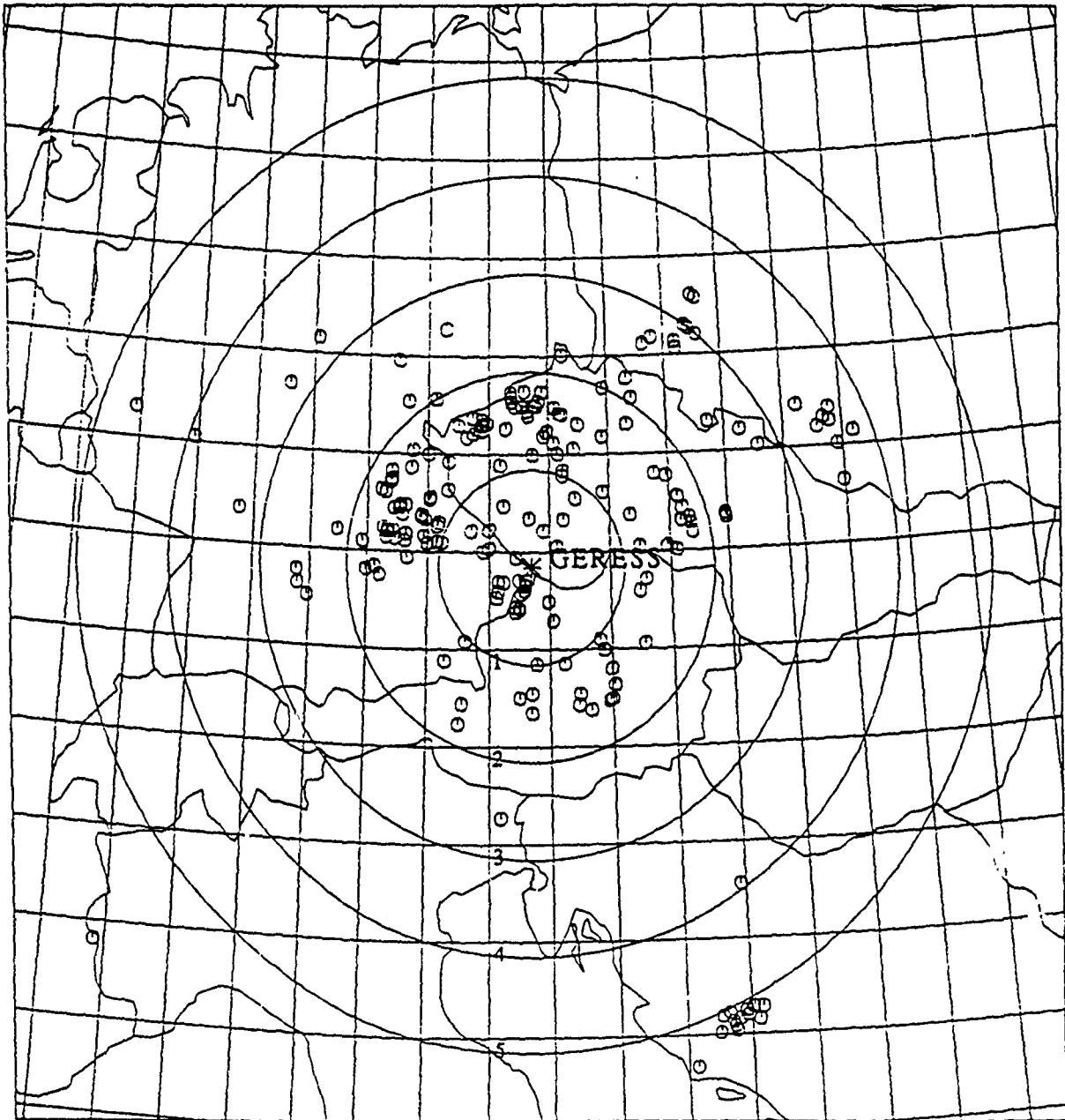


Figure 5-2: All events located by GERESS (Bochum) at regional distances.

# GERESS: Located Events (RONAP)

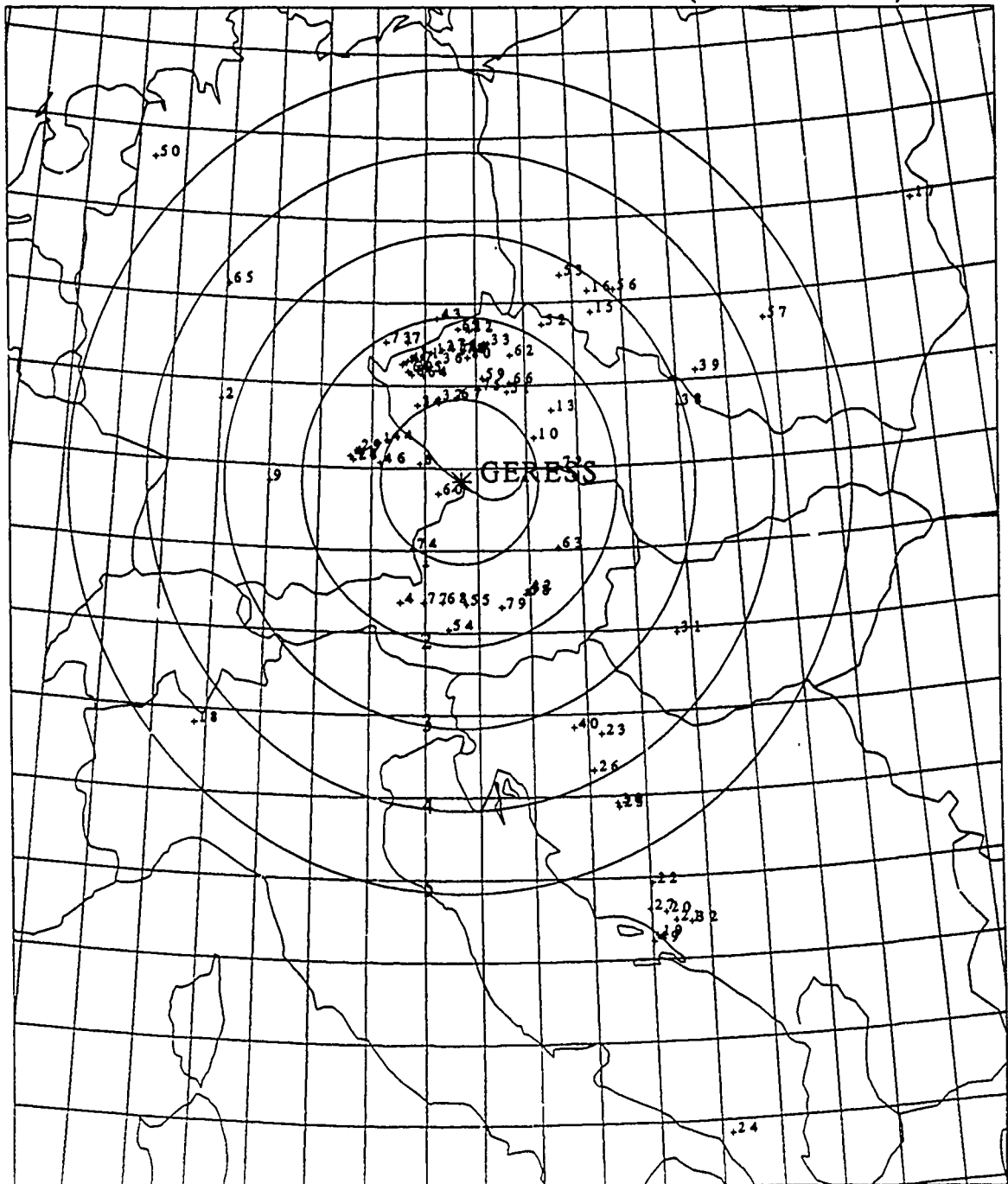


Figure 5-3: RONAPP-locations for events also found in Bochum.

# GERESS: Located Events (Bochum)

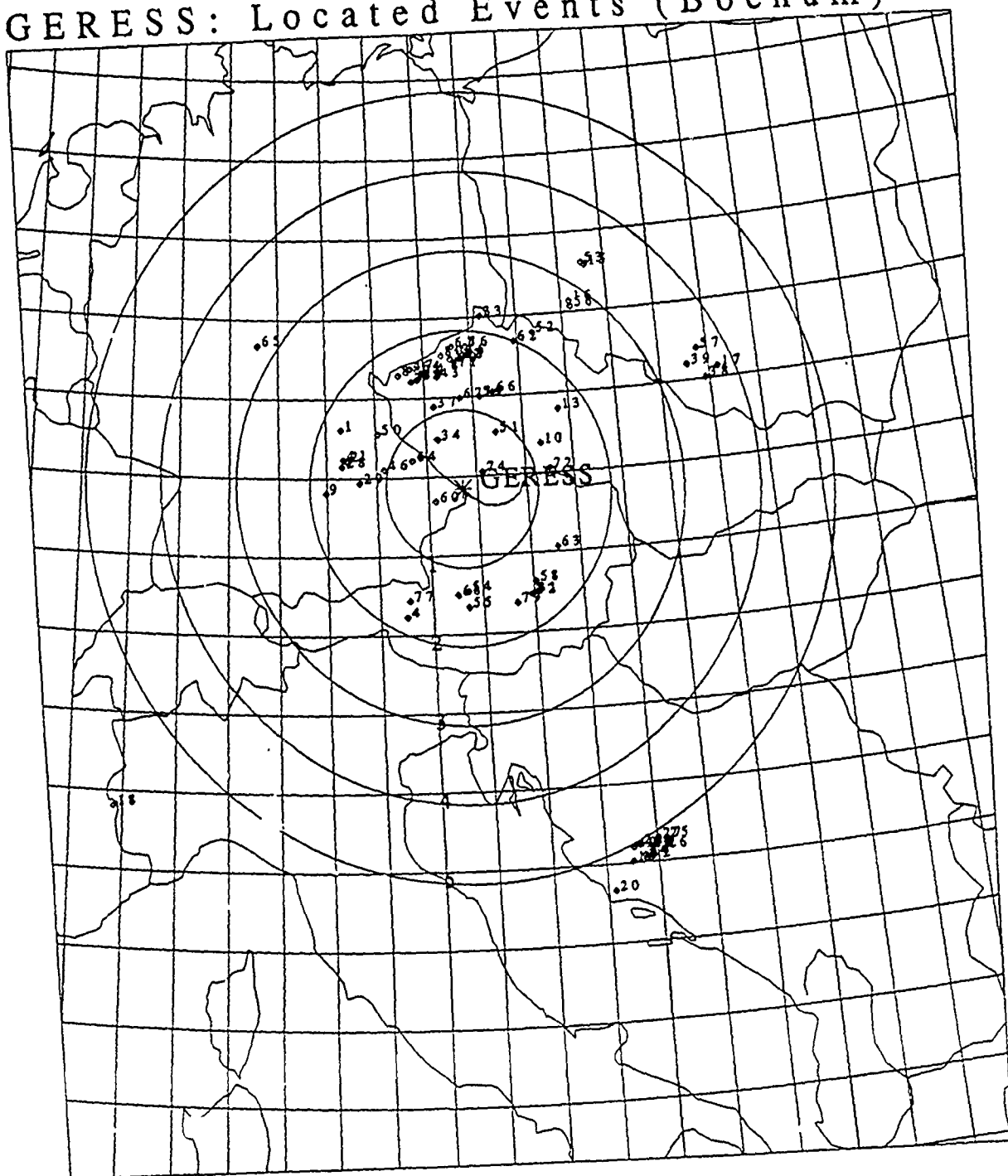
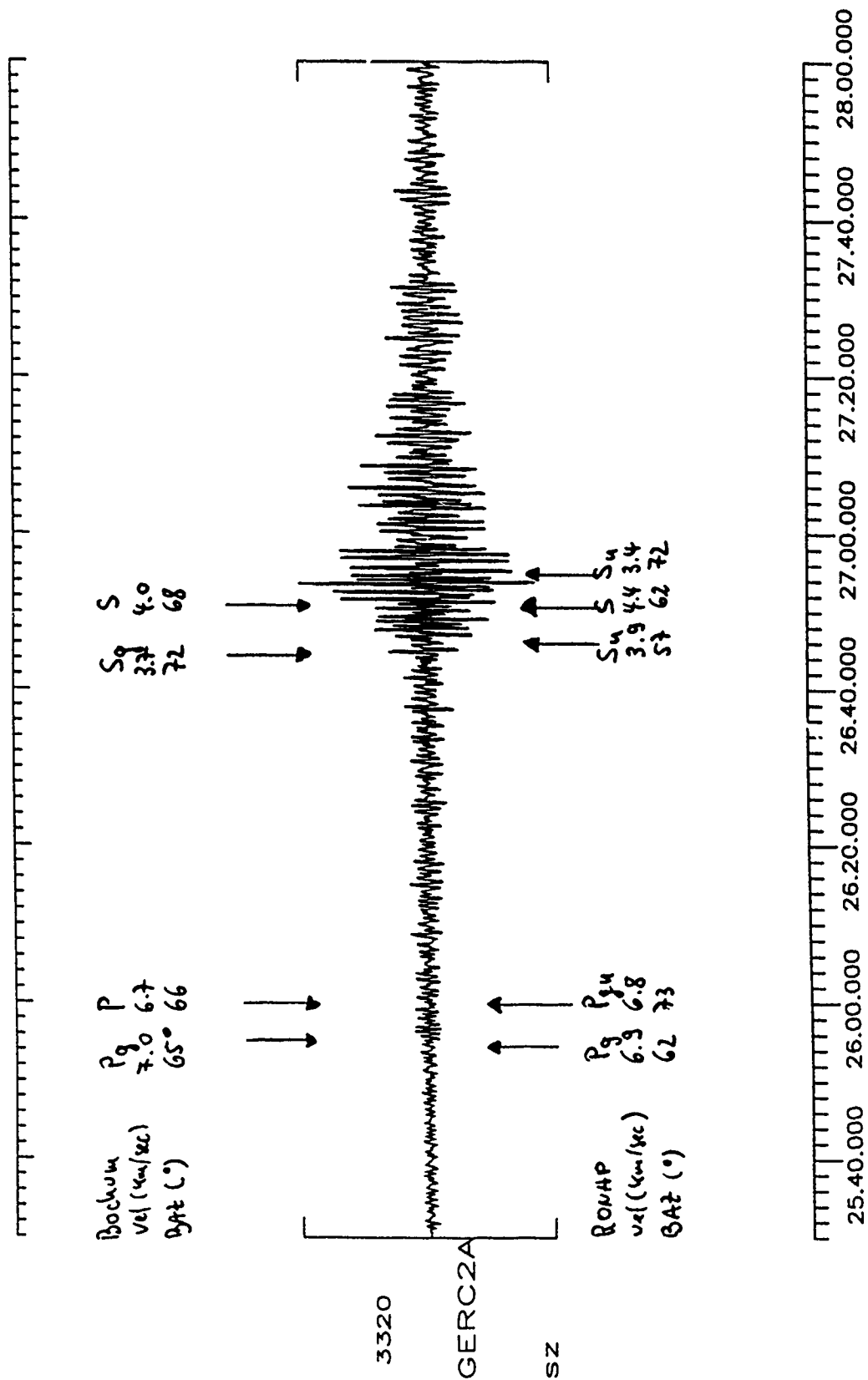


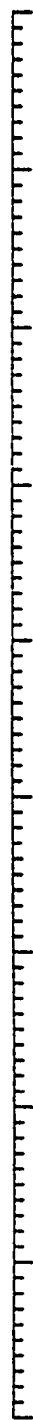
Figure 5-4: Bochum locations for events also found by RONAPP.



1990-331:01.25.30.000

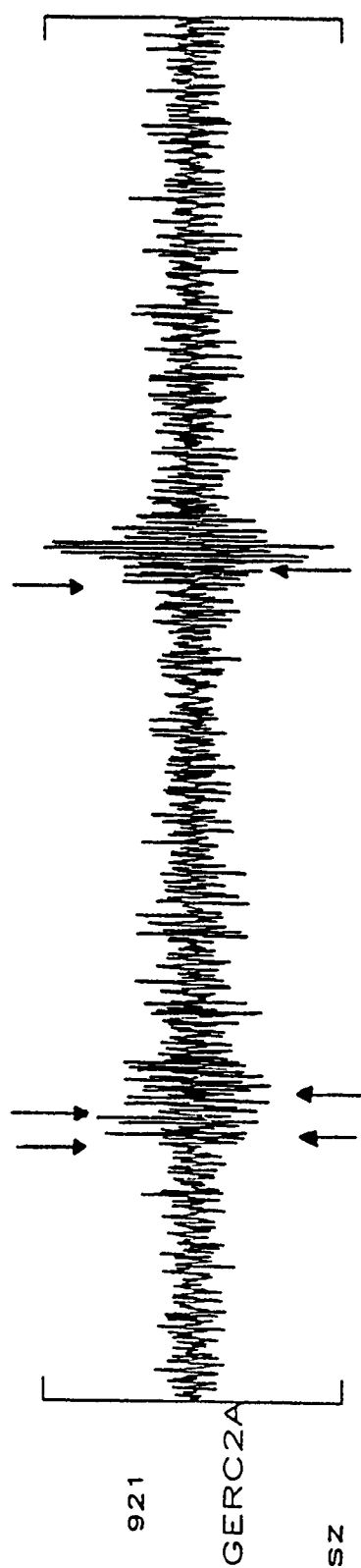
Figure 5-5: Waveform of event no. 17 (Upper Silesia) and phase identification by analysts (top) and RONAPP (bottom).





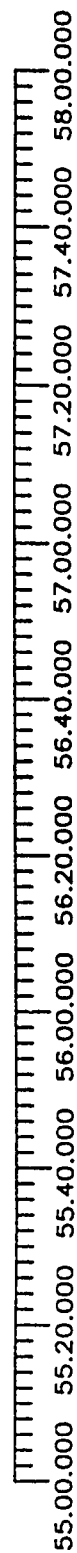
$S_u$   
 4.6  
 235

Backum  
 vel (km/sec)  
 BAT (°)  
 $P_u$   $P_u$   
 8.7 8.7  
 229 227



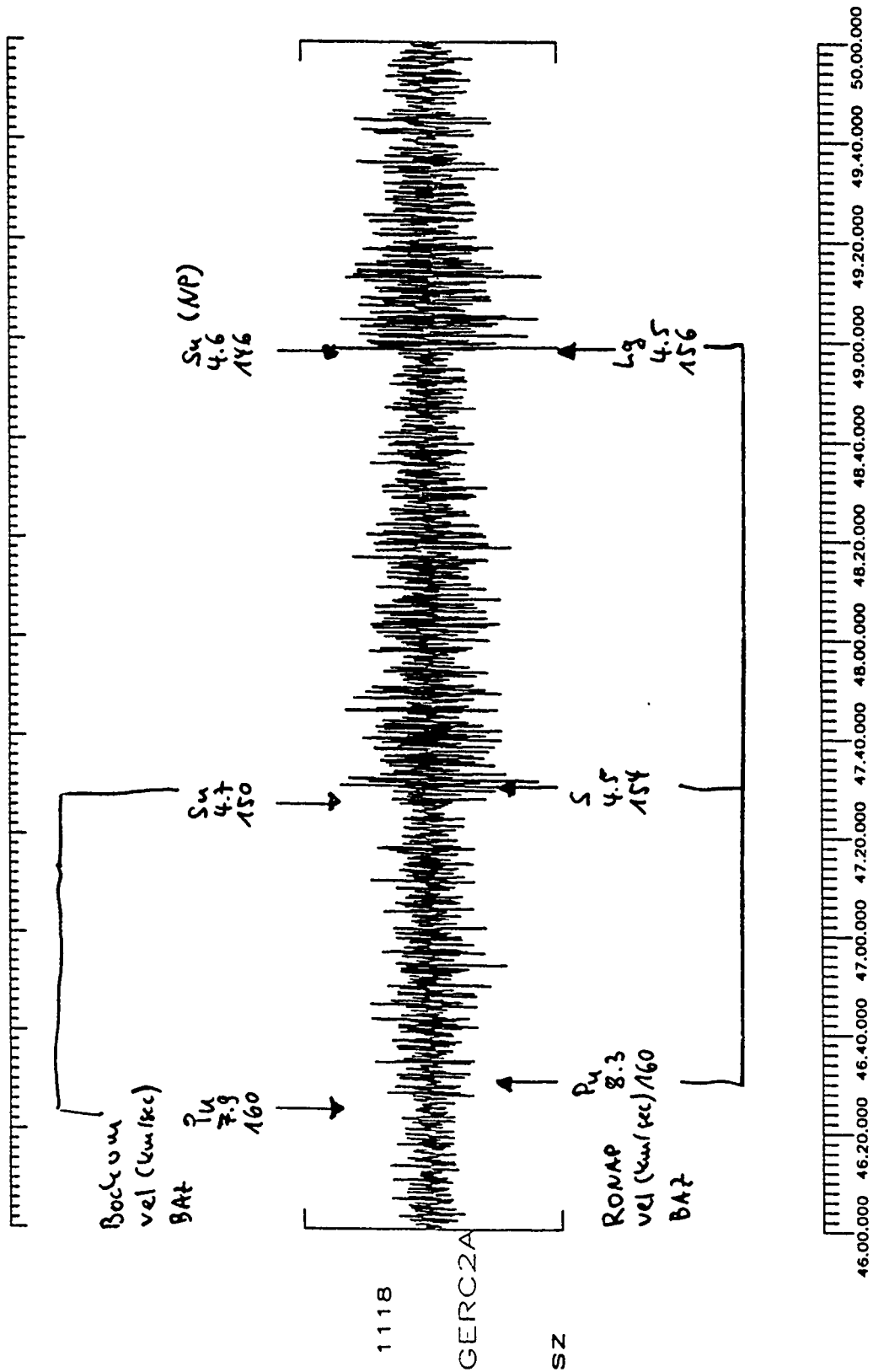
$L_g$   
 4.8  
 235

RONAP  
 vel (km/sec)  
 BAT (°)  
 $P_u$   $P_{gu}$   
 8.2 8.6  
 224 226



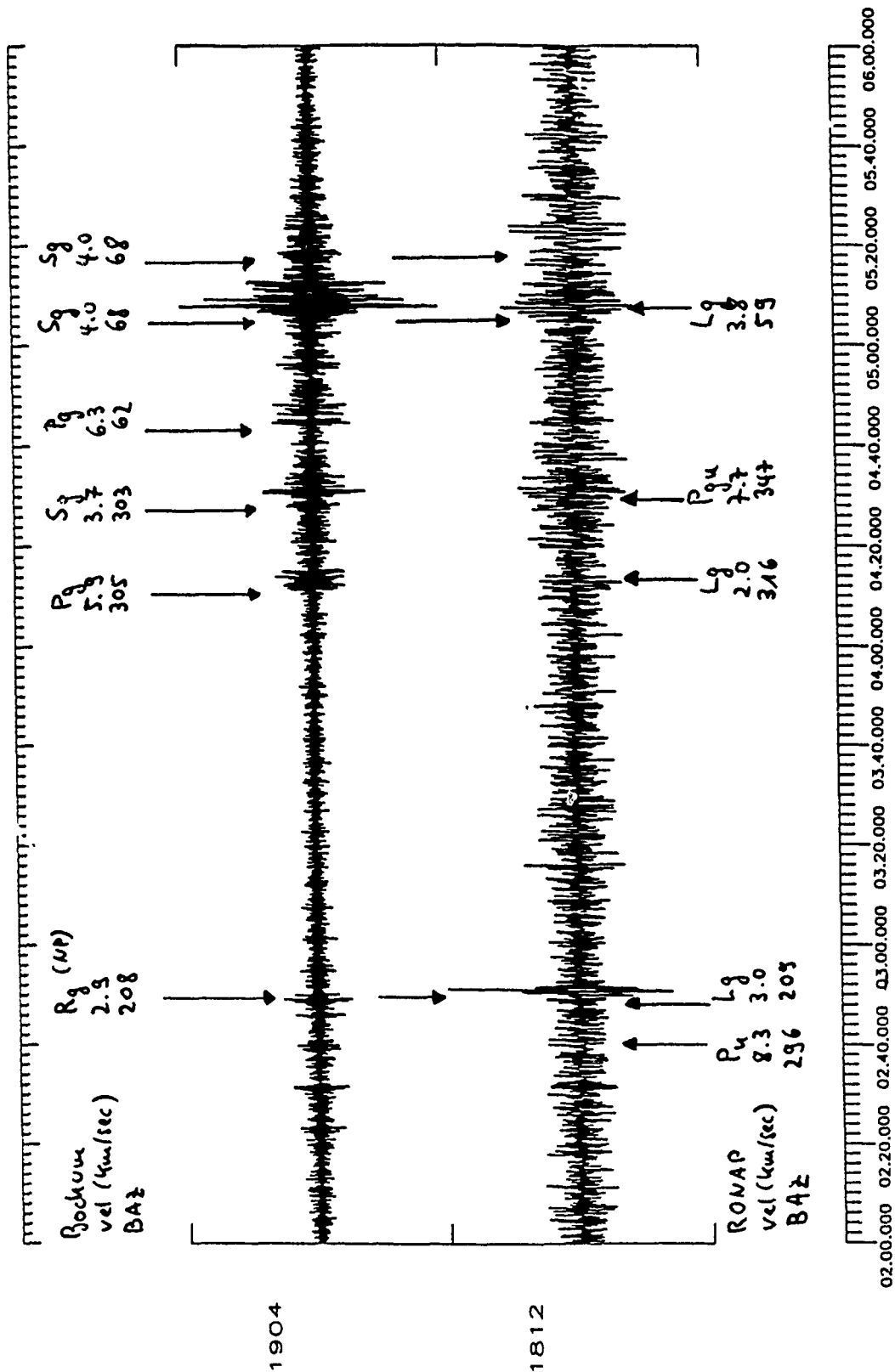
1990-331:01.55.00.000

Figure 5-6: Waveform of event no. 18 (Italian - French Border Region) and phase identification by analysts (top) and RONAPP (bottom).



1990-331:05.46.00.000

Figure 5-7: Waveform of event no. 24 (Yugoslavia) and phase identification by analysts (top) and RONAPP (bottom).



1990-332:13.02.00.000 GERC2A.SZ  
Figure 5-8: Waveform of event no 50 (local quarry) and phase identification by analysts (top) and RONAPP (bottom). Traces were filtered with a bandpass between 6 - 10 Hz (top) and 0.7 - 4 Hz (bottom).

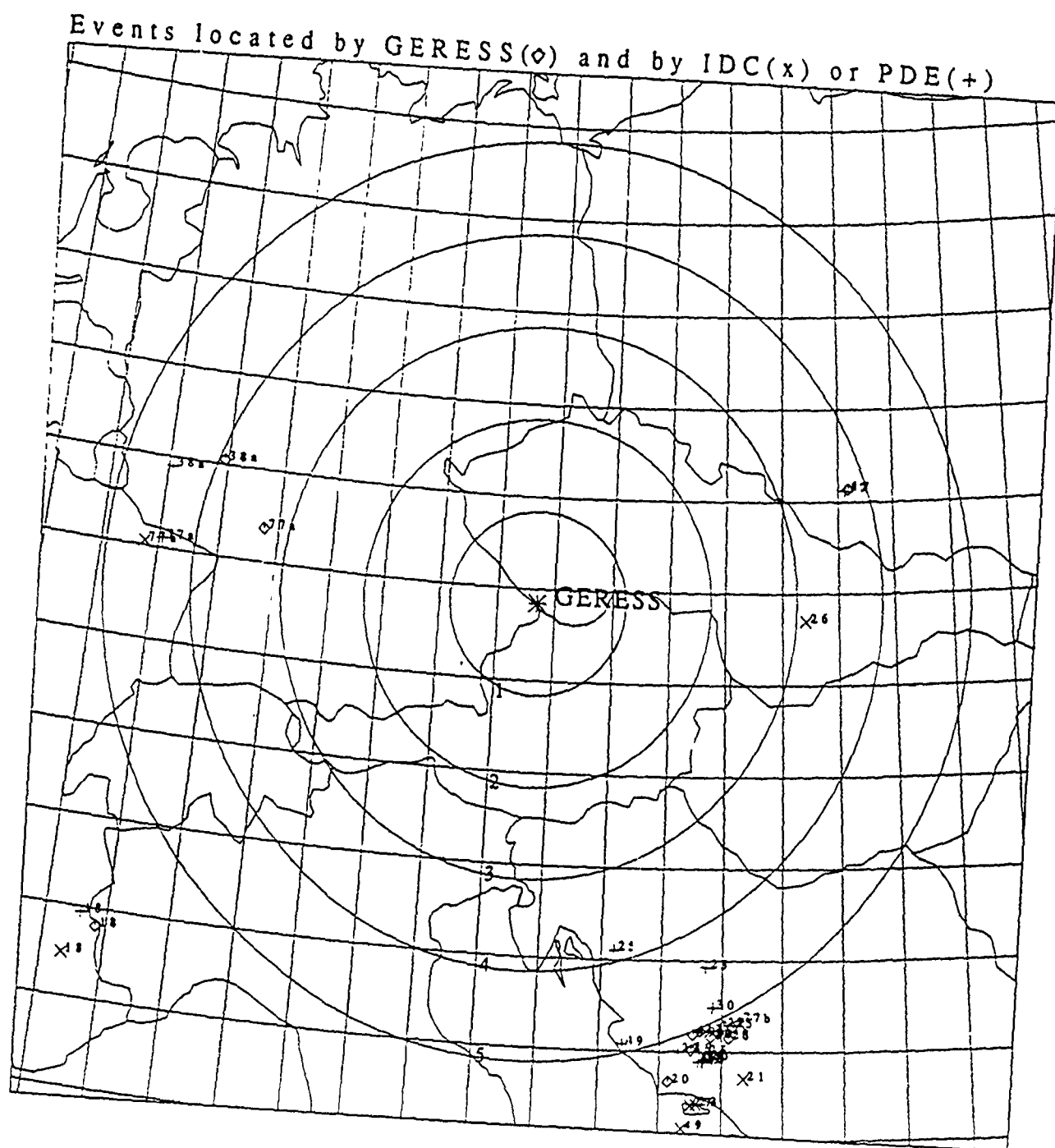


Figure 5-9: Common event locations from GERESS data (Bochum) compared to IDC- and PDE-epicenter determinations.

## 6. NUCLEAR TESTS OBSERVED WITH THE GERESS ARRAY IN 1990

### 6.1 INTRODUCTION

The GERESS array was planned and installed in southern Germany in 1990 for monitoring the local and regional seismicity in central Europe and surrounding areas. GERESS was planned as part of a four element array network in Europe, but it is also possible to locate local and regional earthquakes and explosions using GERESS exclusively. Additionally the low noise level (e.g. Harjes, 1990), especially in the frequency band lower than 2 Hz, results in good monitoring conditions for all teleseismic distances from the GERESS site. Although the aperture of the array is only about 4 km, it was possible to determine backazimuths (BAZ) and slownesses (P) for all teleseismic distances up to 160°. The uncertainty of these parameters could not be investigated, because the array is still (March 1991) not fully operational. The most important problem is, that the time base for the different channels is not stable i.e. some channels show unexpectable time drifts (plus and minus) of up to 1 sec. Though random, not recognizable time drifts affect all following slowness and backazimuth determinations. Nevertheless most of identified or presumed nuclear tests of 1990 could be observed and investigated:

Country	Test Site	Epicentral Distance	# of Tests	# of GERESS Registrations
China	(Nop Lor)	51.3°	2	1
France	(Mururoa)	145.4°	4	4
France	(Fangataufa)	145.6°	2	2
USA	(Nevada)	83.5°	8	4
USSR	(Novaya Zemlya)	30.4°	1	1

The differences between the total number of tests (17) and recorded events (12) is caused either by downtime of the GERESS acquisition system (2) or by tests, which were too small (3) to produce an observable signal at the GERESS site.

In the following I will describe all observations of presumed nuclear explosions by the different test sites. The data of all available GS13 vertical channels are shown either unfiltered or filtered with a third order butterworth bandpass from 0.5 Hz to 2.5 Hz. The general results of the analysis are listed in Tab. 6-1. Station GEC2 was used as reference for all investigations (fk-analysis and beam forming). All times, amplitudes, signal to noise ratios (SNR), and periods have been measured on the beam.

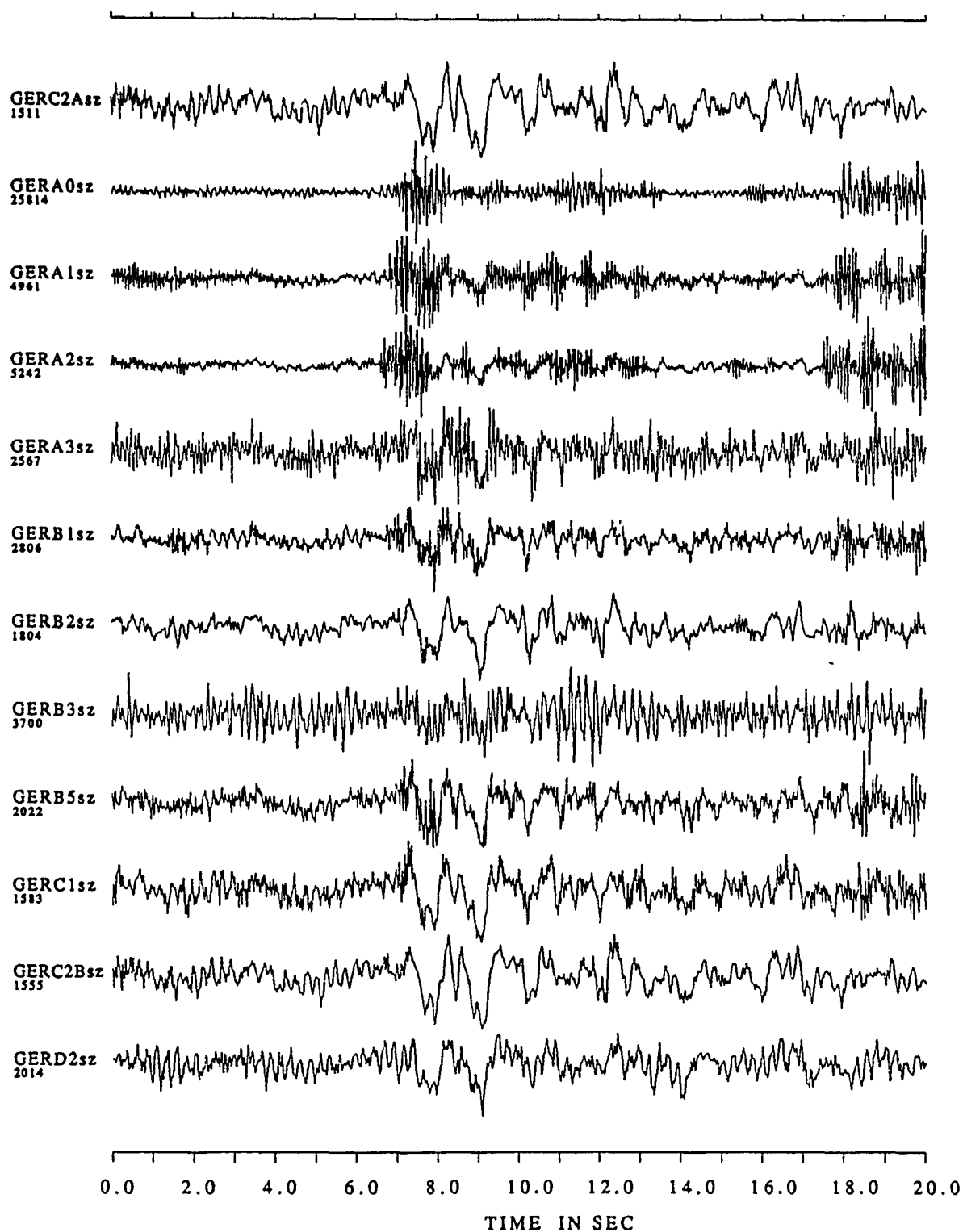
Tab. 6-1: Observed parameters of presumed nuclear tests recorded at GERESS in 1990.

Location	Date	Onset Time	Ampli. [nm]	Period [sec]	Time of Ampli.	SNR	$m_b$	BAZ [deg]	P [sec/deg]
Nop Lor	May 26	08:09:07.4	6.48	0.90	09:09.4	10.0	4.6	68.0	7.84
Mururoa	Jun 02	17:49:38.6	32.69	0.88	49:40.0	58.0		319.7	2.38
Mururoa	Jun 07	17:49:39.5	5.77	0.90	49:40.9	16.4		297.6	2.52
Nevada	Jun 13	16:12:29.8	57.52	1.11	12:32.8	93.5	5.7	325.3	2.98
Fangataufa	Jun 26	18:19:39.9	148.54	1.57	19:43.3	102.2		307.7	1.35
Mururoa	Jul 04	18:19:39.5	14.68	0.87	19:40.9	28.4		297.8	1.90
Nevada	Jul 25	15:12:30.5	4.38	0.99	12:31.8	8.3	4.7	327.5	2.87
Nevada	Oct 12	17:42:30.1	31.07	1.07	42:32.9	55.9	5.5	319.9	3.60
Novaya-Zemlya	Oct 24	15:04:14.0	85.87	1.12	04:18.3	90.3	5.5	29.2	9.02
Fangataufa	Nov 14	18:31:39.9	142.79	1.50	31:42.5	111.5		321.5	2.23
Nevada	Nov 14	19:29:29.9	22.53	0.97	29:31.8	59.1	5.4	329.1	4.58
Mururoa	Nov 21	17:19:39.6	64.65	0.81	19:41.0	89.8		320.2	1.63

## 6.2 NOP LOR

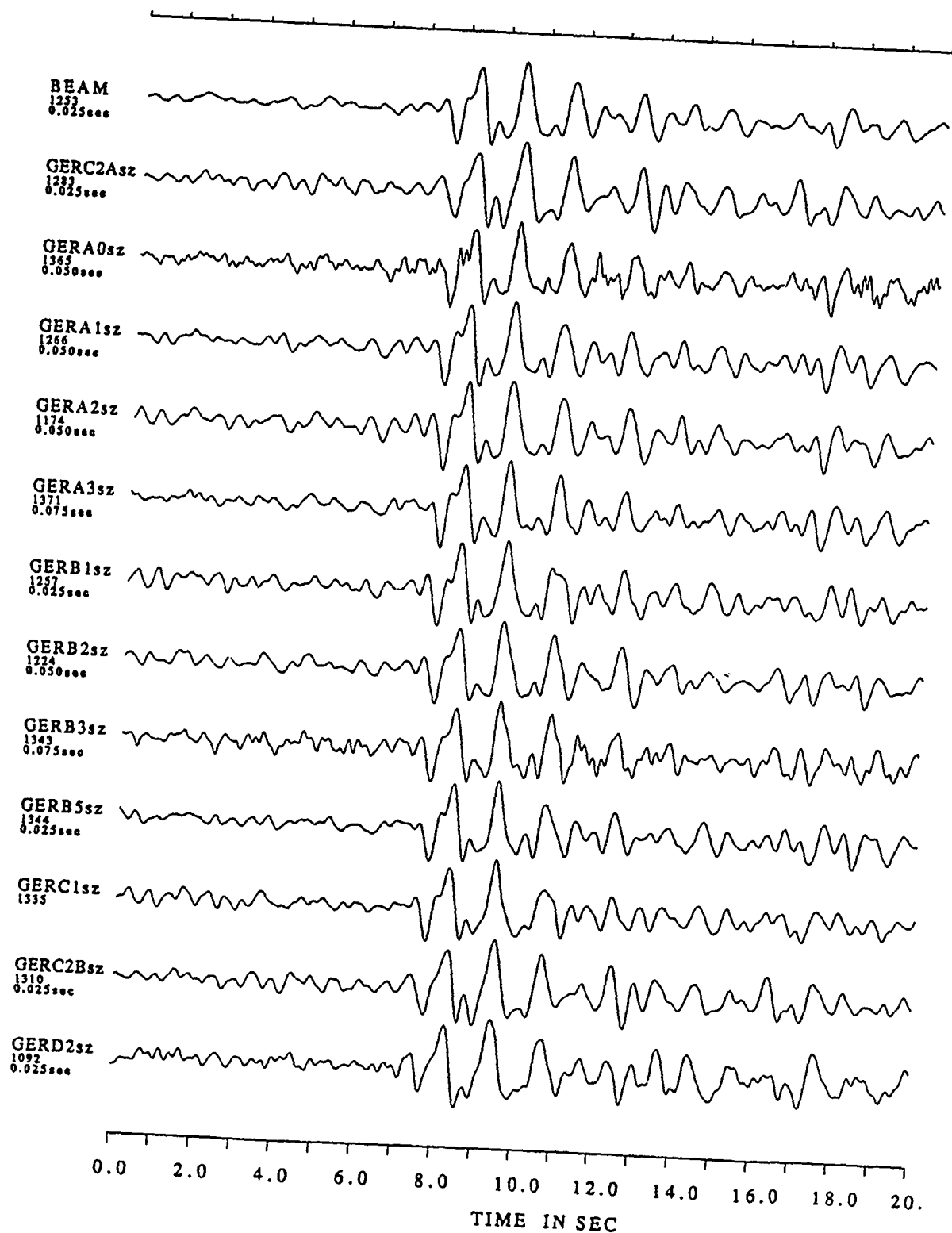
The first presumed nuclear test, which could be recorded with the GERESS array, was an event at the Chinese test site Nop Lor on May 26, 1990. Fig. 6-1 shows the original recordings, in Fig. 6-2 additionally to the filtered seismograms the best beam for the P-phase is also shown. The observed magnitude of  $m_b = 4.6$  is unexpected low for an explosion with a network magnitude of  $m_b = 5.4$  (PDE).

This observed discrepancy needs further investigations. Either it is a true effect of Earth's structure or it is the result of a general malfunction of the array at this time. If new tests will confirm our results, the GERESS array would have a magnitude residuum of -0.8 magnitude units for Nop Lor events. With an STA/LTA detection threshold of 4.0, as used for the GERESS detector, this implies a detection threshold for events at Lop Nor with a network magnitude of  $m_b = 5.0$ . Unfortunately the whole array was down, when the second Chinese nuclear test occurred on August 16, 1990.



event : CSS90-146:08.08  
start-time : 26.5 .1990 8 : 9 : 0.0

Fig. 6-1: Unfiltered seismograms of the Chinese nuclear test on May 26, 1990 at Nop Lor. The traces are normalized and each maximum amplitude is given in counts of the GERESS 24 bits analog/digital converter. For details of the GERESS transfer function see the contribution in this report.



event : CSS90-146:08.08  
start-time : 26.5 .1990 8 : 9 : 0.0

Fig. 6-2: Filtered seismograms (0.5-2.5 Hz) of the Chinese nuclear test on May 26, 1990 at Nop Lor. The traces are shifted for the best P-wave beam (values see Tab. 6-1). The beam is shown as the top trace.



### 6.3 FANGATAUFA and MURUROA

In the epicentral distance range between  $140^\circ$  and  $150^\circ$  the structure of the Earth's core amplifies - like a focusing lens - seismic waves, which travel through the Earth's core as PKP-phases. The comparison of the daily detection list of GERESS with bulletins of international seismic centers shows, that GERESS is therefore very sensitive for the seismicity in the Southern Pacific. The two French nuclear test sites Mururoa and Fangataufa are located very close to each other in the Tuamotu Archipelago. They have an epicentral distance to GERESS of about  $145.5^\circ$ , right where the maximum of the PKP-caustic is observed (Fig. 6-3). Therefore we expect a low detection level for seismic events at these test sites. The seismograms of all observed French explosions are shown in Fig. 6-4 - Fig. 6-10.

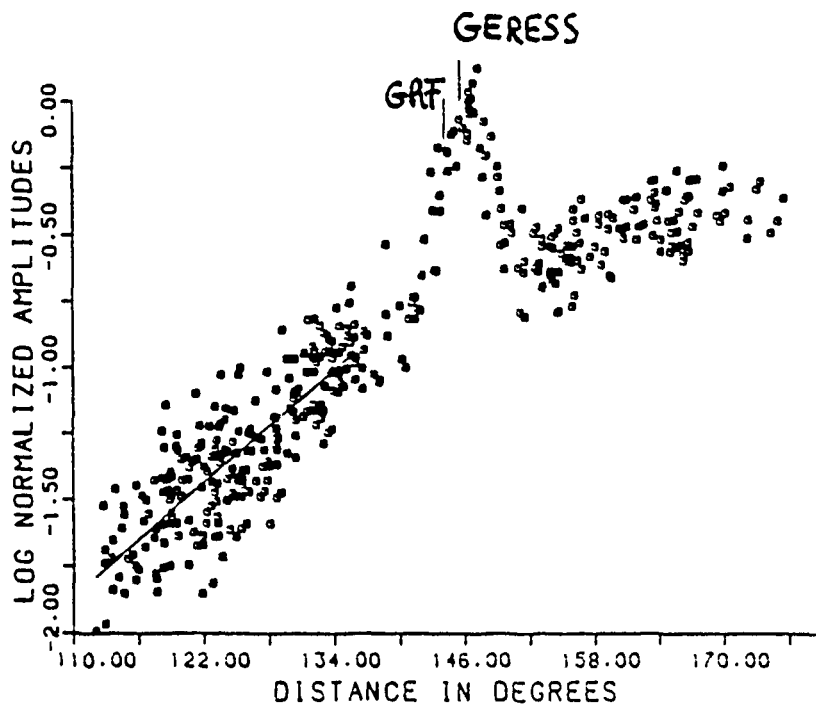


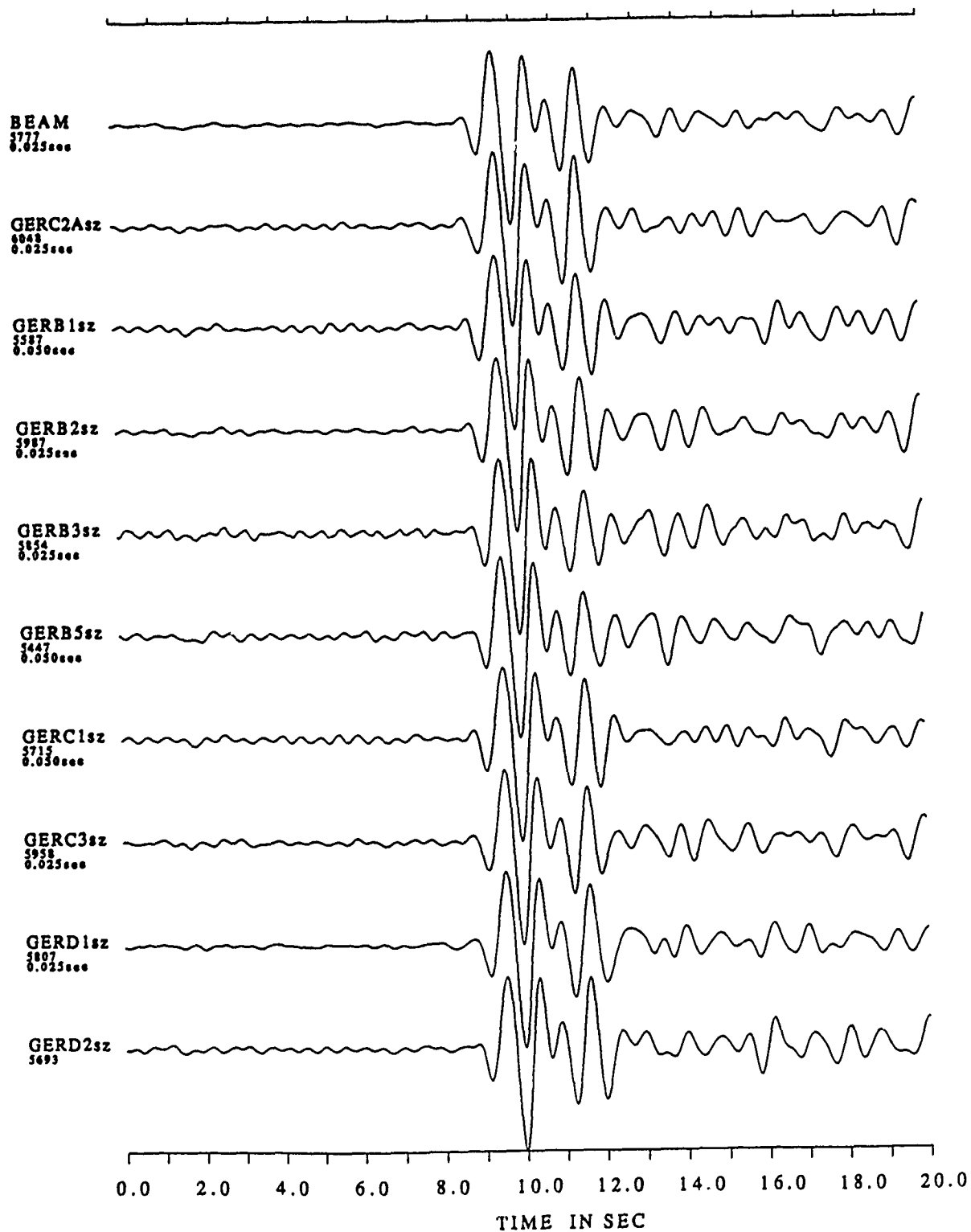
Fig 6-3: Cumulative logarithmic amplitude plot containing normalized PKP-amplitudes (from: Häge, 1981). The epicentral distances from the French test sites to GERESS and GRF are marked.

Tab. 6-2: Amplitude and magnitude observations of French nuclear tests in 1990.

Date		Amplitude [nm]	Period [sec]	$\log(A/T)$	$m_b$ (PKP)	$m_b$ (PDE)	SNR	Det. Thr. [ $m_b$ ]
Jun	02	32.69	0.88	1.57	5.07	5.3	57.99	3.91
Jun	07	5.77	0.90	0.81	4.31		6.42	3.70
Jun	26	148.54	1.57	1.98	5.48	5.5	102.17	4.07
Jul	04	14.68	0.87	1.23	4.73	5.1	28.45	3.88
Nov	16	142.79	1.50	1.98	5.48	5.6	111.45	4.03
Nov	21	64.65	0.81	1.90	5.40	5.4	89.82	4.05

Because the body wave magnitude  $m_b$  is not defined for events with an epicentral distance of more than about  $100^\circ$ , I could not determine  $m_b$ -values for these explosions directly. Schlittenhardt (1988) introduced a body wave magnitude for PKP-observations of the French explosions at the Gräfenberg array (GRF). Although the distance between GRF and GERESS is only about 150km, we cannot use his results to calculate  $m_b$ -values, because the amplitude-distance behaviour of the PKP-phases changes in this distance range drastically (see Fig. 6-3). Therefore I corrected the observed  $\log(A/T)$  values with the attenuation curve of Blandford and Sweetser (1973) for PKP-phases. With the correction value of 3.50 for an epicentral distance of  $145.5^\circ$  I determined the  $m_b(\text{PKP})$ -values for the French explosions. For five of these events our  $m_b(\text{PKP})$ -values can be compared with "classical"  $m_b$ -determinations in the PDE by NEIS. The agreement between the  $m_b$ -values calculated with different methods confirms the proposed usage of PKP-phases for regular worldwide monitoring of as well the seismicity as the nuclear test activities (Harjes, 1985).

The detection threshold (Det. Thr.) was calculated from the observed signal to noise ratio (SNR), the detector threshold of 4.0, and the calculated values for  $m_b(\text{PKP})$ . The mean value for the detection threshold of Tuamotu Archipelago events at GERESS is about  $m_b(\text{PKP}) = 3.9$ .



event : CSS90-153:17.49  
start-time : 2 . 6 . 1990 17:49:30.0

Fig. 6-4: As Fig. 6-2, but now for the French nuclear test on June 2, 1990 at Mururoa.

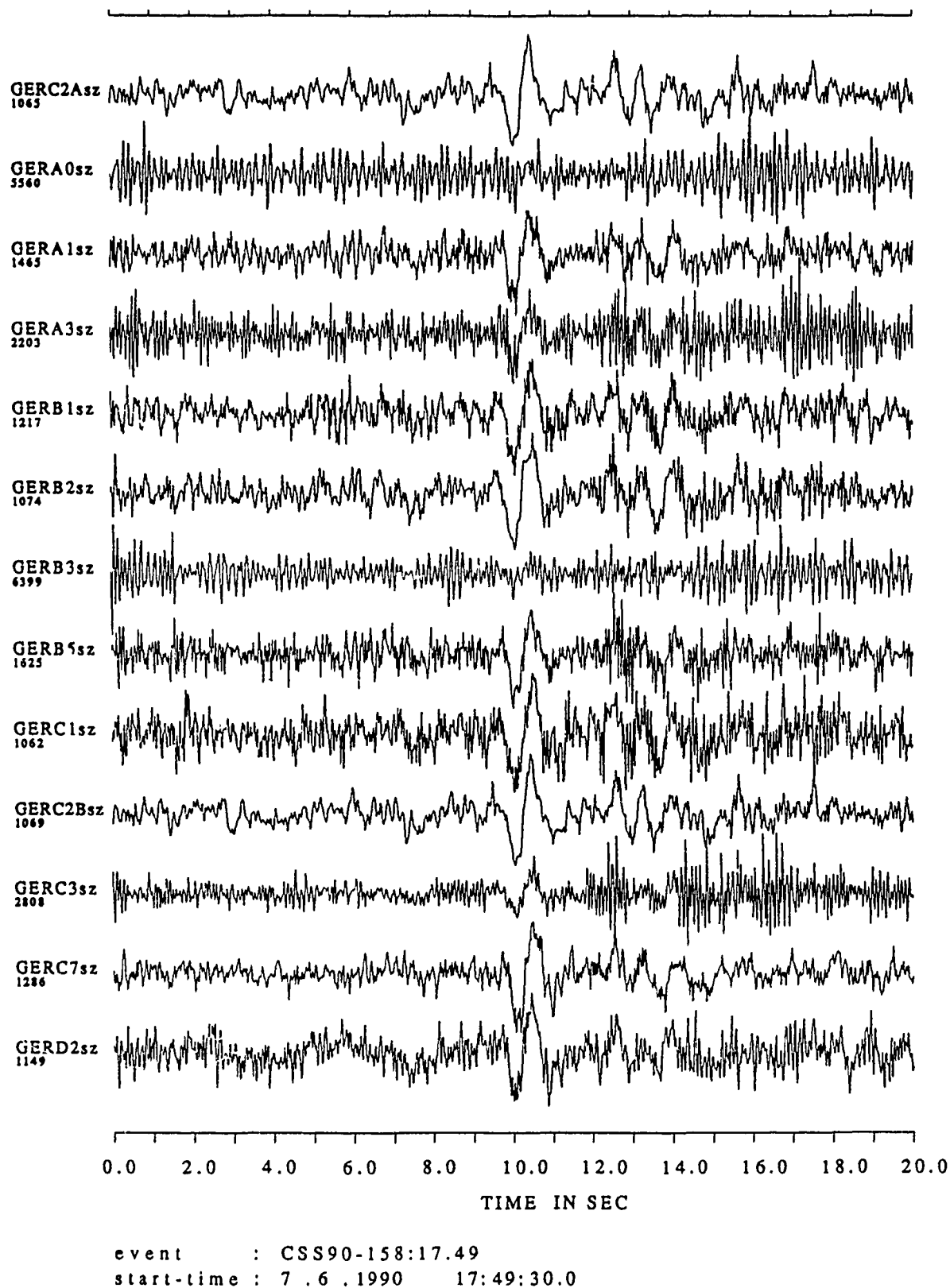


Fig. 6-5: As Fig. 6-1, but now for the French nuclear test on June 7, 1990 at Mururoa. This was the smallest test in 1990 at the French test site Mururoa. Note that the seismic signal of this test with magnitude  $m_b = 4.7$  and a presumed yield of about 7 kt TNT (R. Smith, pers. communication) is seen on the unfiltered single channels. In the PDE (monthly listing) no reference is given for this event.

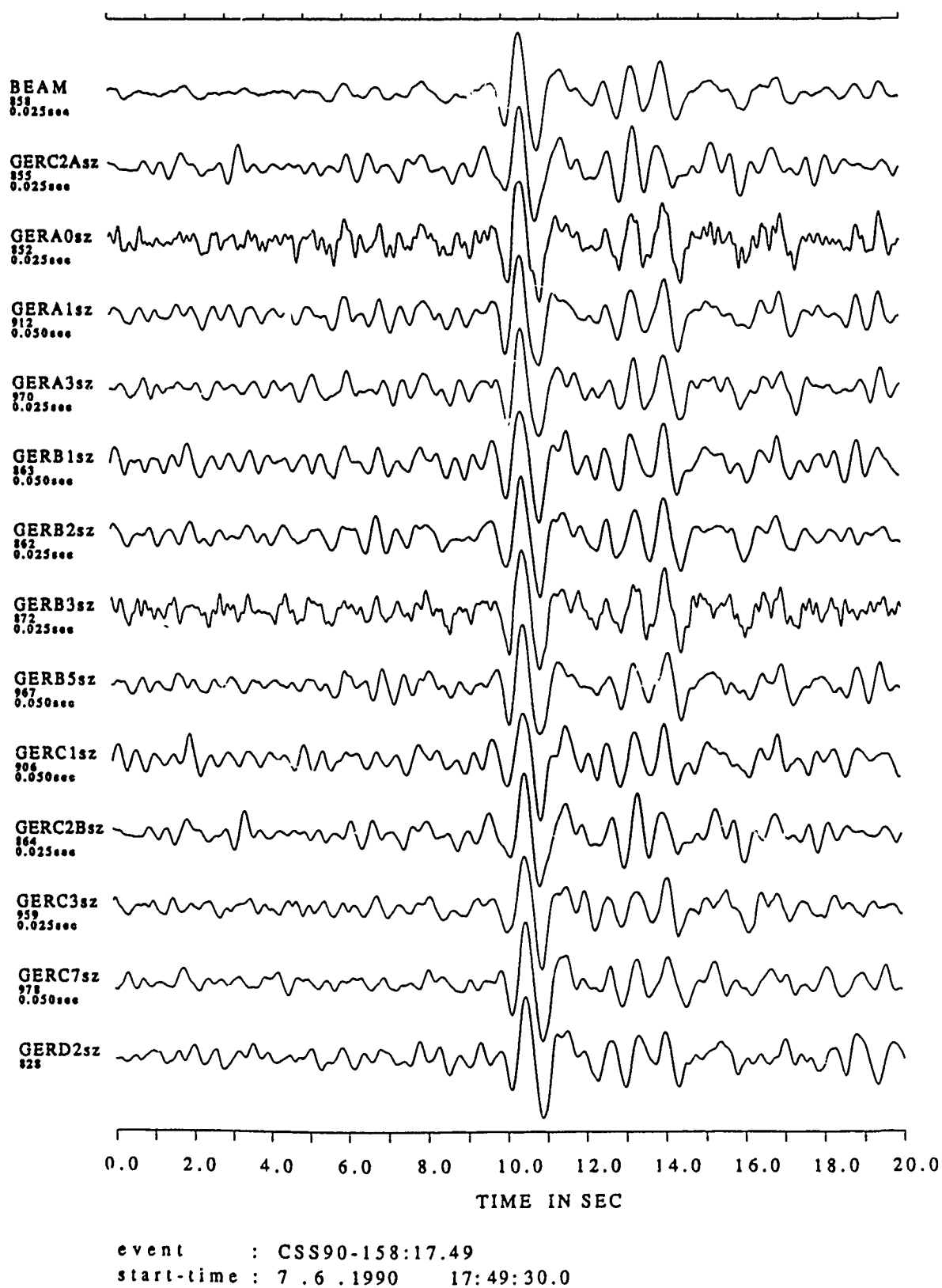


Fig. 6-6: As Fig. 6-2, but now for the French nuclear test on June 7, 1990 at Mururoa.

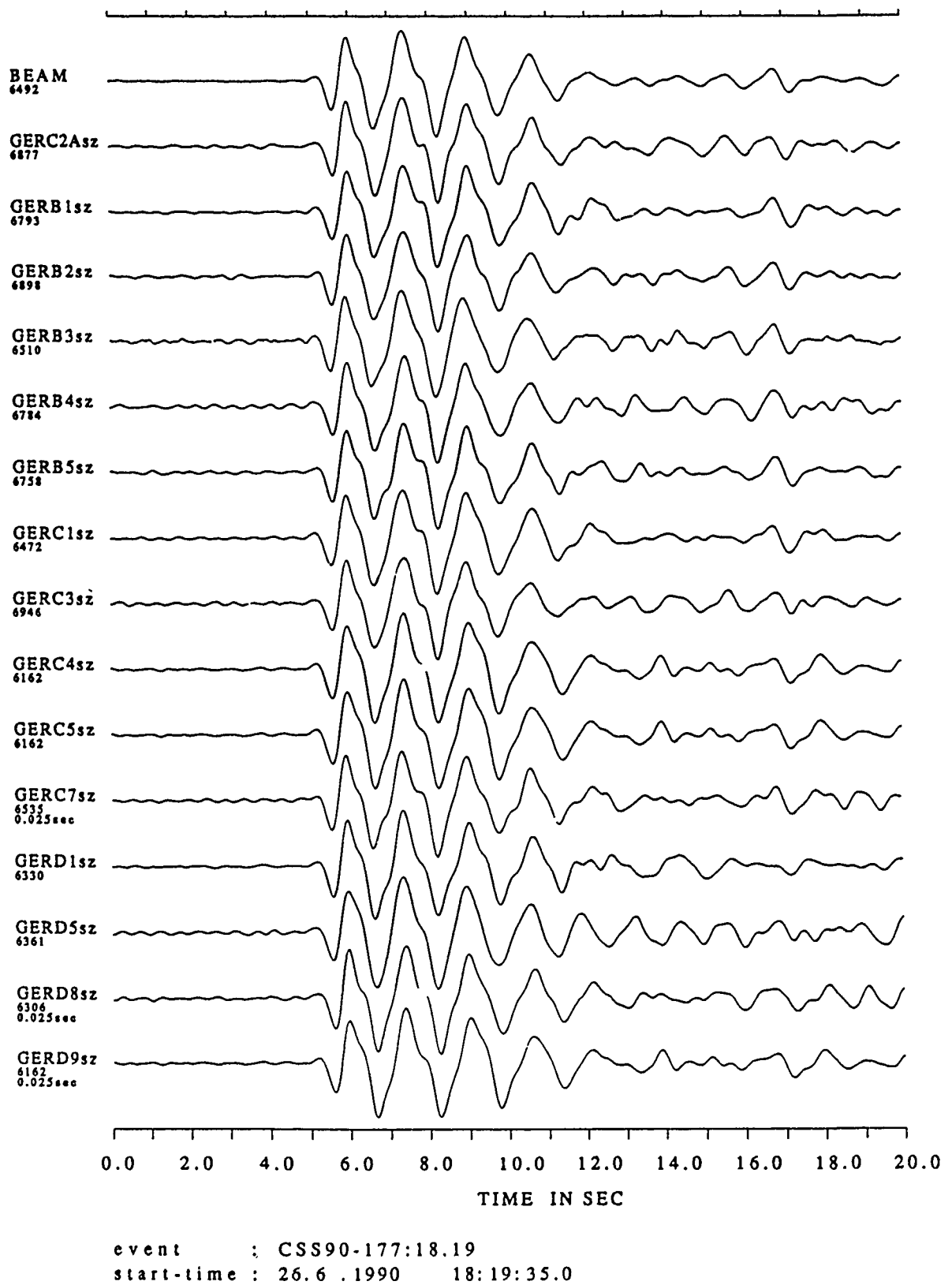
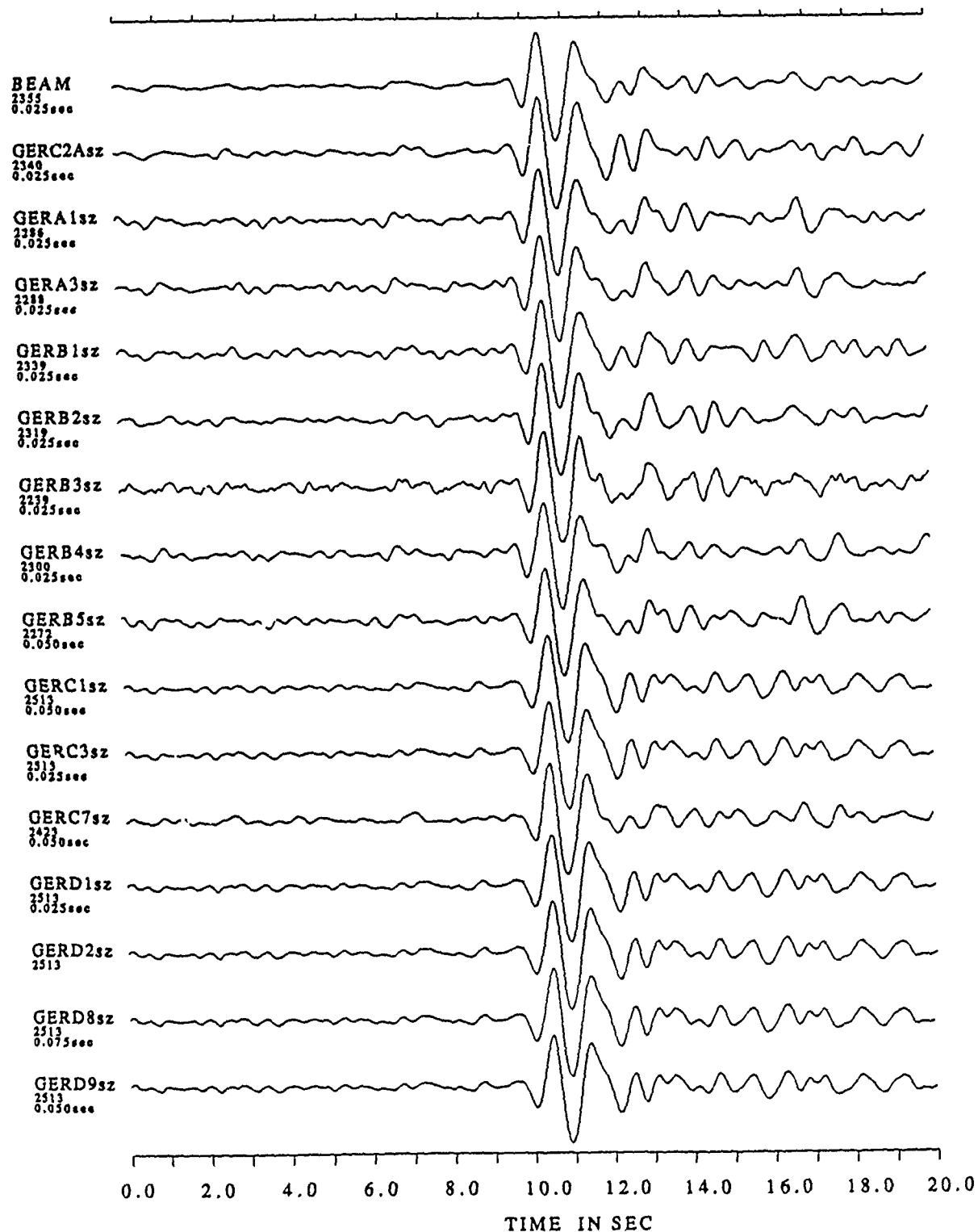
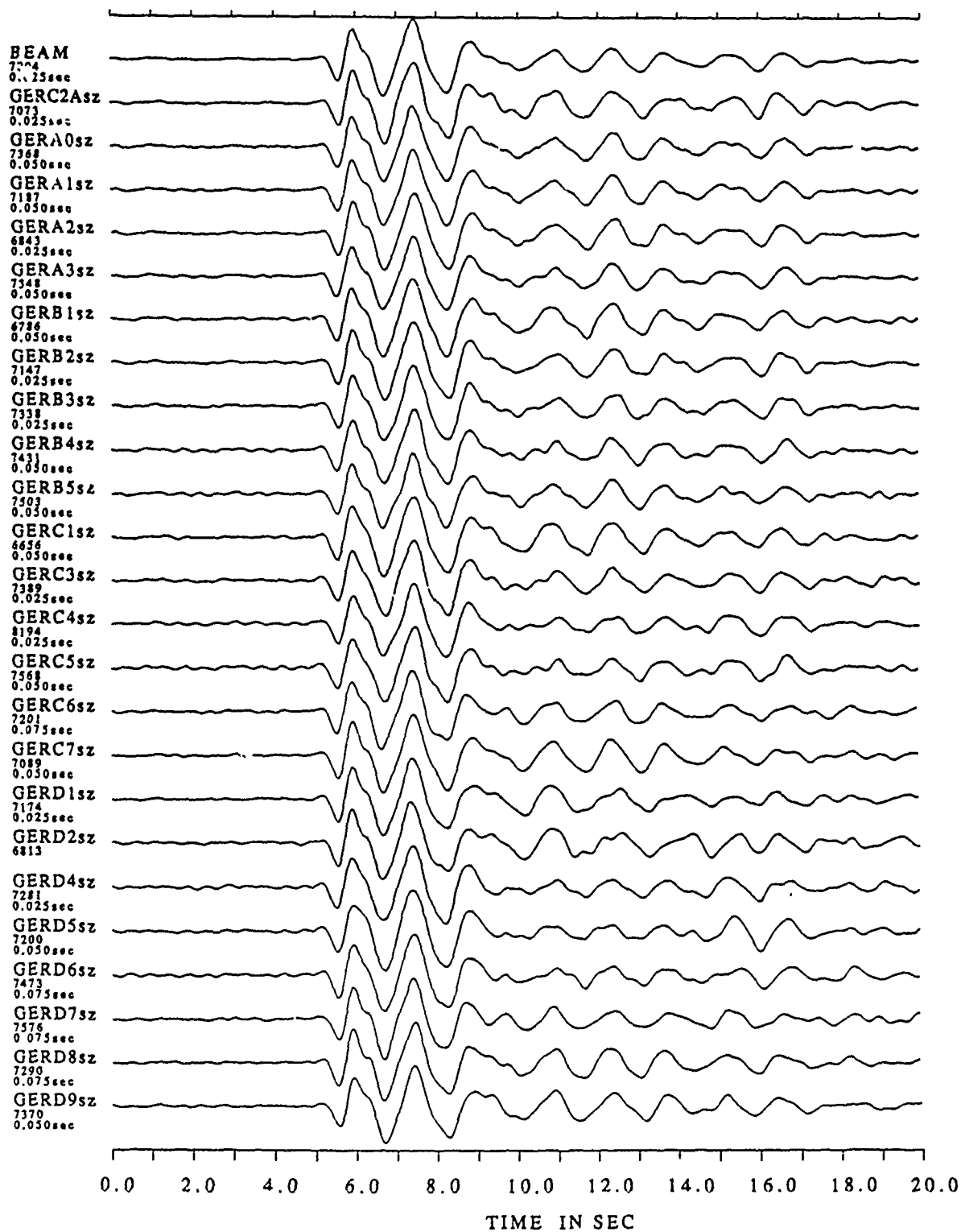


Fig. 6-7: As Fig. 6-2, but now for the French nuclear test on June 26, 1990 at Fanga-  
taufa.



event : CSS90-185:18.19  
start-time : 4 . 7 . 1990 18:19:30.0

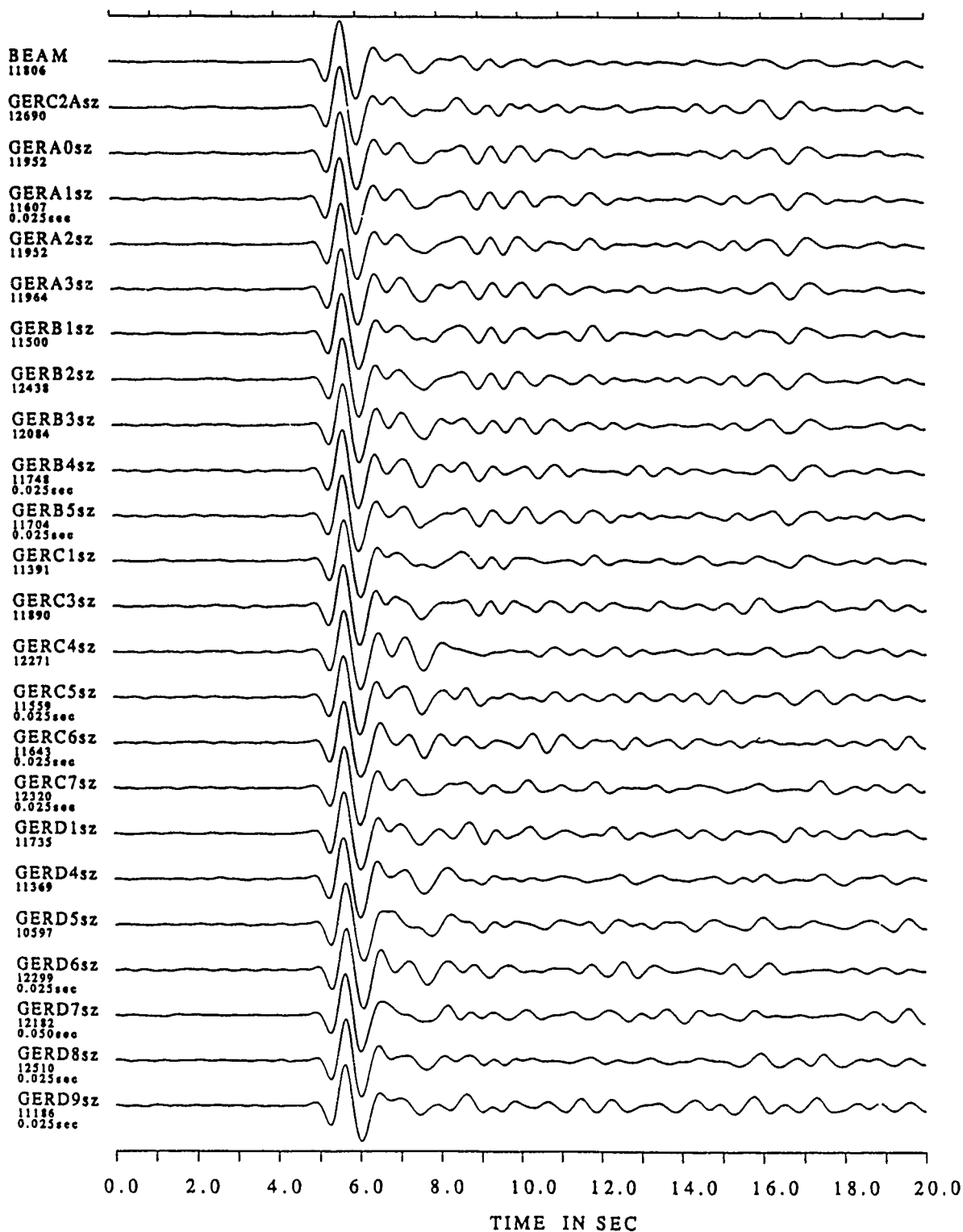
Fig. 6-8: As Fig. 6-2, but now for the French nuclear test on July 4, 1990 at Mururoa.



event : CSS90-318:18.31  
start-time : 14.11.1990 18:31:35.0

Fig. 6-9: As Fig. 6-2, but now for the French nuclear test on November 14, 1990 at Fangataufa.





event : CSS90-325:17.19  
start-time : 21.11.1990 17:19:35.0

Fig. 6-10: As Fig. 6-2, but now for the French nuclear test on November 21, 1990 at Mururoa.

## 6.4 NEVADA

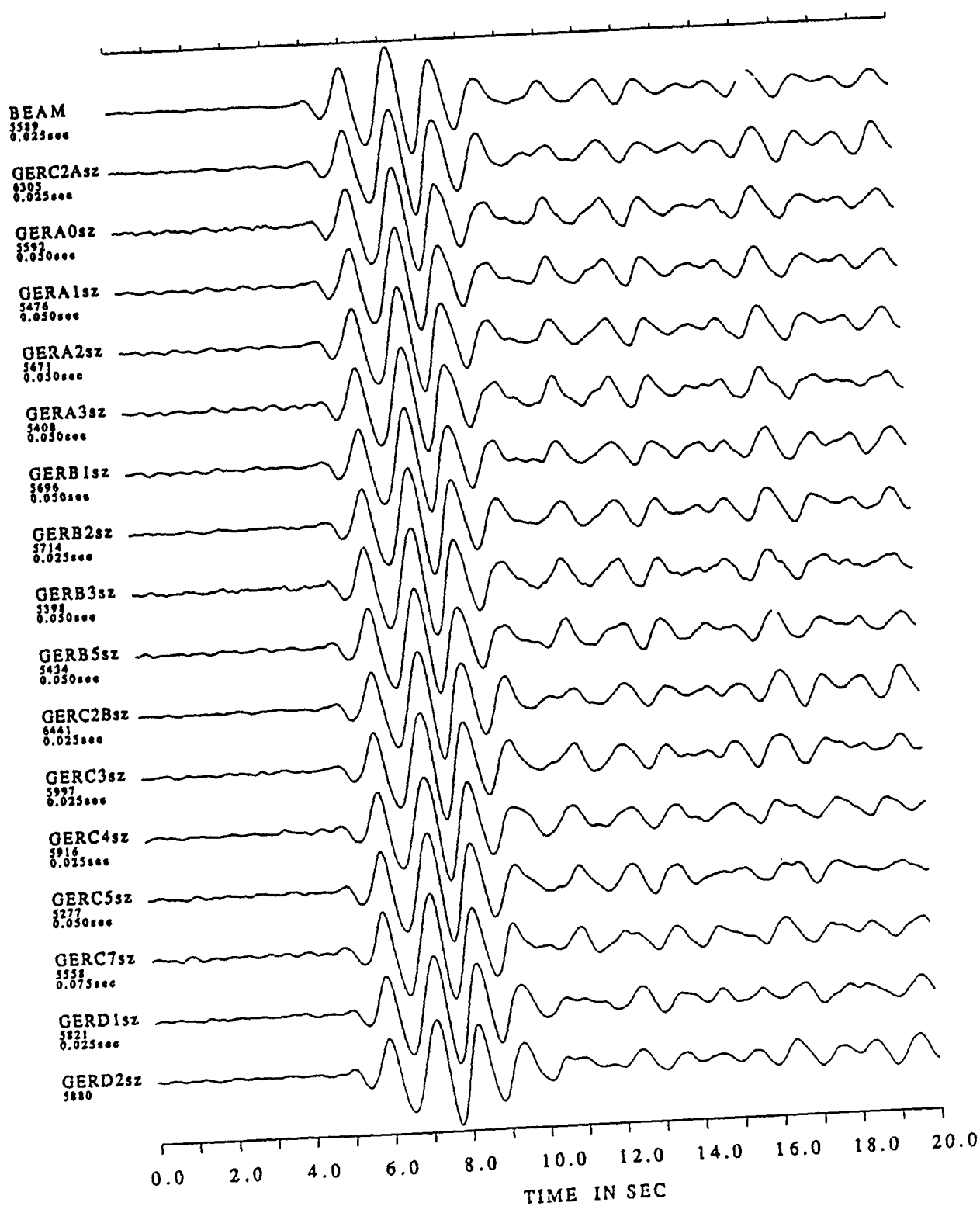
Four of eight nuclear tests at the Nevada test site (NTS) could be observed with the GERESS array. Records of all events are shown in Fig. 6-11 - Fig. 6-15. The calculated  $m_b$ -values are in good agreement with the network magnitudes published by NEIS (PDE, either monthly or weekly listings). In Tab. 6-3, I listed a detection threshold in  $m_b$ , considering the observed SNR for all NTS events respectively. From these numbers the mean value of the detection threshold for NTS explosions can be determined as  $m_b = 4.4$ .

One surprising observation is, that for these events extremely small slowness values have been determined (see Tab. 6-1). Only one value (November 14, 1990) is close to the theoretical value (Herrin Tables) of  $P = 5.09$  sec/deg. But because of the timing problems (see Introduction), this problem was not investigated in more detail.

If the time base of all channels of the array is stable, it will become also possible to investigate the P-wave coda of these events. The PKP-waves from the French explosions arrive more or less from the same backazimuth at GERESS and show a similar picture: Coherent energy, which cannot be explained with a spherical Earth model. Obviously, a large amount of this energy is scattered off the great circle path.

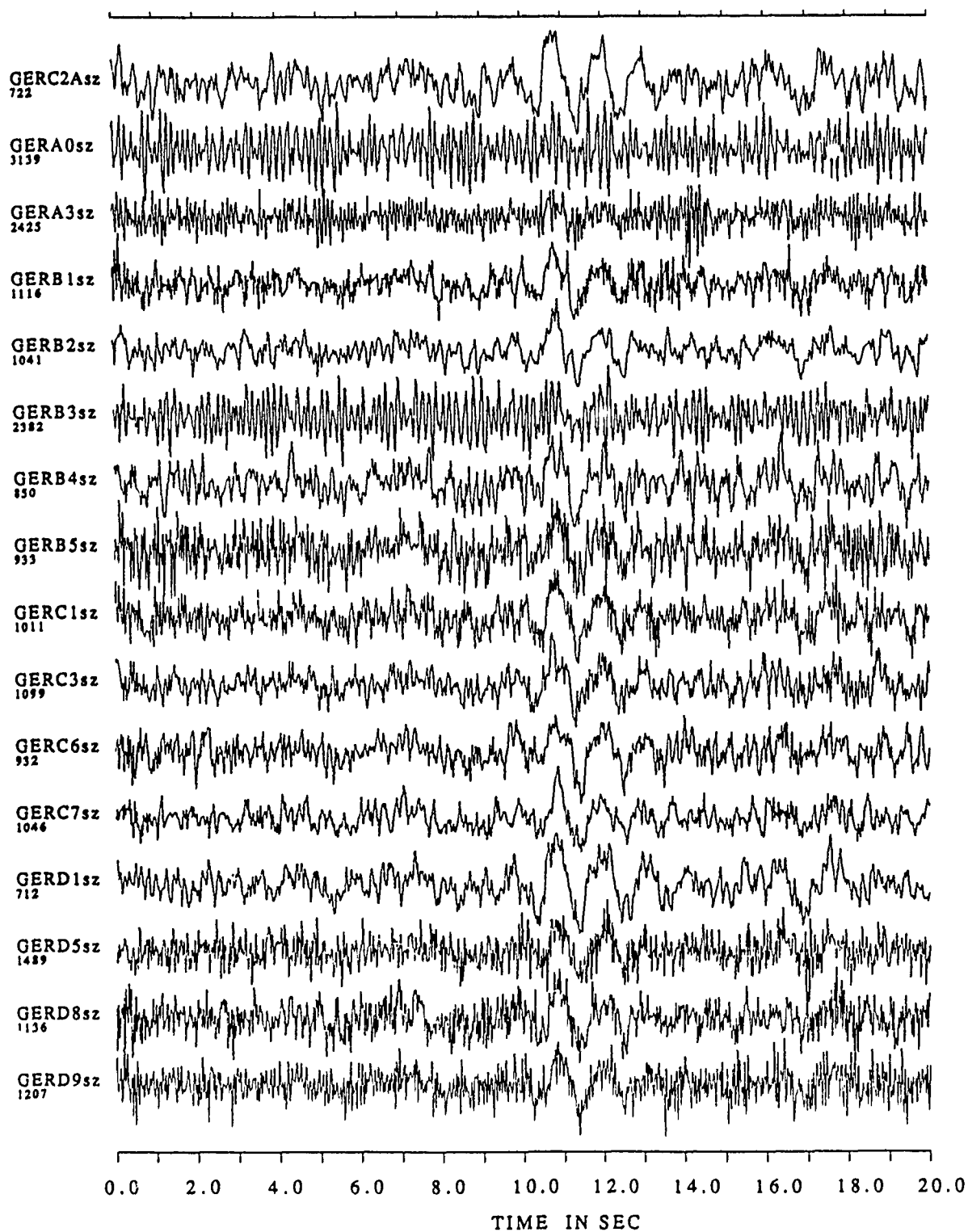
Tab. 6-3: Magnitudes and detection thresholds for the NTS-explosions in 1990.

Date		$m_b$ GERESS	$m_b$ PDE	SNR	Det. Thr. [ $m_b$ ]
Jun	13	5.7	5.7	93.5	4.3
Jul	25	4.7	4.7	8.3	4.4
Oct	12	5.5	5.6	55.9	4.5
Nov	14	5.4	5.4	59.1	4.2



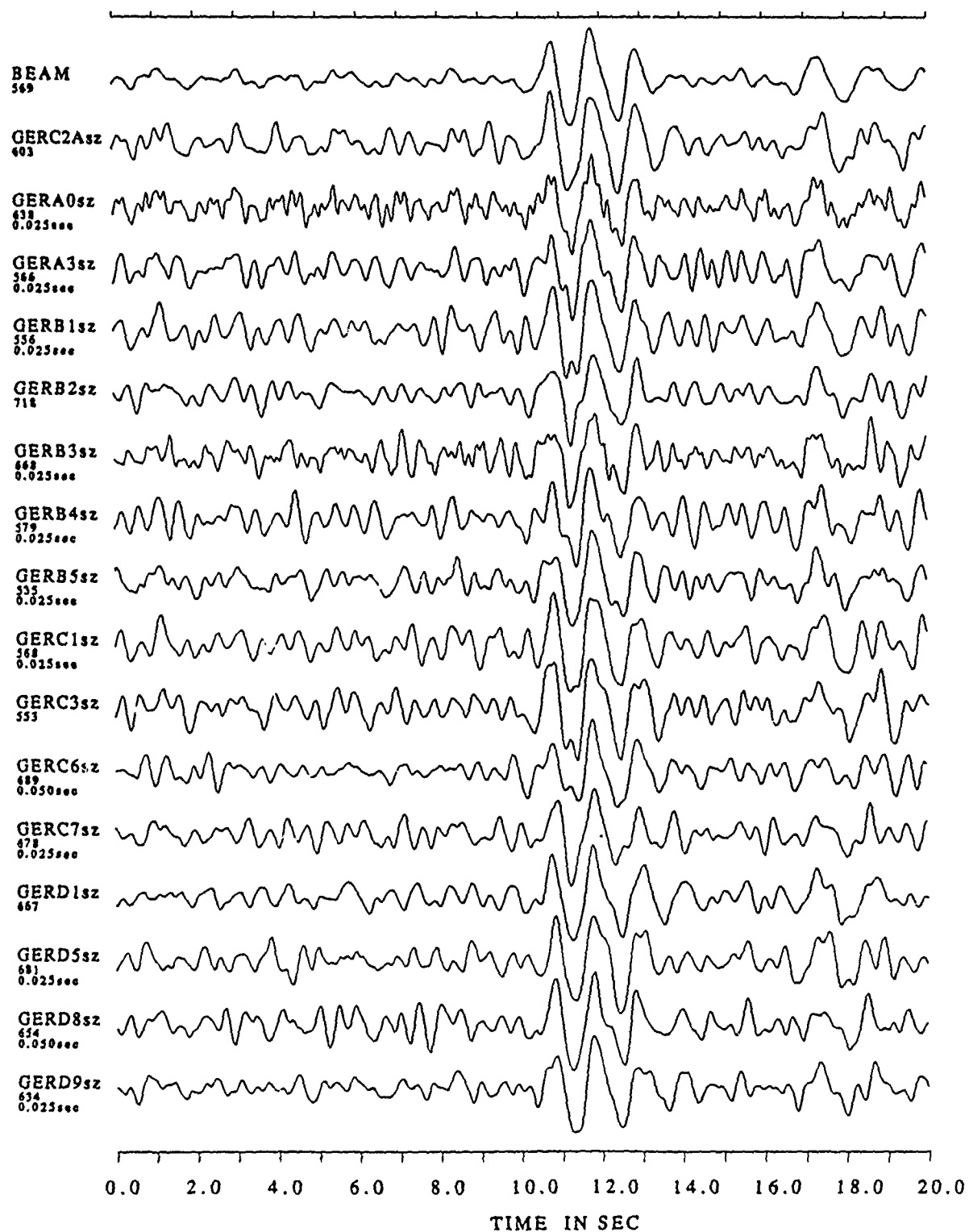
event : CSS90-164:16.12  
start-time : 13.6 .1990 16:12:25.0

Fig. 6-11: As Fig. 6-2, but now for the USA nuclear test on June 13, 1990 at Nevada.



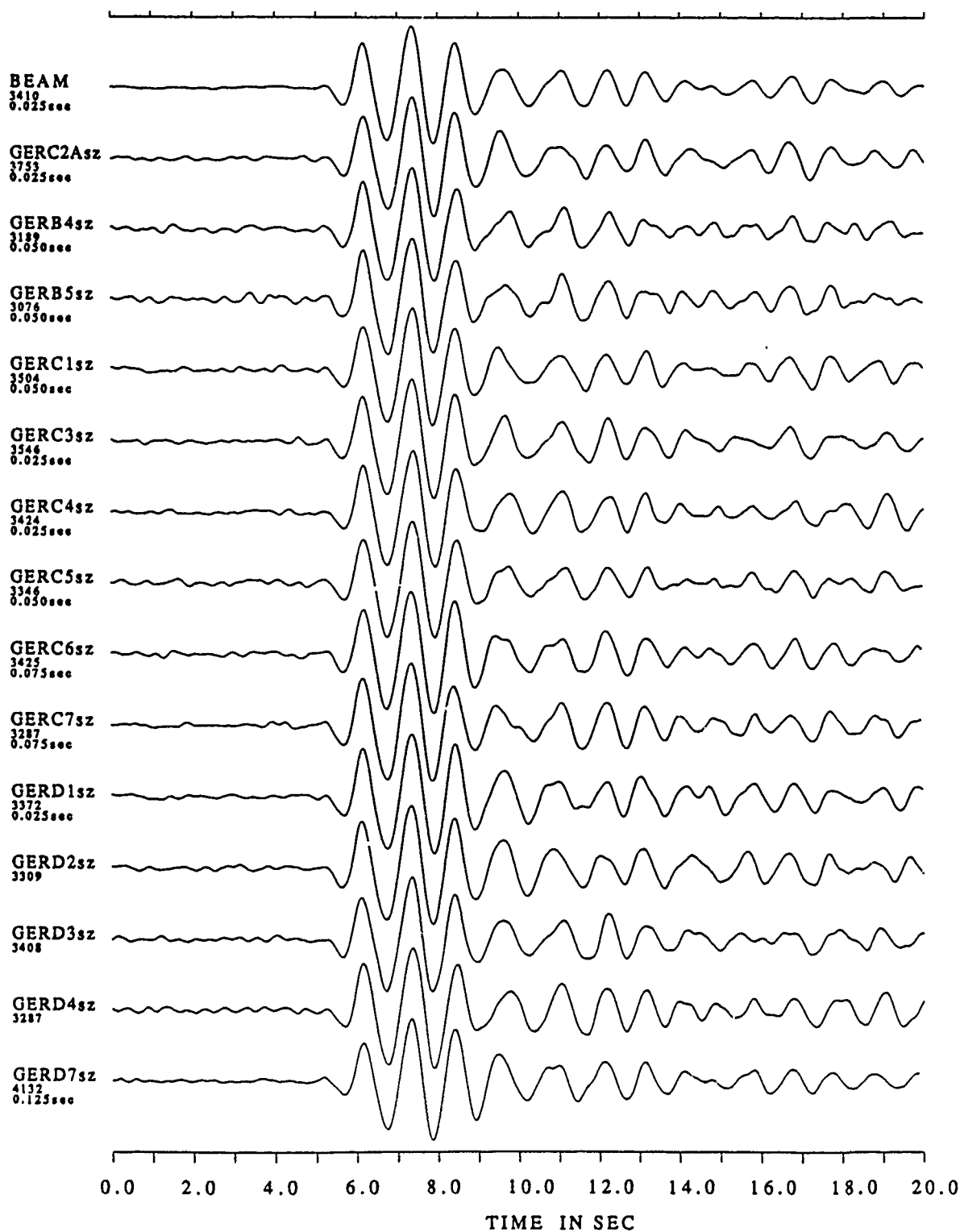
event : CSS90-206:15.12  
start-time : 25.7 . 1990 15:12:20.0

Fig. 6-12: As Fig. 6-1, but now for the USA nuclear test on July 25, 1990 at Nevada. Note the P-wave onset on most of the unprocessed channels.



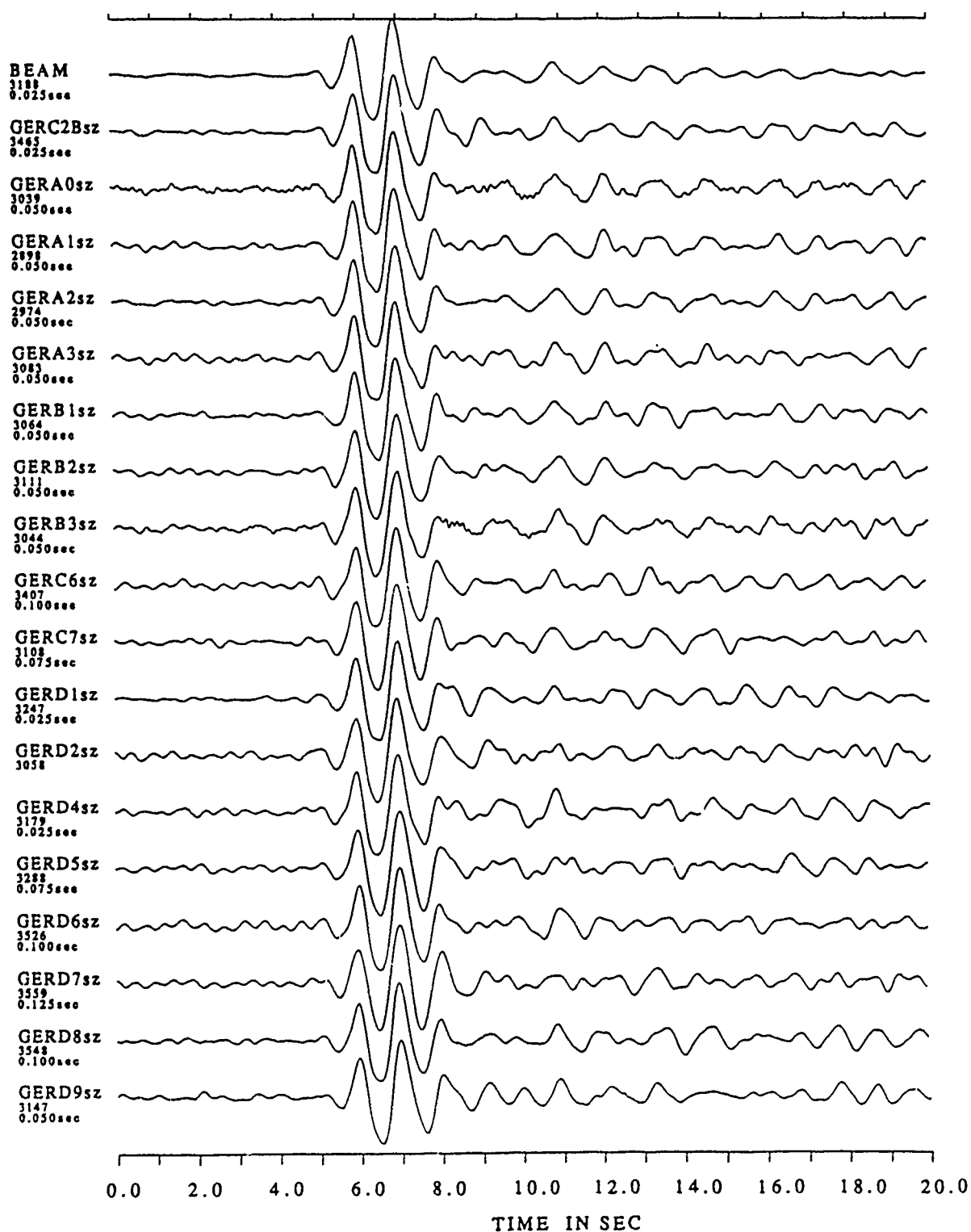
event : CSS90-206:15.12  
start-time : 25.7.1990 15:12:20.0

Fig. 6-13: As Fig. 6-2, but now for the USA nuclear test on July 25, 1990 at Nevada.



event : CSS90-285:17.42  
start-time : 12.10.1990 17:42:25.0

Fig. 6-14: As Fig. 6-2, but now for the USA nuclear test on October 12, 1990 at Nevada.



event : CSS90-318:19.28  
start-time : 14.11.1990 19:29:25.0

Fig. 6-15: As Fig. 6-2, but now for the USA nuclear test on November 14, 1990 at Nevada.

## 6.5 NOVAYA ZEMLYA

In 1990 the Soviet Union carried out only one nuclear test. This test on October 24 was the nuclear explosion, which had been recorded at GERESS in 1990 with the smallest epicentral distance of  $30.4^\circ$ . The records are dominated by the very prominent P-wave coda (Fig. 6-16), and a very complex pulse form of the direct P-wave (Fig. 6-17). This feature must be explained by contributions from the direct waves of the upper mantle triplications, by converted phases, multipathing, and by a lateral heterogeneous structure of crust and upper mantle in Europe. The observed magnitude  $m_b = 5.5$  for this explosion is once more in good agreement with the PDE (weekly listing) investigation ( $m_b = 5.6$ ). With the observed SNR of 90.3 the detection threshold for this test site at the GERESS array is  $m_b = 4.1$ .

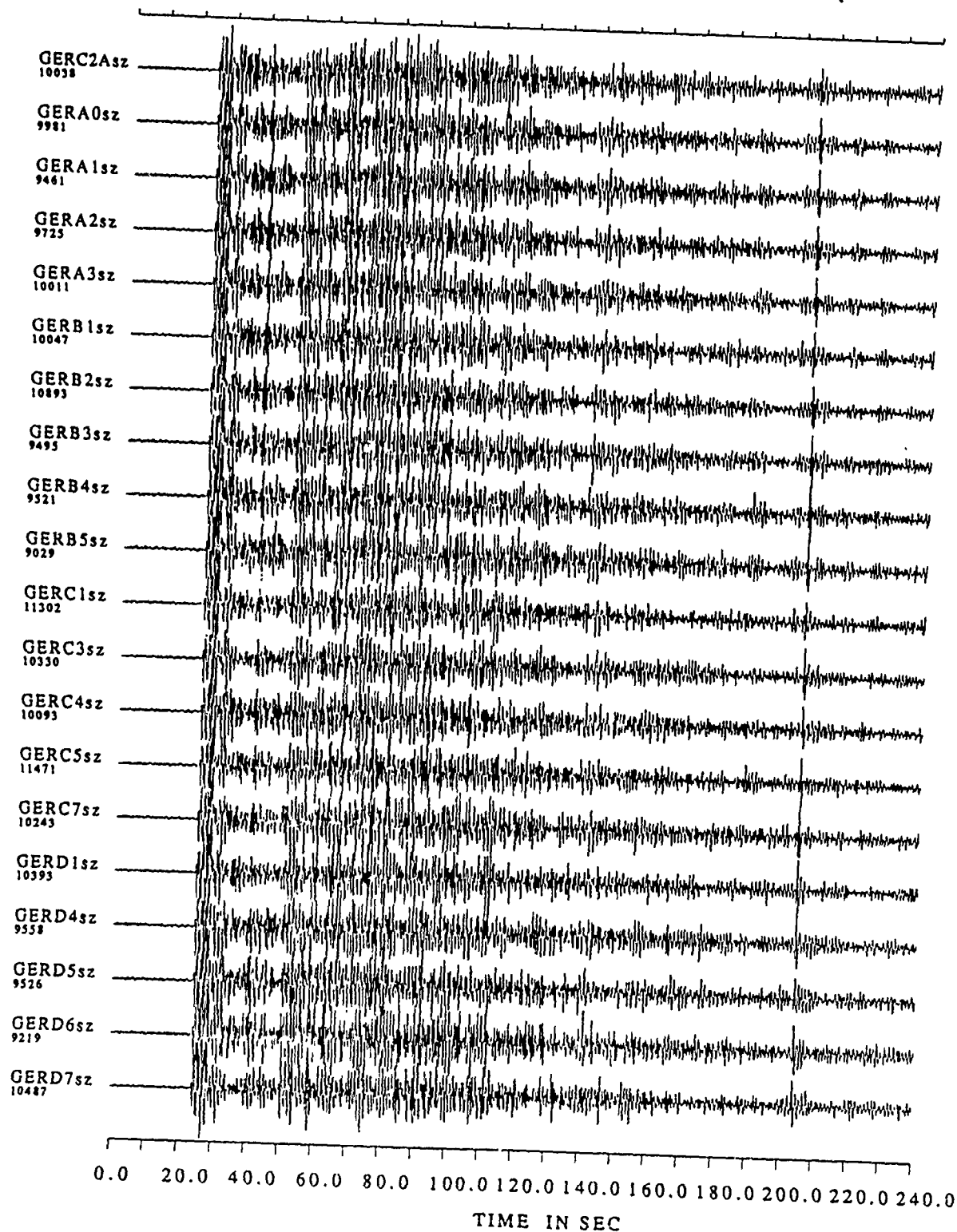
In Fig. 6-16 one clear coherent onset about three minutes after the first arrival is seen. This phase could be identified as PcP (Fig. 6-18) with its onset time and the results of the f-k analysis. This phase has the right slowness (2.6 sec/deg) for a PcP-phase in an epicentral distance of  $30^\circ$ . An unexplained observation at this moment is the anomalous high PcP/P amplitude ratio. A possible explanation would be a focusing structure for PcP elsewhere on its ray path. This leads me to look for other PcP-observations in epicentral distances smaller than  $35^\circ$ . When we have a greater collection of PcP-observations in this distance range, it will become possible to discuss this problem in more detail.

## 6.6 LITERATURE

- Blandford, R. R. and E. I. Sweetser (1973): Seismic distance-amplitude relation for short period P,  $P_{diff}$ , PP and compressional core phases for  $\Delta > 90^\circ$ . Report, Teledyne-Geotech, SDAC-TR-73-9, Alexandria, VA.
- Häge, H. (1981) : P and S-velocity jump at the inner-core boundary from PKP amplitudes. In: E. S. Husebye and S. Mykkeltveit (eds.): Identification of seismic sources - earthquake or underground explosion. Dordrecht 1981.
- Harjes, H. P. (1985) : Global seismic network assessment for teleseismic detection of underground nuclear explosions. J. Geophys. 57, 1-13.
- Harjes, H. P. (1990) : Design and siting of a new regional array in Central Europe. Bull. Seism. Soc. Amer. 80, 1801-1817.
- Schlittenhardt, J. (1988) : Seismic yield estimation using teleseismic P- and PKP-waves recorded at the GRF-(Gräfenberg) array. Geophys. J. 95, 163-179.

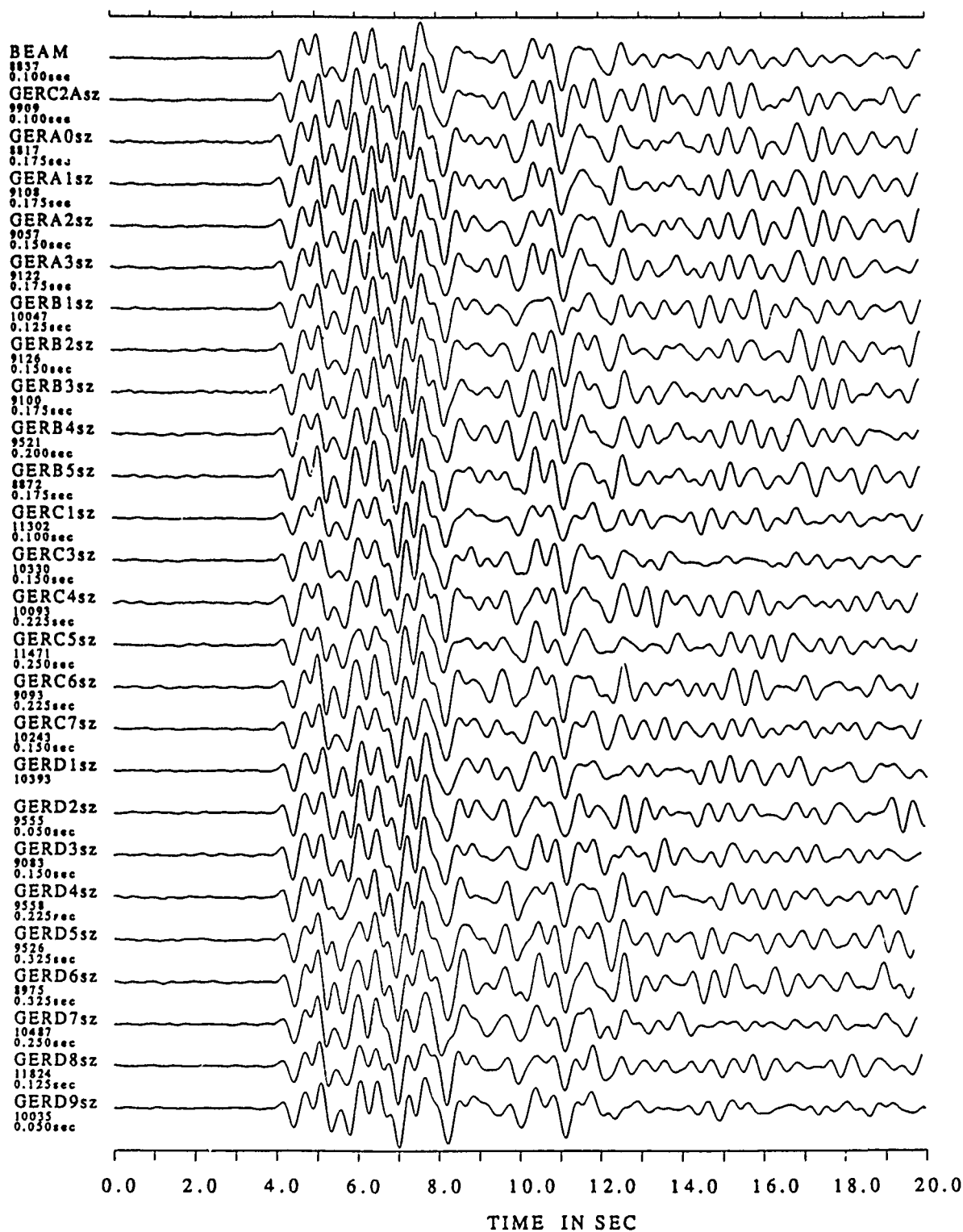


RP



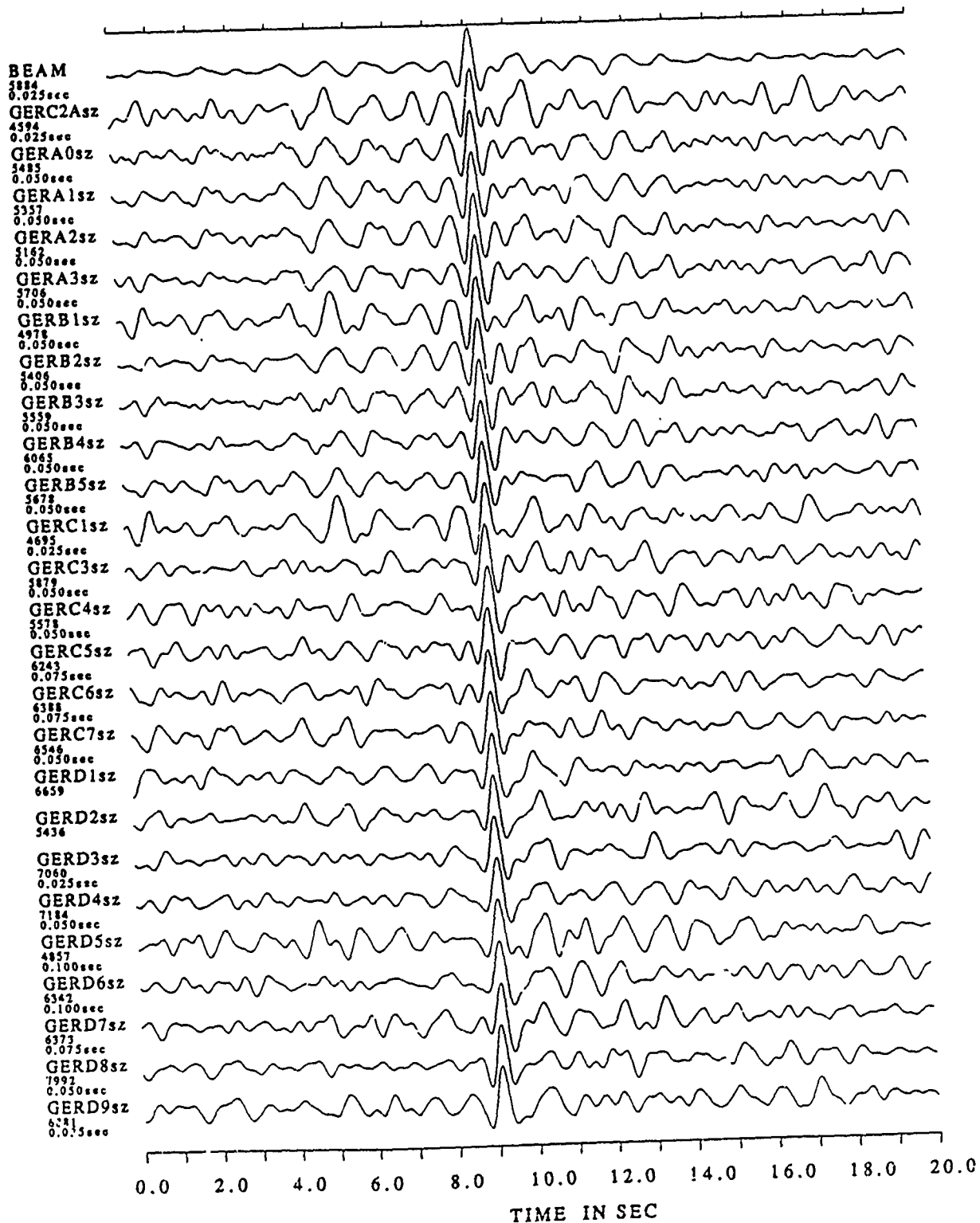
event : CSS90-297:15.03  
start-time : 24.10.1990 15:3 :50.0

Fig. 6-16: As Fig. 6-2, but now for the first four minutes of the records of the Soviet nuclear test on October 24, 1990 at Novaya Zemlya. Note the prominent P-coda and the clear PcP-onset about three minutes after the first arrival.



event : CSS90-297:15.04  
start-time : 24.10.1990 15:4:10.0

Fig. 6-17: As Fig. 6-2, but now for the Soviet nuclear test on October 24, 1990 at Novaya Zemlya.



event : CSS90-297:15.04  
start-time : 24.10.1990 15:7:5.0

Fig. 6-18: As Fig. 6-2, but now for the Soviet nuclear test on October 24, 1990 at Novaya Zemiya and the time window of the PcP-phase with anomalous high amplitudes. The top trace shows the best PcP-beam.

## 7. REGIONAL WAVEFORM ANALYSIS WITH GERESS DATA

### 7.1 INTRODUCTION

One of the main purposes of the GERESS array is the detection and localization of regional and local events. The localization depends mainly on the velocity analysis of dominant onsets in the seismograms and the ability to discriminate between P- and S-phases. If the structure of the crust is well known, a detailed classification is possible. In this paper, the velocity analysis is extended to the whole time-window of the event, to identify additional phases and to find indications of azimuth dependent structure. For a better interpretation, the same analysis is repeated with synthetic seismograms for a simple crustal model.

The configuration of the array is most favorable for the investigation of events in the local and regional distance-range up to 30°. Phase-velocities of the dominant signals range from 2 km/sec to 10 km/sec. Undercritically reflected phases may have significantly higher velocities. The frequency-range of the analyzed phases generally extends from 1 Hz to 20 Hz. For some events we could observe signal frequencies above 50 Hz. Aside from the frequency-wavenumber characteristics of the investigated signals, their coherence across the array is important for the configuration of the array. The coherence length depends on frequency but also on the local geology. Strong inhomogeneties below the seismometer locations may reduce the coherence length.

To study the coherence of noise and signals, a test-array had been installed near the proposed place for the final array (Harjes, 1990). The signal coherence was derived from events recorded with this test array. The investigation of noise was made for a time-window before the first onset. Defining correlation length  $L$  as the characteristic separation between stations, for which the coherence coefficient  $C$  drops below 0.25, the correlation length  $L$  for the noise is about 800 m in the 1 - 2 Hz passband and 400 m in the 2 - 4 Hz passband. The signal-coherence is greater than 0.95 and 0.85 for the two frequency-bands, respectively. Station AG was omitted to avoid coherent noise influencing the results of this study. Thus the minimum station distance increased from 161 m

to 241 m, and only a few station distances remain below the coherence length of the noise.

The determination of phase-velocity and azimuth for seismic onsets was done with the conventional broad-band  $f,k$  power spectrum technique (Capon, 1973). The maximum resolution of this method is given by the width of the main lobe of the array response function (fig. 7.1), depending only on the array configuration. A comparison of methods for various azimuth and phase velocity estimation techniques was done by Kvaerna and Ringdal (1986) and Kvaerna (1987) with data from the NORESS array. They concluded that conventional  $f,k$  processing of vertical data provides more stable estimates than results obtained by similar processing of three-component data. Their final conclusion was that the broad-band  $f,k$  estimation approach clearly provides the most stable estimates of azimuth and apparent velocities. In our own investigations we did not achieve a significant improvement using the high resolution  $f,k$  technique (Capon, 1973).

In this study, the  $f,k$  power spectrum was calculated for time-windows of 1 second duration moving along the whole recorded event or the synthetic data. Consecutive time-windows were allowed to overlap by 0.5 seconds. Within each time-window the maximum of this function defines phase-velocity and azimuth of the wavegroup, which propagates across the array. These values were associated with the respective time-window. In addition to azimuth and phase velocity, a quality value was calculated which reflects the signal coherence inside each time-window. This quality value ranges from 0 to 1.

The investigations described below have been limited to the frequency band from 0.8 Hz to 4 Hz because of the good signal to noise ratio in this passband.

## 7.2 INVESTIGATION OF GERESS DATA

Two events with almost equal distance, but different azimuths have been selected for velocity and azimuth analyzes (table 7.1 and figure 7.2).

The first event is a recording of a quarry blast from the Vogtland area in the north-eastern part of CSFR. This area is well known for many small earthquakes and extensive quarry blast activities. During a test from 26.11.90 to 2.12.90 (phase 3 of GSETT 2), 12 events could be detected and located in this region (figure 7.3). At 3 of the 7 days of the test, no events could be detected

from this area. The second event is a small earthquake from the Alps near the village of Kitzbühl in Austria.

The filtered seismograms (0.8 - 4.0 Hz) from the first event are shown in figure 7.4. The spectra for the two time-windows containing P and S energy and a third time-window with noise preceding the first onset (figure 7.5) show the best signal to noise ratio in the frequency band from 1.5 to 4.0 Hz. The dominant noise maximum at 4 - 5 Hz is supposed to originate from a saw mill at a distance of a few kilometers from the GERESS array. The spectra of P and S surpass the noise level up to 30 Hz and 20 Hz, respectively. The high frequency element at C2, sampled at 120 Hz, was used for calculating the power spectra.

Amplitudes of Pg-impulse vary greatly between different array stations. Some stations show a simple strong Pg impulse (e. g. station D8), but for other stations, the onset is hardly visible (D4). Lg/Pg amplitude ratios for different array stations vary between 0.9 to 5.8 for the 0.8 - 4.0 Hz bandpass and between 0.9 - 6.1 for the unfiltered seismograms. This may be due to different coupling of the seismometers to the solid underground as well as to inhomogeneities along the whole propagation path and underneath the seismometer location. Contrary to Pg, the Pn onset is visible without additional filtering for a few stations only (e. g. A1, C1 and C2).

The results of the f,k analysis for this first event are displayed in figure 7.6. Marked onsets and phases are the results of standard interpretation. Azimuth values for the individual time-windows scatter within a range of  $\pm 15^\circ$  around the mean value of  $331^\circ$ . The calculated mean value has been found to be very stable, generally deviating no more than  $1 - 2^\circ$  from the theoretical azimuth. Azimuth deviations could have the following reasons:

- General heterogeneities exist along the travel path and underneath the array, reducing the signal coherence and producing travel-time residues between the stations of the array.
- Each time-window contains a superposition of wavegroups with different phase velocities, which cannot be resolved because in each time-window only the maximum of the f,k power spectrum is considered. This is even true for the synthetic seismograms where azimuth variations are substantially smaller, however.
- Large-scale structures along the travel path reflect the waves laterally. Thereby producing alternative ray paths giving rise to real azimuth

variations.

- Coherent noise contributes to these variations.

As described in section one, the effect due to coherent noise cannot be large enough to explain the observed azimuth variations completely, because only a few seismometer distances are smaller than the coherence length. The  $f,k$  analysis of synthetic signals calculated for a station distribution identical to the GERESS array confirmed these results. Heterogeneities below the array appear to be the most probable reason for the azimuth variations, since they also can explain the observed Pg amplitude variations.

The observed variations of the velocities between the individual time- windows seem to be smaller. A clear velocity decrease is visible across the Pg coda and the Lg wave-train. Additional to this general trend, coherent energy with higher velocity can be seen inside the Pg coda. This could be attributed to onsets from waves reflected between surface and Moho at angles less than the critical angle. Before including these phases in the interpretation of crustal structure, the azimuth variations must be explained and their possible effects on the associated velocities must be estimated.

The onset of the Sn phase is characterized by a step in velocity to 4.5 km/sec (figure 7.6). The phase velocity of the following Sg phase is smaller than 4.0 km/sec. The derived velocities of Pn and Pg are 7.7 km/sec and 7.1 km/sec respectively.

The interpretation of the refraction seismic measurement by Miller and Gebrande (1976) for the international profile VII, which crosses the GERESS location from SW to NE, showed P-velocities of about 8.2 km/sec below the Moho. P wave velocity corresponds to an S-velocity of 4.7 km/sec assuming a fixed  $v_s$  to  $v_p$  ratio of  $\sqrt{3}$ . This S-velocity would be slightly higher than the phase velocity of 4.5 km/sec derived from the  $f,k$  analyses for the Sn phase.

The single  $f,k$  analysis of the time-window including the Pn phase and the corresponding beam are plotted in figure 7.7. The time function of the Pg impulse matches a 2nd order K pper impulse in the first approximation, whereas the time function of the Pn-onset resembles more closely a 1st order K pper impulse. If Pg is a diving wave, the Pg impulse would be proportional to the source function. With this assumption, Pn is a classical head wave with a time function like the integrated source function. The calculated Pn velocity of about 7.7 km/sec would be significantly smaller in this case than the expected velocity of 8.2 km/sec. On the other hand, this velocity would be consistent

with the Sn velocity of 4.5 km/sec by a fixed ratio of  $\sqrt{3}$ . Assuming Pg to be a refracted wave, the difference between the impulse of Pn and Pg cannot be explained.

The seismograms of the second event of 30.11.90 are plotted in figure 7.8. They were filtered from 0.8 to 4.0 Hz. The results of f,k analysis are shown in figure 7.9. The Pg wave-train is more complex than the one for the first event. The variations for the Lg/Pg amplitude ratio described above cannot be observed for this event.

The calculated azimuth values for the individual time-windows vary over a range of  $\pm 15^\circ$  around the mean value of  $206^\circ$  as observed for the first event. Deviations are, however, significantly smaller for the first 5 seconds after the beginning of the Pg wave-train. This indicates that influence of scattered energy increases in the course of the coda.

In contrast to the first event, no general increase in velocity along the Pg coda is observed, moreover, single bursts of coherent energy with increasing velocity towards the end of the Pg coda are significant. For the Lg wave-train, no definite velocity trend can be recognized.

The phase velocity of about 7.5 km/sec for the Pn phase could only be calculated by a time-window with individual length and a special frequency band because this phase is hardly visible. Onsets of Sn and Sg are not as clearly defined as the ones for the first event. The calculated velocities are 4.9 km/sec and 4.0 km/sec for the Sn and Sg phase, respectively.

### 7.3 ANALYSIS OF SYNTHETIC DATA

Synthetic seismograms were calculated with the reflectivity method for the station distribution of the GERESS array, disregarding differences in elevation. The model used is given in figure 7.10 (Campillo et al., 1984). The S velocity is derived from P velocities with the assumption of a fixed ratio of  $\sqrt{3}$ . The density is given by the Nafe-Drake relation (Talwani et al, 1950). An explosion source is used, which lies inside the first layer in the depth of 500 m. The time dependence of the source is given by a 2nd order Küpper impulse with a dominant period of 0.25 seconds. The distance between source and central station C2 is 150 km.



The unfiltered seismograms, convolved with the GS-13 characteristic are plotted in figure 7.12. The dominant onset in the seismograms are Rayleigh waves with a clear onset of that part of the surface waves, which can be described by the inverse part of the dispersion relation. After filtering the seismograms with a pass-band of 1 to 6 Hz (figure 7.13), the part of the surface waves with regular dispersion is no longer visible. The selected time-window of 1 second length for the f,k analysis would be too small for these waves. The amplitude spectrum of the seismogram of C2 is shown in figure 7.11. The frequency band selected for the f,k analysis extends from 1 to 6 Hz.

The variations in azimuth are about  $\pm 0.5^\circ$  around the theoretical value of  $360^\circ$  (figure 7.14). They must be due to superposition of coherent signals with different phase velocities inside the individual time-window and to the finite resolution in the wavenumber domain, since the f,k analysis technique was applied to synthetic seismograms without noise. The numbered onsets in figure 7.14 correspond to visible onsets in the seismograms.

Although the model is simple, the phase velocities cannot be completely explained by the theoretical travel-times because of their complexity. P wave travel-time curves are plotted in figure 7.15 for the direct wave, under- and overcritically reflected waves for each discontinuity, the corresponding head waves, as well as that waves which are reflected one and two times at the surface. The seismograms in figure 7.12 and 7.13 are shifted by 20 seconds compared to the travel-times in figure 7.15.

The first onset (1) will be generated by the head wave from the lowest discontinuity with a velocity of 8.2 km/sec. The calculated phase velocity is correct for the corresponding time-window, although the weaker head wave from the first discontinuity with a velocity of 4.5 km/sec, as well as the surface reflections not included in figure 7.15, arrive within the same time-window. The following dominant P wave-train will be generated by many onsets, as seen in figure 7.15 with velocities in the range from 6.0 km/sec to 6.7 km/sec. An example is the reflected wave from the lowest discontinuity with a phase velocity of 6.7 km/sec. The phase velocity, calculated with the f,k power spectrum for this time-window is about 6.6 km/sec. The onset (3) (figure 7.14), characterized by the increasing phase velocity from 6.4 km/sec to 8.1 km/sec is well recognizable in the seismograms. The arrival of the wave  $P_{41}$ , (reflected between surface and lowest discontinuity) and the wave  $P_{22}$  (reflected twice between surface and second discontinuity) (figure 7.15) with phase velocity between 8.2 km/sec and 7.0 km/sec respectively contribute among others to this

onset. In contrast to the real data, the velocity is significantly higher after this onset.

The arrival of the S waves (5, 6), characterized by a step in phase velocity to 4.5 km/sec, was not analyzed in detail using travel-times. Because the explosion source generates only P waves only, these arrivals must be P-SV-converted phases.

#### 7.4 CONCLUSIONS

It was shown for the two events analyzed, that phase velocities are different for the whole Pg coda and along the Lg wave-train. Future analysis of more events will be necessary to establish an azimuth-dependent trend and allow interpretation in terms of azimuth-dependent crustal models. Further investigations must explain azimuth scattering and the possible inaccuracy of the phase velocity determination. This concerns interpretation of the well-known phases recorded at regional distances like Pn, Pg, Sn, Sg and Lg but effects even stronger the interpretation of high velocity onsets inside the Pg coda. If heterogeneities lead to the azimuth variations, they offer the possibility to judge on models for describing these heterogeneities. The calculated mean azimuth seems to be a stable value especially for weak events. The velocity underneath the Moho deduced from Pn and Sn velocities seems to be smaller than expected from other investigations.

Analysis of the synthetic data showed, that visible onsets in the seismograms are always composed of pulses of coherent energy with different phase velocity. This inaccuracy, however, is an order of magnitude below the azimuth variations observed in natural events and thus cannot be used in their explanation.

Nicolai Gestermann

## REFERENCES

Campillo, M., M. Bouchon, and B. Massinon (1984). The theoretical study of the excitation, spectral characteristics, and geometrical attenuation of regional seismic phases, *Bull. Seism. Soc. Am.*, 74, 79-90.

Capon, J. (1973). Signal processing and frequency-wavenumber spectrum analysis for a large aperture seismic array. *Methods in Computational Physics*, Vol. 13, 2-59, Academic Press.

Harjes, H.-P. (1990). Design and siting of a new regional array in central Europe, *Bull. Seism. Soc. Am.*, 80, Part B, 1801-1817.

Kvaerna, T. and F. Ringdal (1986). Stability of various F-K estimation techniques, in: *NORSAR Semiannual Technical Summary*, 1-86/87, Kjeller, Norway, 29-40.

Kvaerna, T. (1987). Wide-band slowness estimation using a small aperture seismic array, in: *NORSAR Semiannual Technical Summary*, 2-86/87, Kjeller, Norway, 29-40.

Miller, H. and H. Gebrande (1976). Crustal structure in Southeastern Bavaria derived from seismic-refraction measurements by ray-tracing methods. In: *Explosion Seismology in Central Europe*. Editor P. Giese, C. Prodehl, A. Stein. Springer, 339-346.

Talwani, M., Sutton, G. H., Worzel, J. L. (1959). A crustal section across the Puerto Rico Trench. *J. Geophys. Res.* 64, 1545-1555.

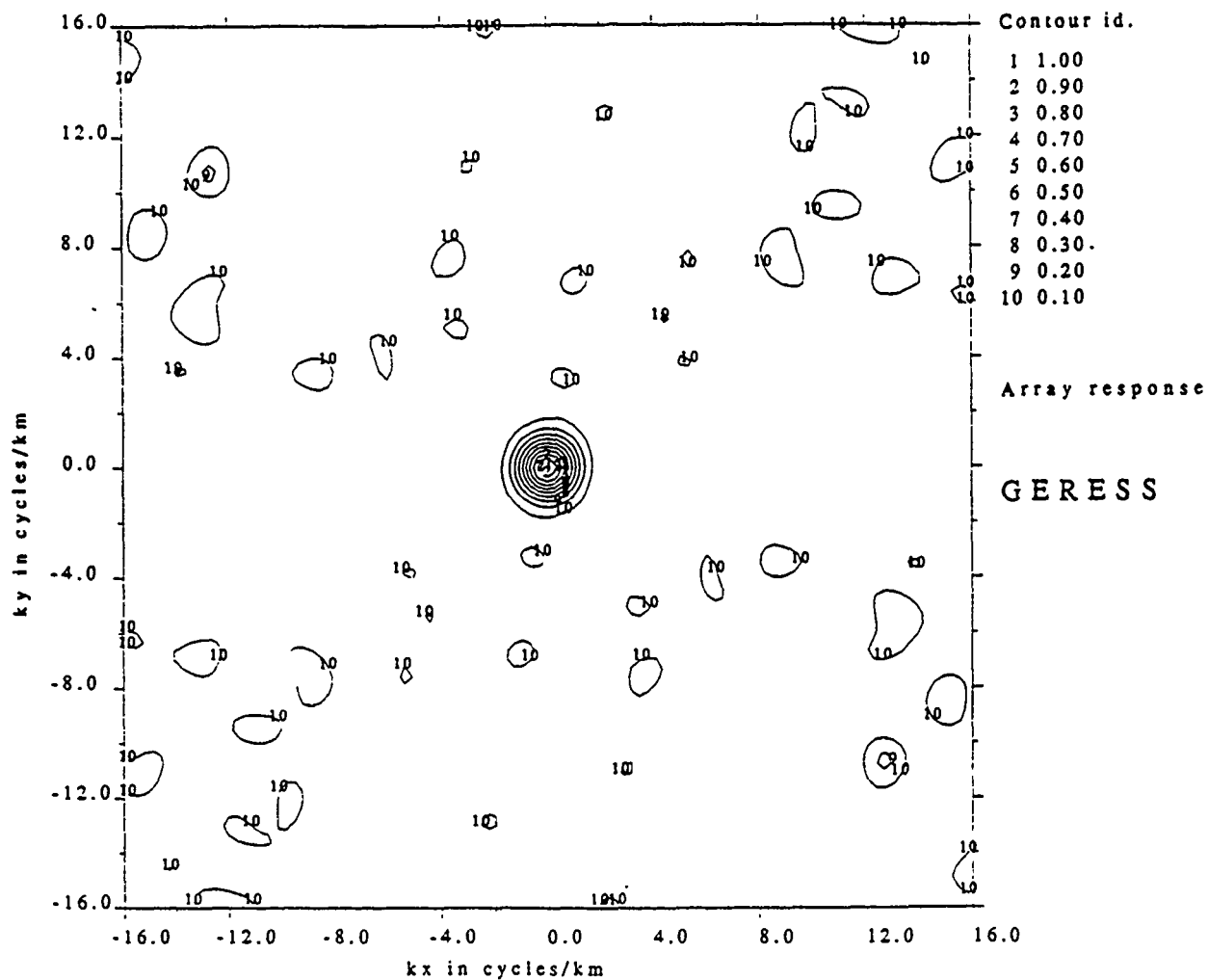


Figure 7.1 Wavenumber characteristics of the GERESS array.

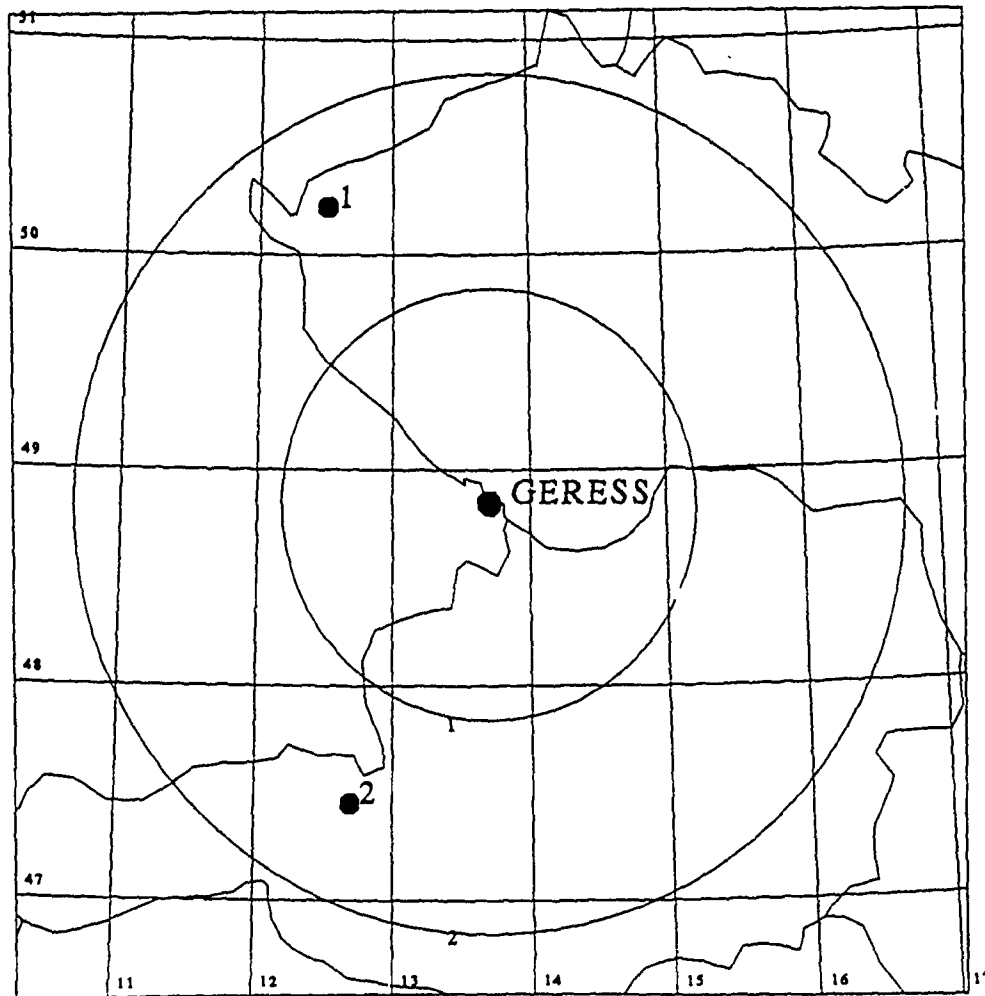


Figure 7.2 Epicenter map of the events used in this study (table 7.1)

	date	first arrival	origin time	$\Delta$ [km]	back-az. [deg]	coordinates	magnitude $m_L$
1.	15.01.91	11:03:58.9 Pn	11:03:29.4	176	331	50.22N 12.51E	1.7
2.	30.11.90	15:44:26.5 Pn	15:43:52.0	172	206	47.46N 12.69E	1.9

Table 7.1 List of events used for the f,k-analysis. The data refer to the central station GEC2.

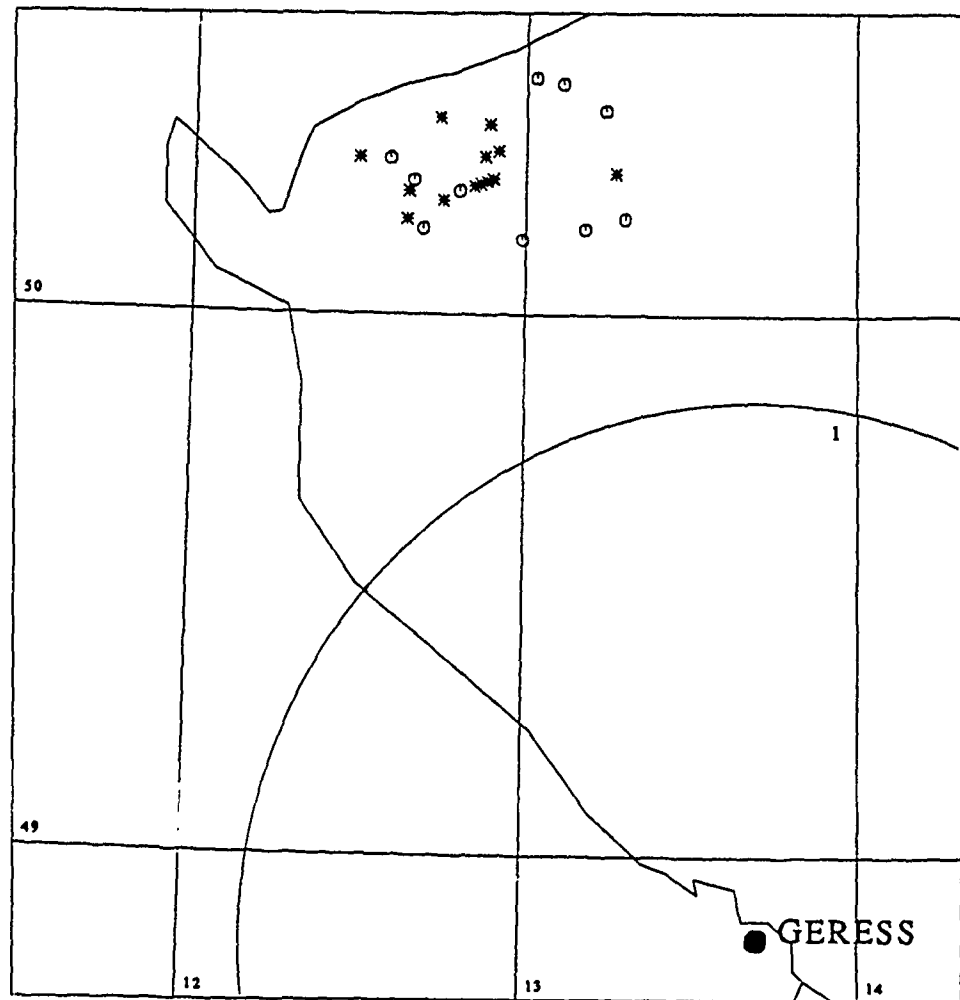


Figure 7.3 Events located by GERESS during the week from 26.11-2.12.90 and known mine locations in the north-eastern part of CSFR.

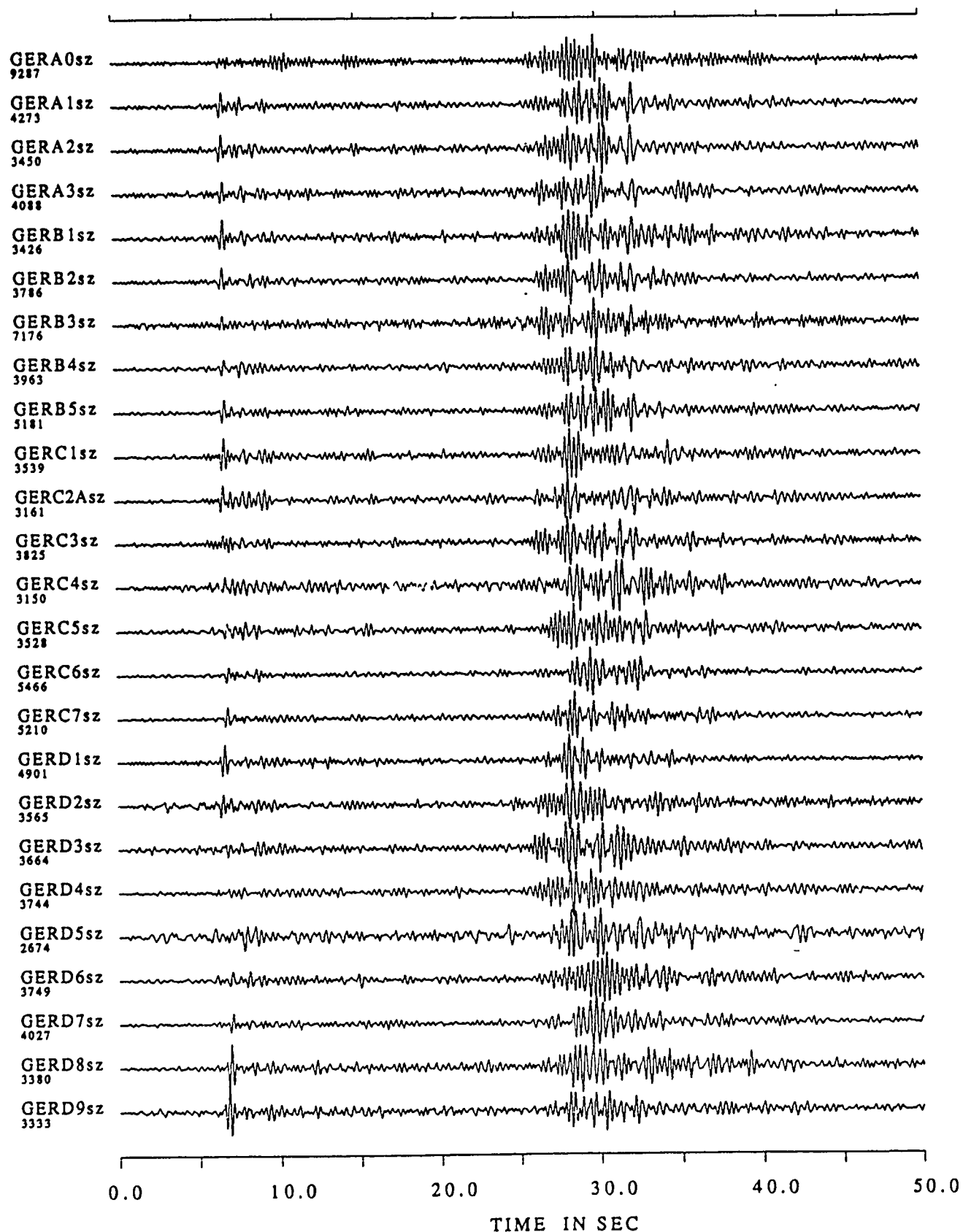


Figure 7.4 Waveforms of the 1. event from table 7.1. Traces were filtered with a bandpass between 0.8-4.0 Hz.

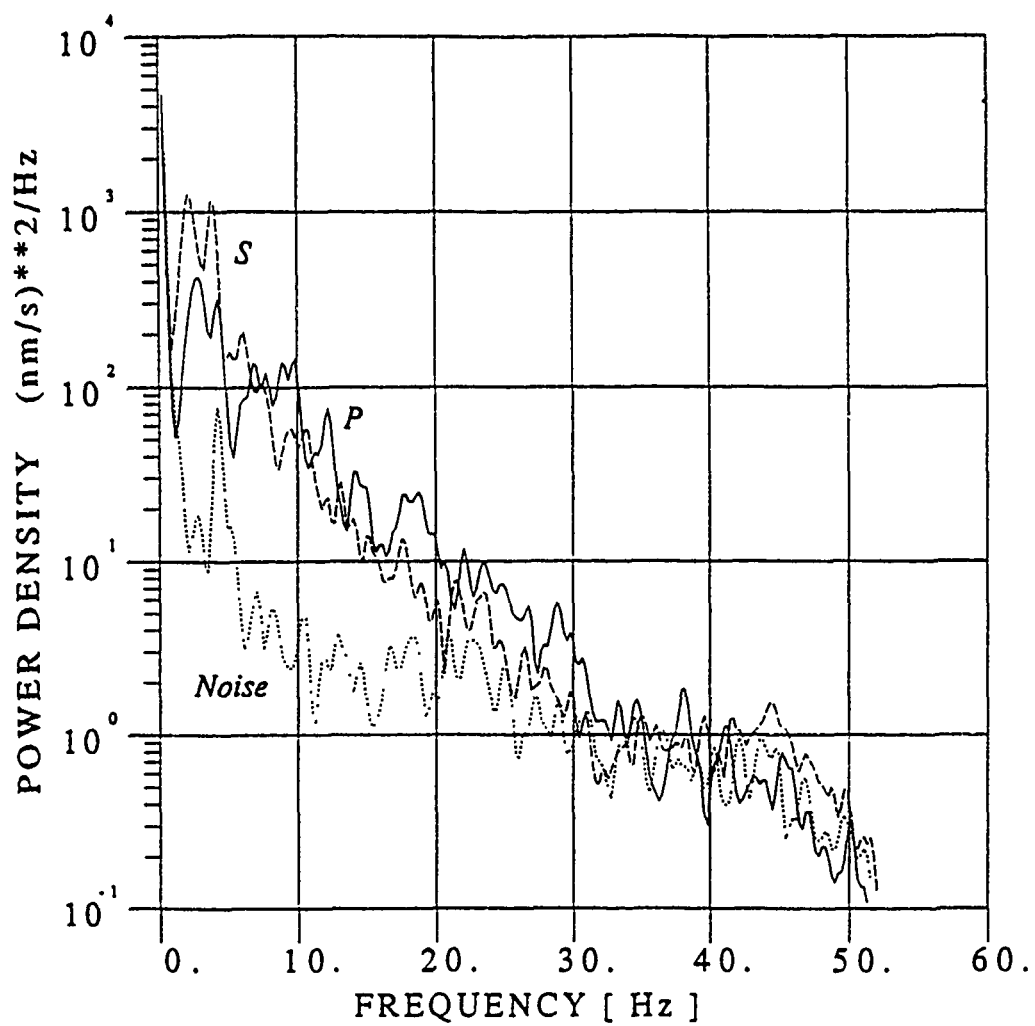


Figure 7.5 Velocity power spectra for time windows containing P and S energy, and for a time window with noise before the first onset.



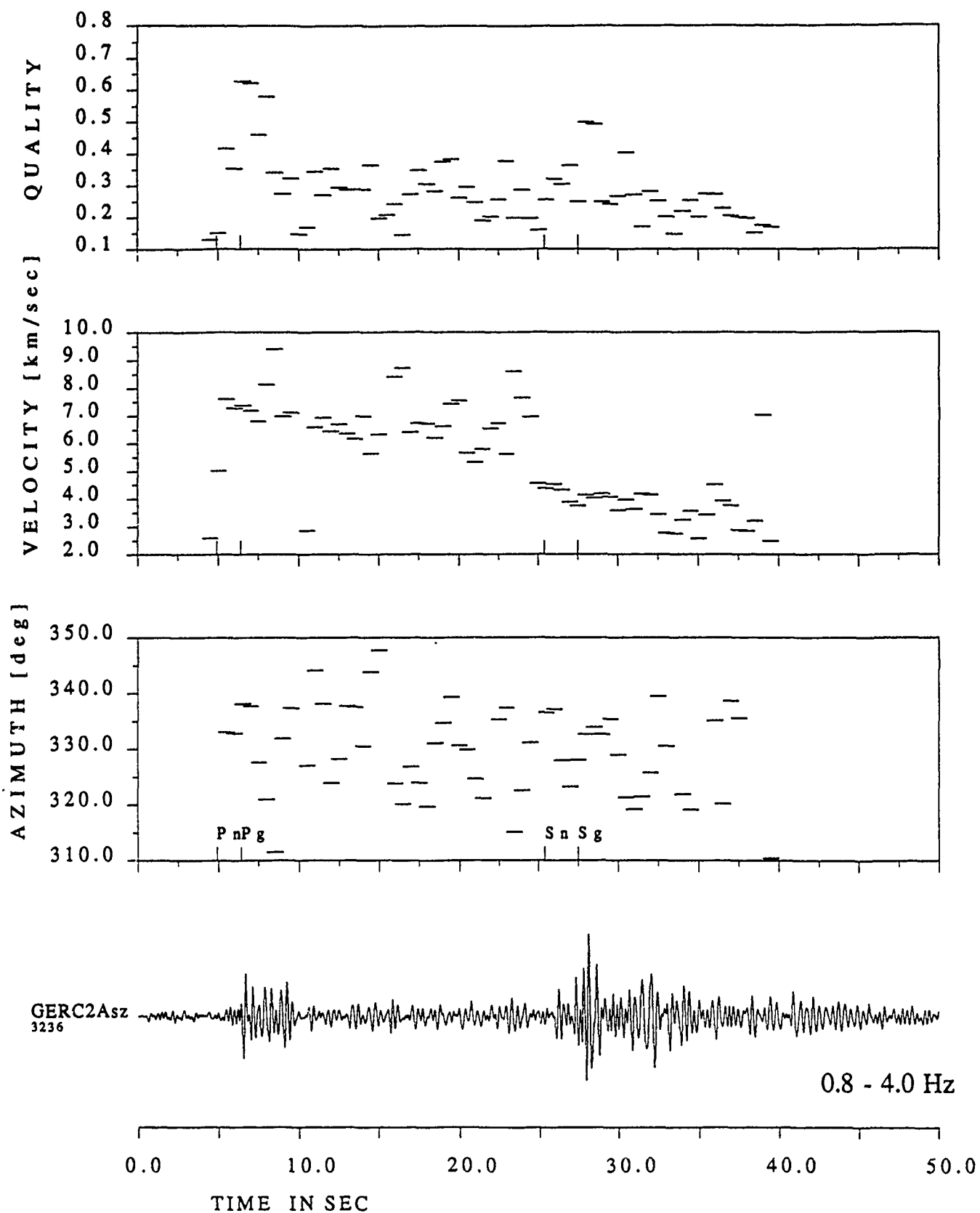


Figure 7.6 Results of the f,k-analysis for the moving time windows of event 1.

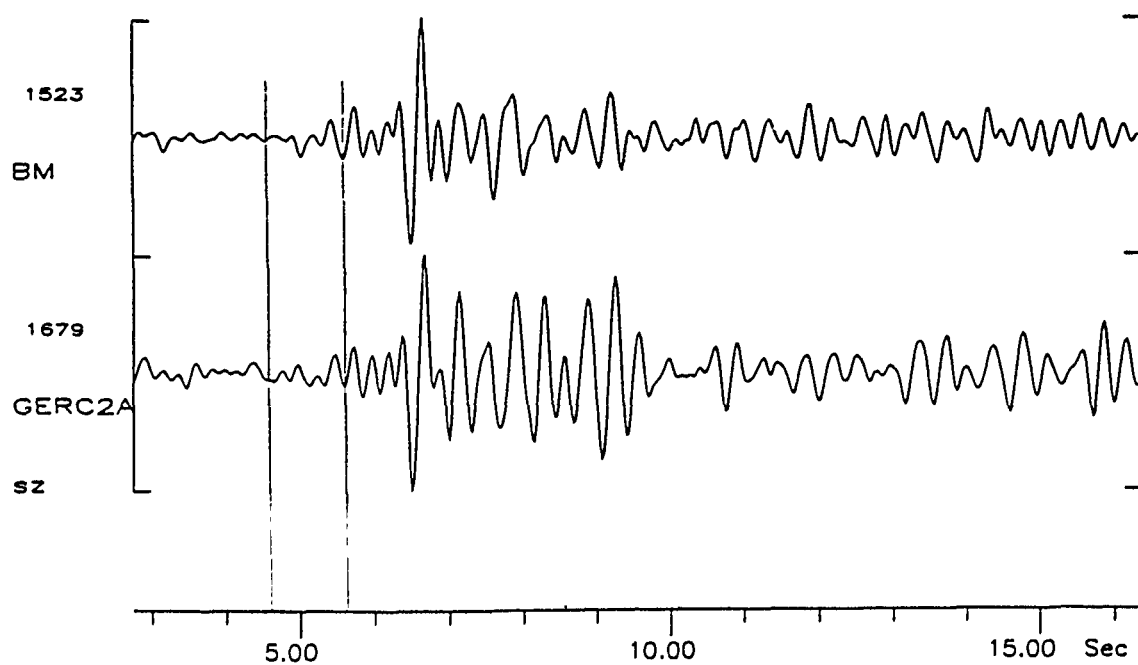
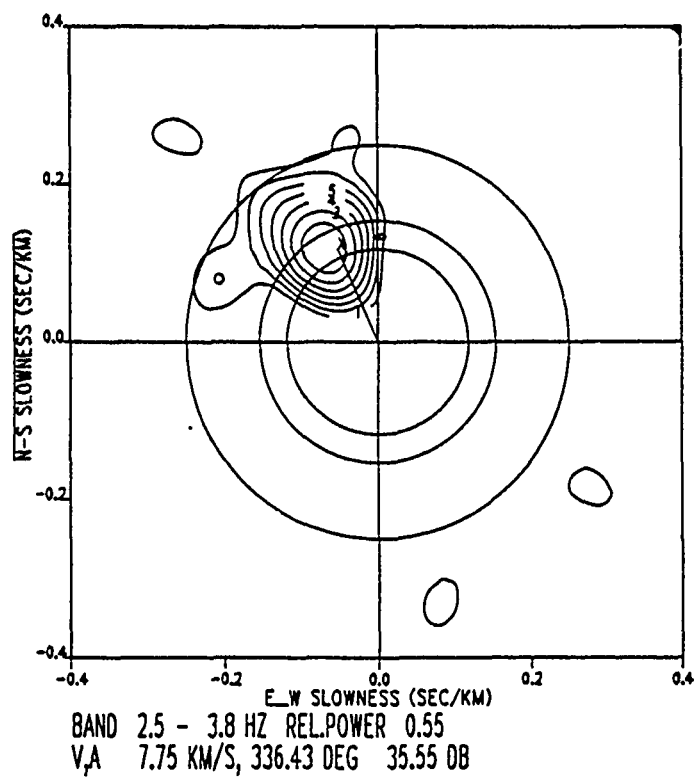


Figure 7.7 F,k analysis for the time window (1 second) containing the Pn onset (top). The calculated beam is displayed together with the waveform of station C2 (bottom).

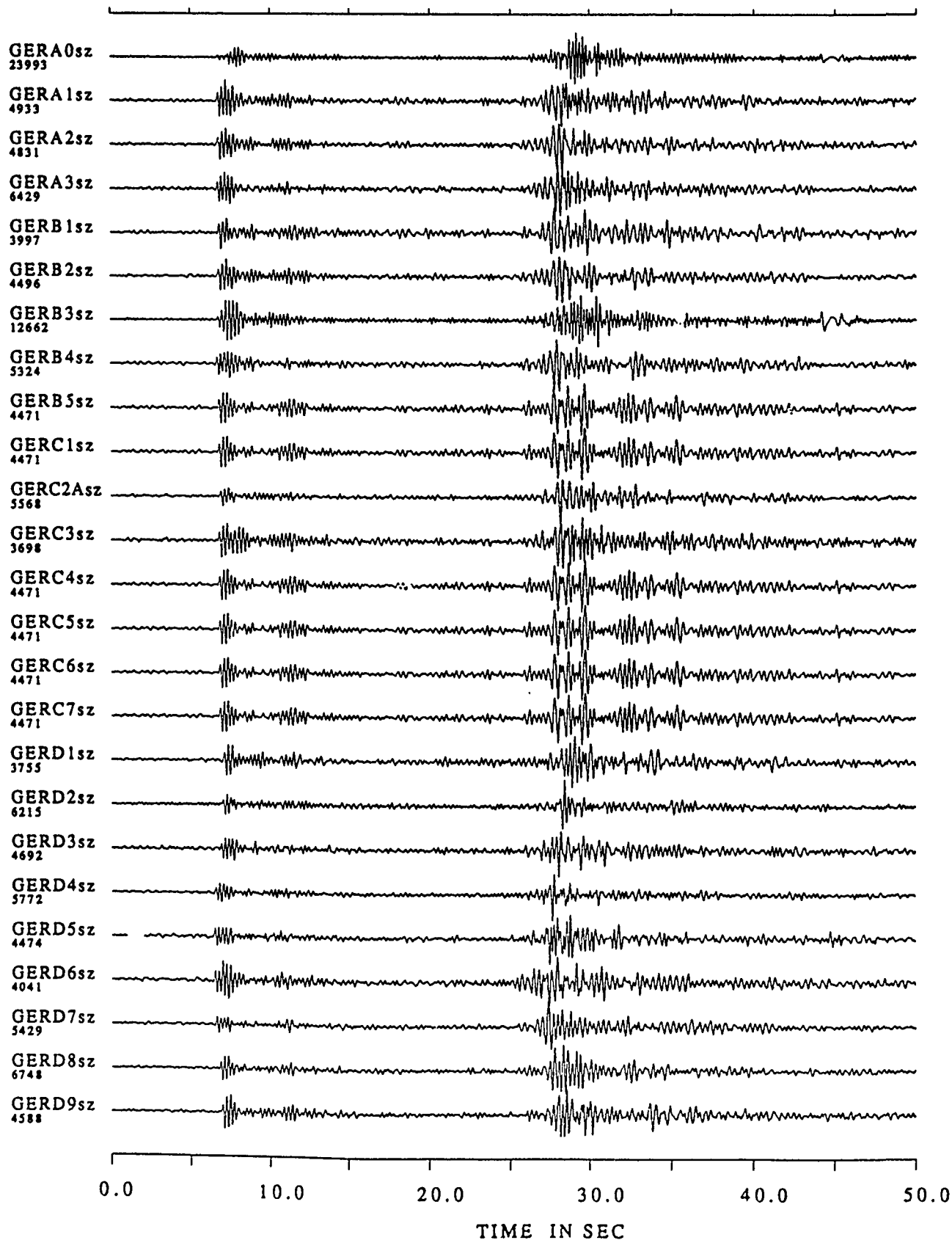


Figure 7.8 Waveform of the 2nd event from table 7.1. Traces are filtered with a bandpass from 0.8-4.0 Hz.

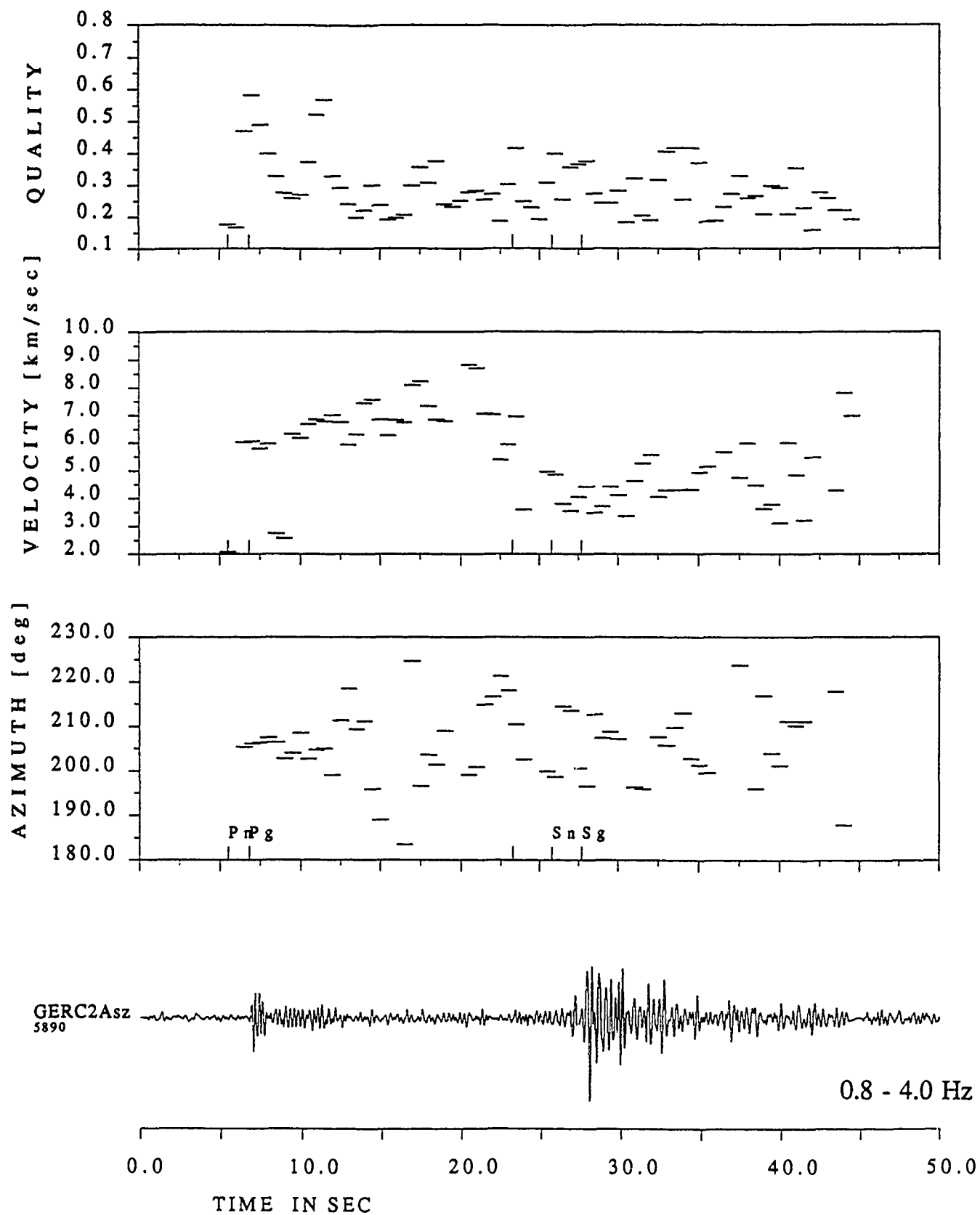


Figure 7.9 Results of the f,k-analysis for the moving time windows of event 2.

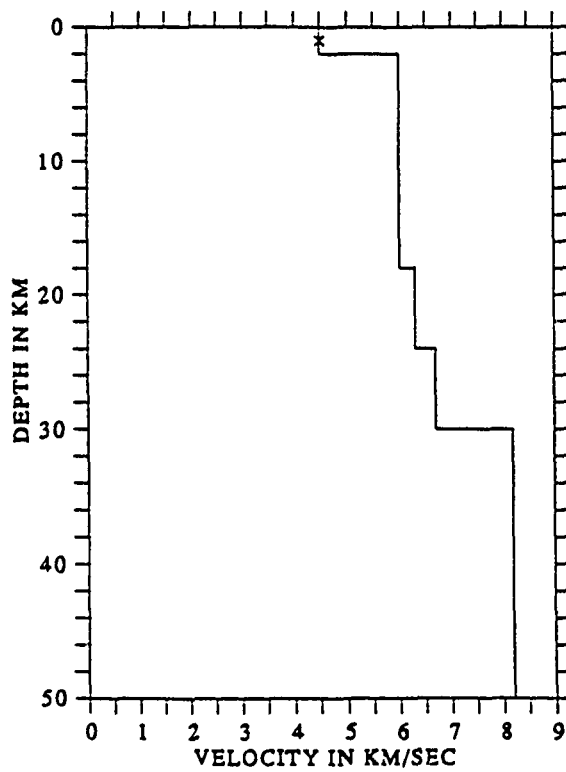


Figure 7.10 P-velocity versus depth function used for calculating synthetic seismograms.

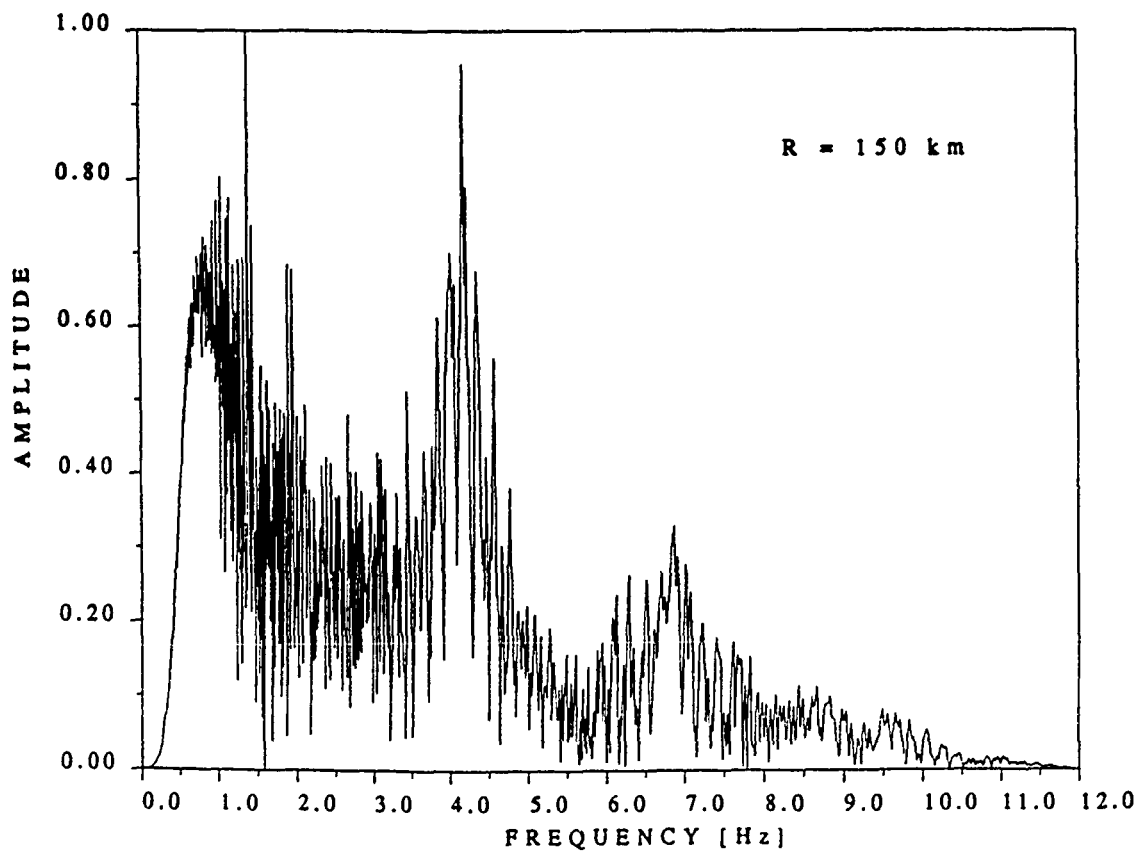


Figure 7.11 Normalized amplitude spectrum for the synthetic seismograms of station C2 in figure 7.12.

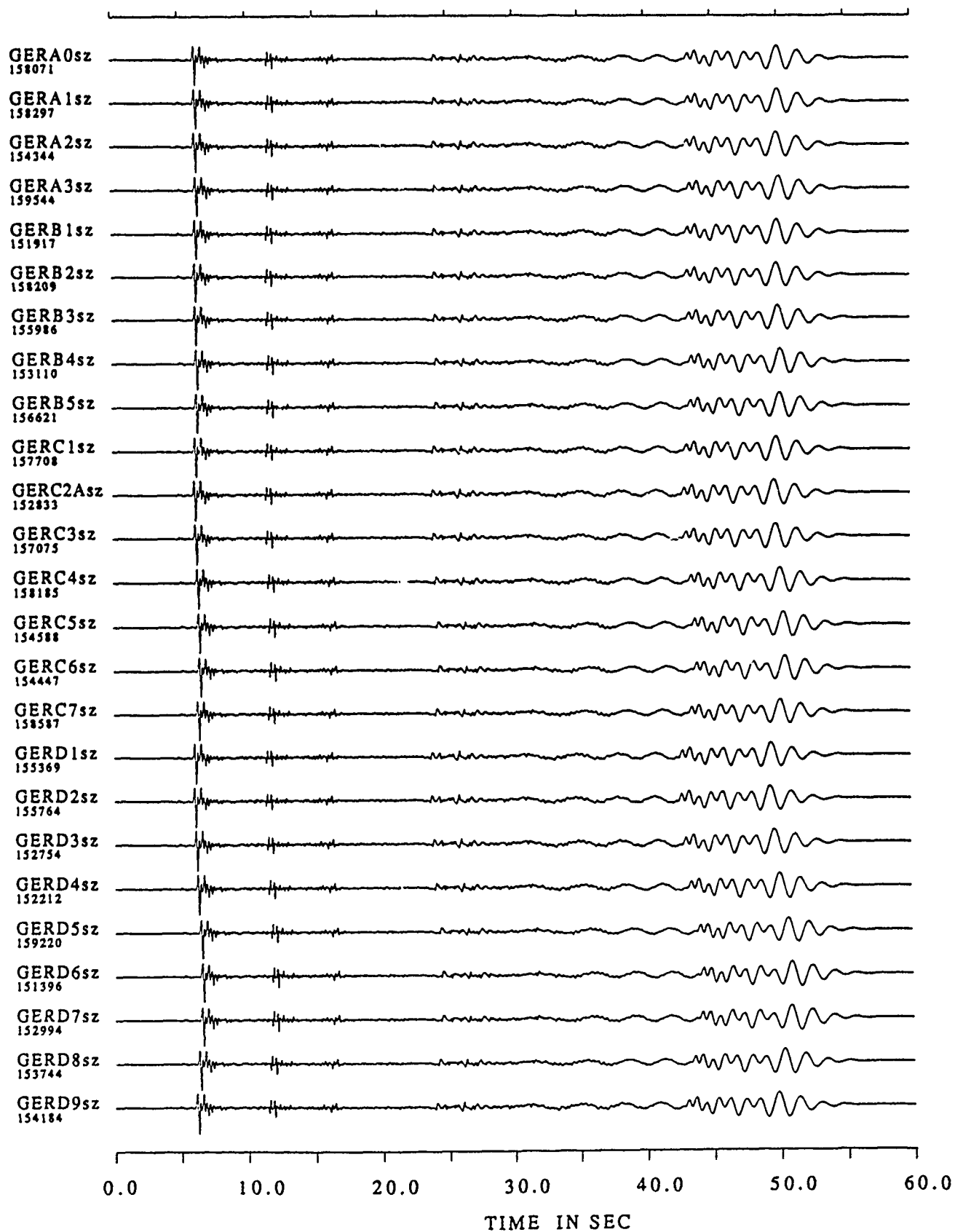


Figure 7.12 Synthetic seismograms (vertical component) calculated for the model in figure 7.10.

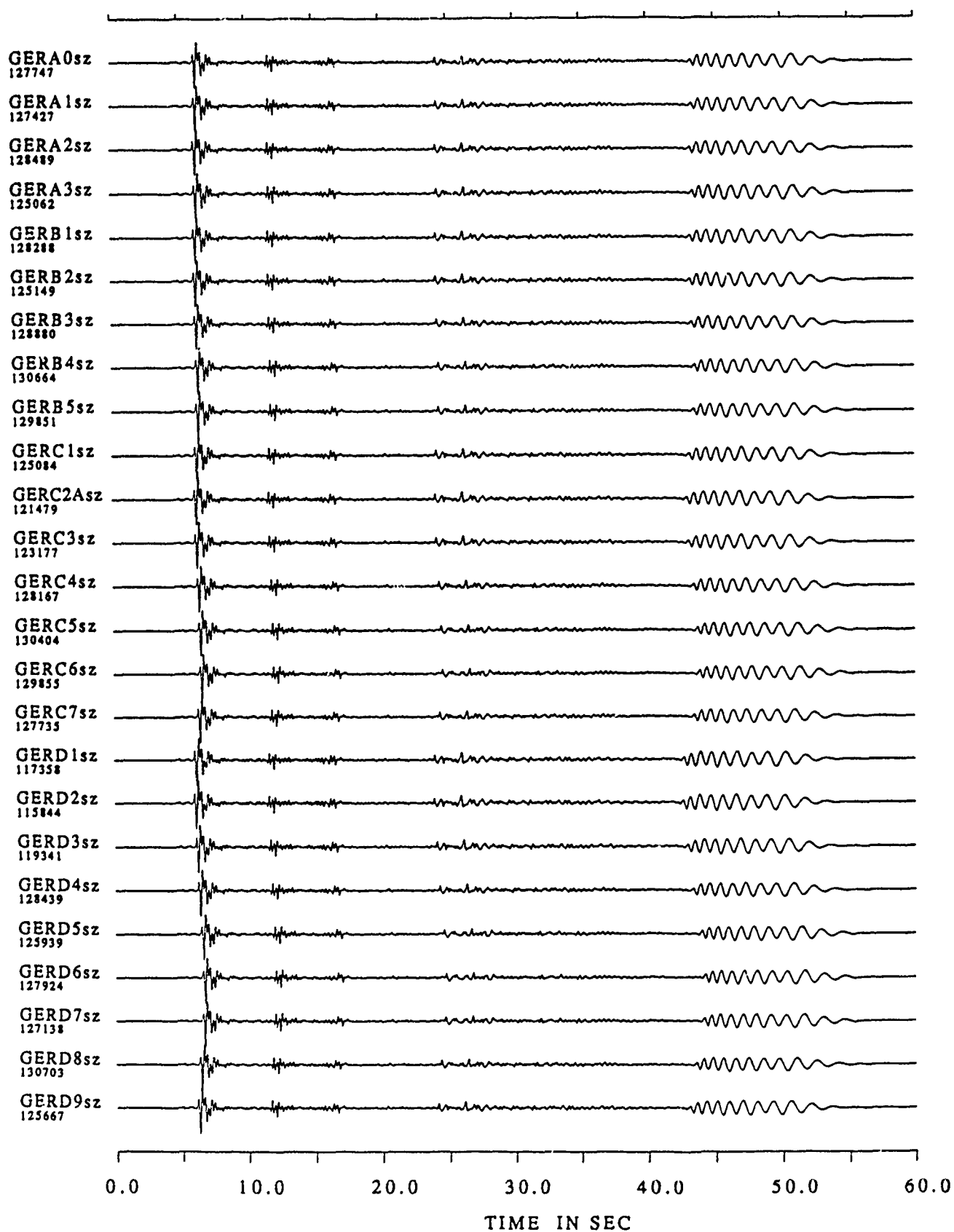


Figure 7.13 Synthetic seismograms (vertical component) of figure 7.12, filtered with a bandpass from 1 - 6 Hz.

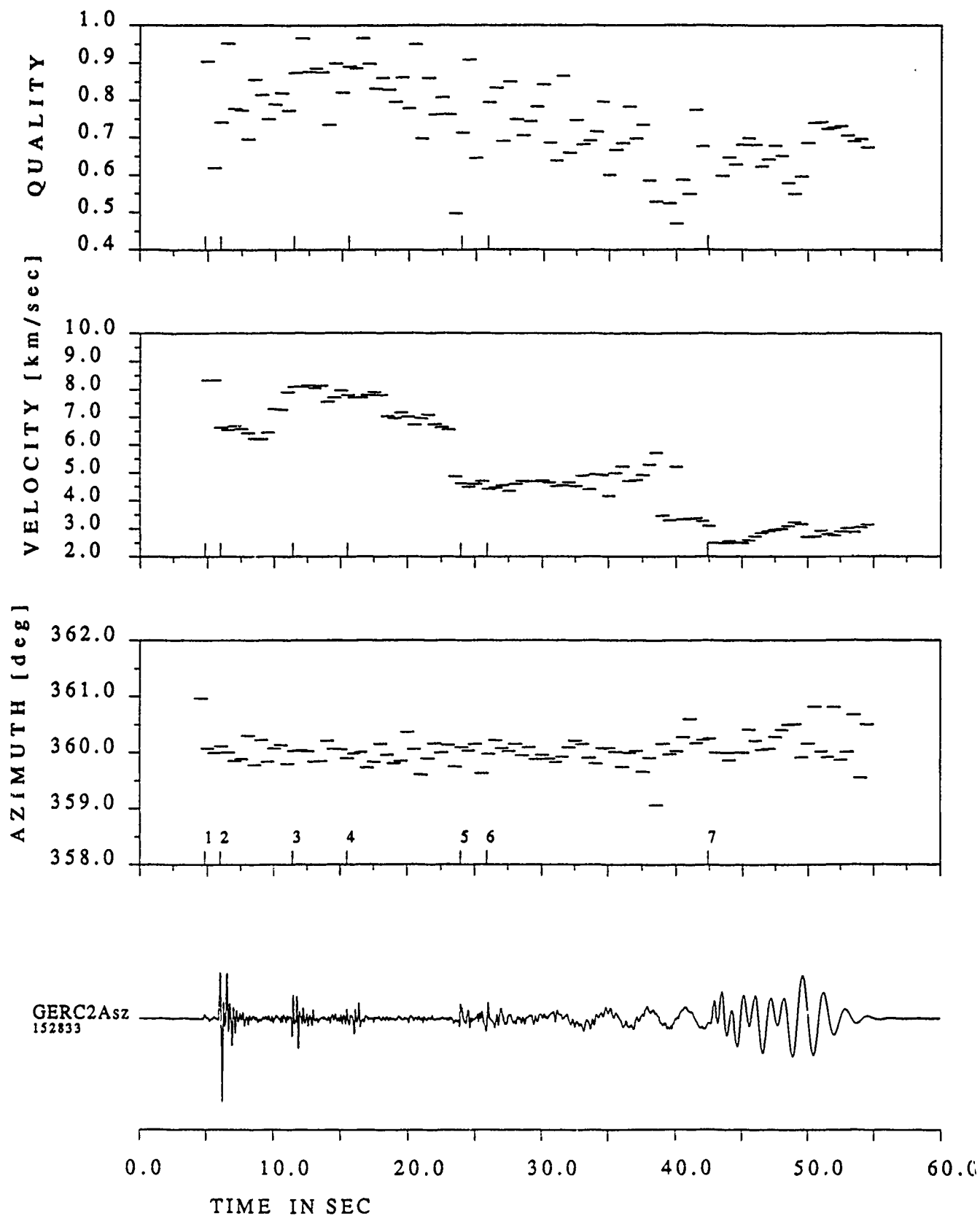


Figure 7.14 Results of the f,k-analysis for the synthetic seismograms from figure 7.12.



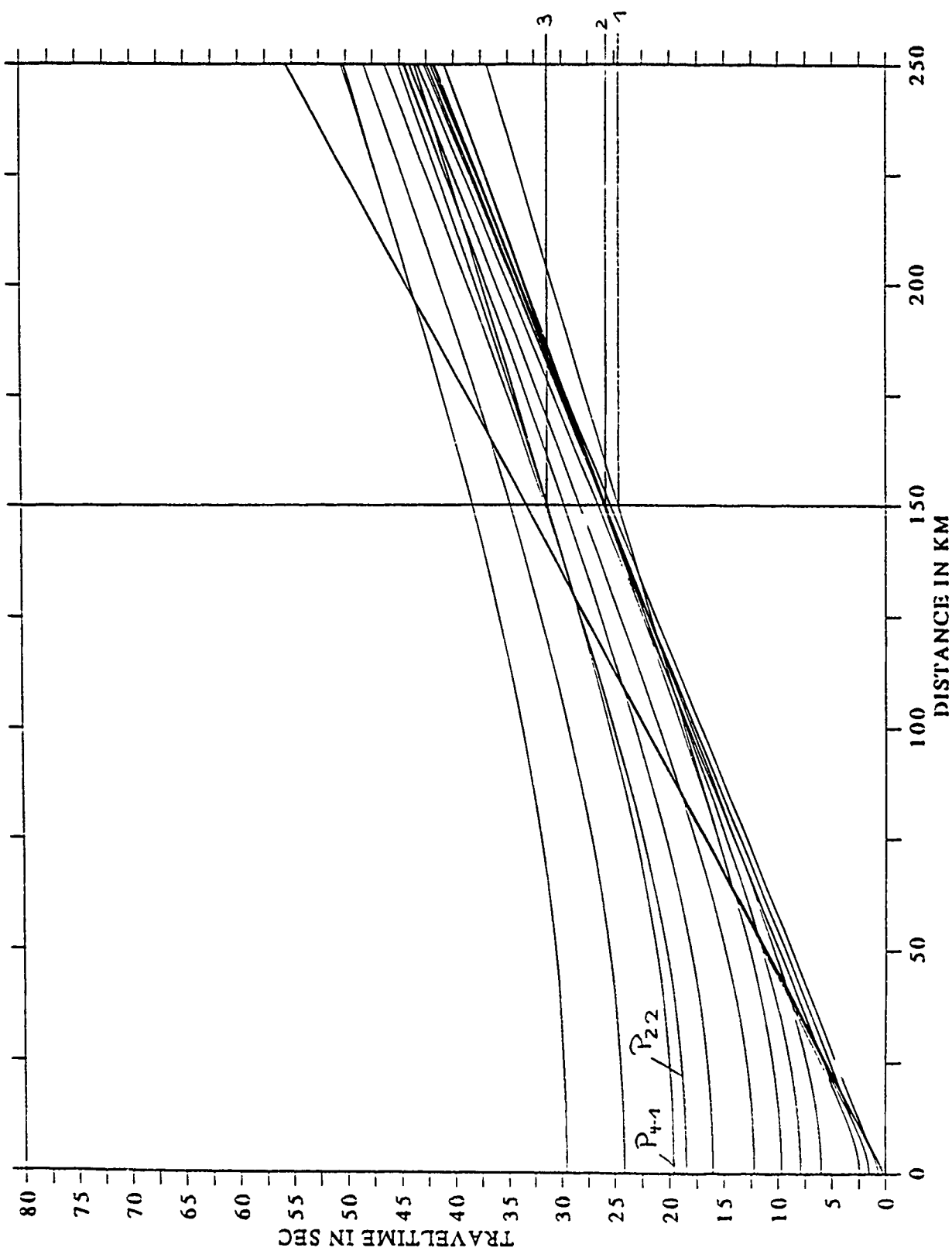


Figure 7.15 Theoretical P wave traveltimes for the velocity model in figure 7.10.

CONTRACTORS (United States)

Prof. Thomas Ahrens  
Seismological Lab, 252-21  
Division of Geological & Planetary Sciences  
California Institute of Technology  
Pasadena, CA 91125

Prof. Charles B. Archambeau  
CIRES  
University of Colorado  
Boulder, CO 80309

Dr. Thomas C. Bache, Jr.  
Science Applications Int'l Corp.  
10260 Campus Point Drive  
San Diego, CA 92121 (2 copies)

Prof. Muawia Barazangi  
Institute for the Study of the Continent  
Cornell University  
Ithaca, NY 14853

Dr. Jeff Barker  
Department of Geological Sciences  
State University of New York  
at Binghamton  
Vestal, NY 13901

Dr. Douglas R. Baumgardt  
ENSCO, Inc  
5400 Port Royal Road  
Springfield, VA 22151-2388

Prof. Jonathan Berger  
IGPP, A-025  
Scripps Institution of Oceanography  
University of California, San Diego  
La Jolla, CA 92093

Dr. Gilbert A. Bollinger  
Department of Geological Sciences  
Virginia Polytechnical Institute  
21044 Derring Hall  
Blacksburg, VA 24061

Dr. Lawrence J. Burdick  
Woodward-Clyde Consultants  
566 El Dorado Street  
Pasadena, CA 91109-3245

Dr. Jerry Carter  
Center for Seismic Studies  
1300 North 17th St., Suite 1450  
Arlington, VA 22209-2308

Prof. Vernon F. Cormier  
Department of Geology & Geophysics  
U-45, Room 207  
The University of Connecticut  
Storrs, CT 06268

Professor Anton W. Dainty  
Earth Resources Laboratory  
Massachusetts Institute of Technology  
42 Carleton Street  
Cambridge, MA 02142

Prof. Steven Day  
Department of Geological Sciences  
San Diego State University  
San Diego, CA 92182

Dr. Zoltan A. Der  
ENSCO, Inc.  
5400 Port Royal Road  
Springfield, VA 22151-2388

Prof. Lewis M. Duncan  
Dept. of Physics & Astronautics  
Clemson University  
Clemson, SC 29634-1901

Prof. John Ferguson  
Center for Lithospheric Studies  
The University of Texas at Dallas  
P.O. Box 830688  
Richardson, TX 75083-0688

Dr. Mark D. Fisk  
Mission Research Corporation  
735 State Street  
P. O. Drawer 719  
Santa Barbara, CA 93102

Prof. Stanley Flatte  
Applied Sciences Building  
University of California  
Santa Cruz, CA 95064

Dr. Alexander Florence  
SRI International  
333 Ravenswood Avenue  
Menlo Park, CA 94025-3493

Dr. Clifford Frohlich  
Institute of Geophysics  
8701 North Mopac  
Austin, TX 78759

Dr. Holy K. Given  
IGPP, A-025  
Scripps Institute of Oceanography  
University of California, San Diego  
La Jolla, CA 92093

Prof. Henry L. Gray  
Vice Provost and Dean  
Department of Statistical Sciences  
Southern Methodist University  
Dallas, TX 75275

Dr. Indra Gupta  
Teledyne Geotech  
314 Montgomery Street  
Alexandria, VA 22314

Prof. David G. Harkrider  
Seismological Laboratory  
Division of Geological & Planetary Sciences  
California Institute of Technology  
Pasadena, CA 91125

Prof. Danny Harvey  
CIRES  
University of Colorado  
Boulder, CO 80309

Prof. Donald V. Helmberger  
Seismological Laboratory  
Division of Geological & Planetary Sciences  
California Institute of Technology  
Pasadena, CA 91125

Prof. Eugene Herrin  
Institute for the Study of Earth and Man  
Geophysical Laboratory  
Southern Methodist University  
Dallas, TX 75275

Prof. Bryan Isacks  
Cornell University  
Department of Geological Sciences  
SNEE Hall  
Ithaca, NY 14850

Dr. Rong-Song Jih  
Teledyne Geotech  
314 Montgomery Street  
Alexandria, VA 22314

Prof. Lane R. Johnson  
Seismographic Station  
University of California  
Berkeley, CA 94720

Dr. Richard LaCoss  
MIT-Lincoln Laboratory  
M-200B  
P. O. Box 73  
Lexington, MA 02173-0073 (3 copies)

Prof. Fred K. Lamb  
University of Illinois at Urbana-Champaign  
Department of Physics  
1110 West Green Street  
Urbana, IL 61801

Prof. Charles A. Langston  
Geosciences Department  
403 Deike Building  
The Pennsylvania State University  
University Park, PA 16802

Prof. Thorne Lay  
Institute of Tectonics  
Earth Science Board  
University of California, Santa Cruz  
Santa Cruz, CA 95064

Prof. Arthur Lerner-Lam  
Lamont-Doherty Geological Observatory  
of Columbia University  
Palisades, NY 10964

Dr. Christopher Lynnes  
Teledyne Geotech  
314 Montgomery Street  
Alexandria, VA 22314

Prof. Peter Malin  
Department of Geology  
Old Chemistry Bldg.  
Duke University  
Durham, NC 27706

Dr. Randolph Martin, III  
New England Research, Inc.  
76 Olcott Drive  
White River Junction, VT 05001

Prof. Thomas V. McEvilly  
Seismographic Station  
University of California  
Berkeley, CA 94720

Dr. Keith L. McLaughlin  
S-CUBED  
A Division of Maxwell Laboratory  
P.O. Box 1620  
La Jolla, CA 92038-1620

Prof. William Menke  
Lamont-Doherty Geological Observatory  
of Columbia University  
Palisades, NY 10964

Stephen Miller  
SRI International  
333 Ravenswood Avenue  
Box AF 116  
Menlo Park, CA 94025-3493

Prof. Bernard Minster  
IGPP, A-025  
Scripps Institute of Oceanography  
University of California, San Diego  
La Jolla, CA 92093

Prof. Brian J. Mitchell  
Department of Earth & Atmospheric Sciences  
St. Louis University  
St. Louis, MO 63156

Mr. Jack Murphy  
S-CUBED, A Division of Maxwell Laboratory  
11800 Sunrise Valley Drive  
Suite 1212  
Reston, VA 22091 (2 copies)

Prof. John A. Orcutt  
IGPP, A-025  
Scripps Institute of Oceanography  
University of California, San Diego  
La Jolla, CA 92093

Prof. Keith Priestley  
University of Cambridge  
Bullard Labs, Dept. of Earth Sciences  
Madingley Rise, Madingley Rd.  
Cambridge CB3 0EZ; ENGLAND

Dr. Jay J. Pulli  
Radix Systems, Inc.  
2 Taft Court, Suite 203  
Rockville, MD 20850

Prof. Paul G. Richards  
Lamont Doherty Geological Observatory  
of Columbia University  
Palisades, NY 10964

Dr. Wilmer Rivers  
Teledyne Geotech  
314 Montgomery Street  
Alexandria, VA 22314

Prof. Charles G. Sammis  
Center for Earth Sciences  
University of Southern California  
University Park  
Los Angeles, CA 90089-0741

Prof. Christopher H. Scholz  
Lamont-Doherty Geological Observatory  
of Columbia University  
Palisades, NY 10964

Thomas J. Sereno, Jr.  
Science Application Int'l Corp.  
10260 Campus Point Drive  
San Diego, CA 92121

Prof. David G. Simpson  
Lamont-Doherty Geological Observatory  
of Columbia University  
Palisades, NY 10964

Dr. Jeffrey Stevens  
S-CUBED  
A Division of Maxwell Laboratory  
P.O. Box 1620  
La Jolla, CA 92038-1620

Prof. Brian Stump  
Institute for the Study of Earth & Man  
Geophysical Laboratory  
Southern Methodist University  
Dallas, TX 75275

Prof. Jeremiah Sullivan  
University of Illinois at Urbana-Champaign  
Department of Physics  
1110 West Green Street  
Urbana, IL 61801

Prof. Clifford Thurber  
University of Wisconsin-Madison  
Department of Geology & Geophysics  
1215 West Dayton Street  
Madison, WI 53706

Prof. M. Nafi Toksoz  
Earth Resources Lab  
Massachusetts Institute of Technology  
42 Carleton Street  
Cambridge, MA 02142

Prof. John E. Vidale  
University of California at Santa Cruz  
Seismological Laboratory  
Santa Cruz, CA 95064

Prof. Terry C. Wallace  
Department of Geosciences  
Building #77  
University of Arizona  
Tucson, AZ 85721

Dr. William Wortman  
Mission Research Corporation  
8560 Cinderbed Rd.  
Suite # 700  
Newington, VA 22122

Prof. Francis T. Wu  
Department of Geological Sciences  
State University of New York  
at Binghamton  
Vestal, NY 13901

OTHERS (United States)

Dr. Monem Abdel-Gawad  
Rockwell International Science Center  
1049 Camino Dos Rios  
Thousand Oaks, CA 91360

Michael Browne  
Teledyne Geotech  
3401 Shiloh Road  
Garland, TX 75041

Prof. Keiiti Aki  
Center for Earth Sciences  
University of Southern California  
University Park  
Los Angeles, CA 90089-0741

Mr. Roy Burger  
1221 Serry Road  
Schenectady, NY 12309

Prof. Shelton S. Alexander  
Geosciences Department  
403 Deike Building  
The Pennsylvania State University  
University Park, PA 16802

Dr. Robert Burrige  
Schlumberger-Doll Research Center  
Old Quarry Road  
Ridgefield, CT 06877

Dr. Kenneth Anderson  
BBNSTC  
Mail Stop 14/1B  
Cambridge, MA 02238

Dr. W. Winston Chan  
Teledyne Geotech  
314 Montgomery Street  
Alexandria, VA 22314-1581

Dr. Ralph Archuleta  
Department of Geological Sciences  
University of California at Santa Barbara  
Santa Barbara, CA 93102

Dr. Theodore Cherry  
Science Horizons, Inc.  
710 Encinitas Blvd., Suite 200  
Encinitas, CA 92024 (2 copies)

Dr. Susan Beck  
Department of Geosciences  
Bldg. # 77  
University of Arizona  
Tucson, AZ 85721

Prof. Jon F. Claerbout  
Department of Geophysics  
Stanford University  
Stanford, CA 94305

Dr. T.J. Bennett  
S-CUBED  
A Division of Maxwell Laboratory  
11800 Sunrise Valley Drive, Suite 1212  
Reston, VA 22091

Prof. Robert W. Clayton  
Seismological Laboratory  
Division of Geological & Planetary Sciences  
California Institute of Technology  
Pasadena, CA 91125

Mr. William J. Best  
907 Westwood Drive  
Vienna, VA 22180

Prof. F. A. Dahlen  
Geological and Geophysical Sciences  
Princeton University  
Princeton, NJ 08544-0636

Dr. N. Biswas  
Geophysical Institute  
University of Alaska  
Fairbanks, AK 99701

Mr. Charles Doll  
Earth Resources Laboratory  
Massachusetts Institute of Technology  
42 Carleton St.  
Cambridge, MA 02142

Dr. Stephen Bratt  
Center for Seismic Studies  
1300 North 17th Street  
Suite 1450  
Arlington, VA 22209

Prof. Adam Dziewonski  
Hoffman Laboratory, Harvard Univ.  
Dept. of Earth Atmos. & Planetary Sciences  
20 Oxford St  
Cambridge, MA 02138

Prof. John Ebel  
Department of Geology & Geophysics  
Boston College  
Chestnut Hill, MA 02167

Eric Fielding  
SNEE Hall  
INSTOC  
Cornell University  
Ithaca, NY 14853

Dr. John Foley  
Phillips Laboratory/LWH  
Hanscom AFB, MA 01731-5000

Prof. Donald Forsyth  
Department of Geological Sciences  
Brown University  
Providence, RI 02912

Dr. Anthony Gangi  
Texas A&M University  
Department of Geophysics  
College Station, TX 77843

Dr. Freeman Gilbert  
IGPP, A-025  
Scripps Institute of Oceanography  
University of California  
La Jolla, CA 92093

Mr. Edward Giller  
Pacific Sierra Research Corp.  
1401 Wilson Boulevard  
Arlington, VA 22209

Dr. Jeffrey W. Given  
SAIC  
10260 Campus Point Drive  
San Diego, CA 92121

Prof. Stephen Grand  
University of Texas at Austin  
Department of Geological Sciences  
Austin, TX 78713-7909

Prof. Roy Greenfield  
Geosciences Department  
403 Deike Building  
The Pennsylvania State University  
University Park, PA 16802

Dan N. Hagedorn  
Battelle  
Pacific Northwest Laboratories  
Battelle Boulevard  
Richland, WA 99352

Dr. James Hannon  
Lawrence Livermore National Laboratory  
P. O. Box 808  
Livermore, CA 94550

Prof. Robert B. Herrmann  
Dept. of Earth & Atmospheric Sciences  
St. Louis University  
St. Louis, MO 63156

Ms. Heidi Houston  
Seismological Laboratory  
University of California  
Santa Cruz, CA 95064

Kevin Hutchenson  
Department of Earth Sciences  
St. Louis University  
3507 Laclede  
St. Louis, MO 63103

Dr. Hans Israelsson  
Center for Seismic Studies  
1300 N. 17th Street, Suite 1450  
Arlington, VA 22209-2308

Prof. Thomas H. Jordan  
Department of Earth, Atmospheric  
and Planetary Sciences  
Massachusetts Institute of Technology  
Cambridge, MA 02139

Prof. Alan Kafka  
Department of Geology & Geophysics  
Boston College  
Chestnut Hill, MA 02167

Robert C. Kemerait  
ENSCO, Inc.  
445 Pineda Court  
Melbourne, FL 32940

William Kikendall  
Teledyne Geotech  
3401 Shiloh Road  
Garland, TX 75041

Prof. Leon Knopoff  
University of California  
Institute of Geophysics & Planetary Physics  
Los Angeles, CA 90024

Prof. Jack Oliver  
Department of Geology  
Cornell University  
Ithaca, NY 14850

Prof. John Kuo  
Aldridge Laboratory of Applied Geophysics  
Columbia University  
842 Mudd Bldg.  
New York, NY 10027

Dr. Kenneth Olsen  
P. O. Box 1273  
Linwood, WA 98046-1273

Prof. L. Timothy Long  
School of Geophysical Sciences  
Georgia Institute of Technology  
Atlanta, GA 30332

Prof. Jeffrey Park  
Department of Geology and Geophysics  
Kline Geology Laboratory  
P. O. Box 6666  
New Haven, CT 06511-8130

Dr. Gary McCartor  
Department of Physics  
Southern Methodist University  
Dallas, TX 75275

Howard J. Patton  
Lawrence Livermore National Laboratory  
L-205  
P. O. Box 808  
Livermore, CA 94550

Prof. Art McGarr  
Mail Stop 977  
Geological Survey  
345 Middlefield Rd.  
Menlo Park, CA 94025

Prof. Robert Phinney  
Geological & Geophysical Sciences  
Princeton University  
Princeton, NJ 08544-0636

Dr. George Mellman  
Sierra Geophysics  
11255 Kirkland Way  
Kirkland, WA 98033

Dr. Paul Pomeroy  
Rondout Associates  
P.O. Box 224  
Stone Ridge, NY 12484

Prof. John Nabelek  
College of Oceanography  
Oregon State University  
Corvallis, OR 97331

Dr. Norton Rimer  
S-CUBED  
A Division of Maxwell Laboratory  
P.O. Box 1620  
La Jolla, CA 92038-1620

Prof. Geza Nagy  
University of California, San Diego  
Department of Ames, M.S. B-010  
La Jolla, CA 92093

Prof. Larry J. Ruff  
Department of Geological Sciences  
1006 C.C. Little Building  
University of Michigan  
Ann Arbor, MI 48109-1063

Dr. Keith K. Nakanishi  
Lawrence Livermore National Laboratory  
L-205  
P. O. Box 808  
Livermore, CA 94550

Dr. Richard Sailor  
TASC Inc.  
55 Walkers Brook Drive  
Reading, MA 01867

Prof. Amos Nur  
Department of Geophysics  
Stanford University  
Stanford, CA 94305

Dr. Susan Schwartz  
Institute of Tectonics  
1156 High St.  
Santa Cruz, CA 95064



John Sherwin  
Teledyne Geotech  
3401 Shiloh Road  
Garland, TX 75041

Dr. Matthew Sibol  
Virginia Tech  
Seismological Observatory  
4044 Derring Hall  
Blacksburg, VA 24061-0420

Dr. Albert Smith  
Lawrence Livermore National Laboratory  
L-205  
P. O. Box 808  
Livermore, CA 94550

Prof. Robert Smith  
Department of Geophysics  
University of Utah  
1400 East 2nd South  
Salt Lake City, UT 84112

Dr. Stewart W. Smith  
Geophysics AK-50  
University of Washington  
Seattle, WA 98195

Donald L. Springer  
Lawrence Livermore National Laboratory  
L-205  
P. O. Box 808  
Livermore, CA 94550

Dr. George Sutton  
Rondout Associates  
P.O. Box 224  
Stone Ridge, NY 12484

Prof. L. Sykes  
Lamont-Doherty Geological Observatory  
of Columbia University  
Palisades, NY 10964

Prof. Pradeep Talwani  
Department of Geological Sciences  
University of South Carolina  
Columbia, SC 29208

Dr. David Taylor  
ENSCO, Inc.  
445 Pineda Court  
Melbourne, FL 32940

Dr. Steven R. Taylor  
Lawrence Livermore National Laboratory  
L-205  
P. O. Box 808  
Livermore, CA 94550

Professor Ta-Liang Teng  
Center for Earth Sciences  
University of Southern California  
University Park  
Los Angeles, CA 90089-0741

Dr. Gregory van der Vink  
IRIS, Inc.  
1616 North Fort Myer Drive  
Suite 1440  
Arlington, VA 22209

Professor Daniel Walker  
University of Hawaii  
Institute of Geophysics  
Honolulu, HI 96822

William R. Walter  
Seismological Laboratory  
University of Nevada  
Reno, NV 89557

Dr. Raymond Willeman  
Phillips Laboratory/LWH  
Hanscom AFB, MA 01731-5000

Dr. Gregory Wojcik  
Weidlinger Associates  
4410 El Camino Real  
Suite 110  
Los Altos, CA 94022

Dr. Lorraine Wolf  
Phillips Laboratory/LWH  
Hanscom AFB, MA 01731-5000

Dr. Gregory B. Young  
ENSCO, Inc.  
5400 Port Royal Road  
Springfield, VA 22151-2388

Dr. Eileen Vergino  
Lawrence Livermore National Laboratory  
L-205  
P. O. Box 808  
Livermore, CA 94550

J. J. Zucca  
Lawrence Livermore National Laboratory  
P. O. Box 808  
Livermore, CA 94550

Dr. Ralph Alewine III  
DARPA/NMRO  
1400 Wilson Boulevard  
Arlington, VA 22209-2308

Mr. James C. Battis  
Phillips Laboratory/LWH  
Hanscom AFB, MA 01731-5000

Harley Benz  
U.S. Geological Survey, MS-977  
345 Middlefield Rd.  
Menlo Park, CA 94025

Dr. Robert Blandford  
AFTAC/TT  
Center for Seismic Studies  
1300 North 17th St. Suite 1450  
Arlington, VA 22209-2308

Eric Chael  
Division 9241  
Sandia Laboratory  
Albuquerque, NM 87185

Dr. John J. Cipar  
Phillips Laboratory/LWH  
Hanscom AFB, MA 01731-5000

Cecil Davis  
Group P-15, Mail Stop D406  
P.O. Box 1663  
Los Alamos National Laboratory  
Los Alamos, NM 87544

Mr. Jeff Duncan  
Office of Congressman Markey  
2133 Rayburn House Bldg.  
Washington, DC 20515

Dr. Jack Evernden  
USGS - Earthquake Studies  
345 Middlefield Road  
Menlo Park, CA 94025

Art Frankel  
USGS  
922 National Center  
Reston, VA 22092

Dr. Dale Glover  
DIA/DT-1B  
Washington, DC 20301

Dr. T. Hanks  
USGS  
Nat'l Earthquake Research Center  
345 Middlefield Road  
Menlo Park, CA 94025

Dr. Roger Hansen  
AFTAC/TT  
Patrick AFB, FL 32925

Paul Johnson  
ESS-4, Mail Stop J979  
Los Alamos National Laboratory  
Los Alamos, NM 87545

Janet Johnston  
Phillips Laboratory/LWH  
Hanscom AFB, MA 01731-5000

Dr. Katharine Kadinsky-Cade  
Phillips Laboratory/LWH  
Hanscom AFB, MA 01731-5000

Ms. Ann Kerr  
IGPP, A-025  
Scripps Institute of Oceanography  
University of California, San Diego  
La Jolla, CA 92093

Dr. Max Koontz  
US Dept of Energy/DP 5  
Forrestal Building  
1000 Independence Avenue  
Washington, DC 20585

Dr. W.H.K. Lee  
Office of Earthquakes, Volcanoes,  
& Engineering  
345 Middlefield Road  
Menlo Park, CA 94025

Dr. William Leith  
U.S. Geological Survey  
Mail Stop 928  
Reston, VA 22092

Dr. Richard Lewis  
Director, Earthquake Engineering & Geophysics  
U.S. Army Corps of Engineers  
Box 631  
Vicksburg, MS 39180

James F. Lewkowicz  
Phillips Laboratory/LWH  
Hanscom AFB, MA 01731-5000

Mr. Alfred Lieberman  
ACDA/VI-OA State Department Bldg  
Room 5726  
320 - 21st Street, NW  
Washington, DC 20451

Stephen Mangino  
Phillips Laboratory/LWH  
Hanscom AFB, MA 01731-5000

Dr. Robert Masse  
Box 25046, Mail Stop 967  
Denver Federal Center  
Denver, CO 80225

Art McGarr  
U.S. Geological Survey, MS-977  
345 Middlefield Road  
Menlo Park, CA 94025

Richard Morrow  
ACDA/VI, Room 5741  
320 21st Street N.W  
Washington, DC 20451

Dr. Carl Newton  
Los Alamos National Laboratory  
P.O. Box 1663  
Mail Stop C335, Group ESS-3  
Los Alamos, NM 87545

Dr. Bao Nguyen  
AFTAC/TTR  
Patrick AFB, FL 32925

Dr. Kenneth H. Olsen  
Los Alamos Scientific Laboratory  
P. O. Box 1663  
Mail Stop D-406  
Los Alamos, NM 87545

Mr. Chris Paine  
Office of Senator Kennedy  
SR 315  
United States Senate  
Washington, DC 20510

Colonel Jerry J. Perrizo  
AFOSR/NP, Building 410  
Bolling AFB  
Washington, DC 20332-6448

Dr. Frank F. Pilotte  
HQ AFTAC/TT  
Patrick AFB, FL 32925-6001

Katie Poley  
CIA-ACIS/TMC  
Room 4X16NHB  
Washington, DC 20505

Mr. Jack Rachlin  
U.S. Geological Survey  
Geology, Rm 3 C136  
Mail Stop 928 National Center  
Reston, VA 22092

Dr. Robert Reinke  
WL/NTESG  
Kirtland AFB, NM 87117-6008

Dr. Byron Ristvet  
HQ DNA, Nevada Operations Office  
Attn: NVCG  
P.O. Box 98539  
Las Vegas, NV 89193

Dr. George Rothe  
HQ AFTAC/TTR  
Patrick AFB, FL 32925-6001

Dr. Alan S. Ryall, Jr.  
DARPA/NMRO  
1400 Wilson Boulevard  
Arlington, VA 22209-2308

Dr. Michael Shore  
Defense Nuclear Agency/SPSS  
6801 Telegraph Road  
Alexandria, VA 22310

Mr. Charles L. Taylor  
Phillips Laboratory/LWH  
Hanscom AFB, MA 01731-5000

Phillips Laboratory  
Attn: XO  
Hanscom AFB, MA 01731-5000

Dr. Larry Turnbull  
CIA-OSWR/NED  
Washington, DC 20505

Phillips Laboratory  
Attn: LW  
Hanscom AFB, MA 01731-5000

Dr. Thomas Weaver  
Los Alamos National Laboratory  
P.O. Box 1663, Mail Stop C335  
Los Alamos, NM 87545

DARPA/PM  
1400 Wilson Boulevard  
Arlington, VA 22209

Phillips Laboratory  
Research Library  
ATTN: SULL  
Hanscom AFB, MA 01731-5000

Defense Technical Information Center  
Cameron Station  
Alexandria, VA 22314 (2 copies)

Phillips Laboratory  
ATTN: SUL  
Kirtland AFB, NM 87117-6008 (2 copies)

Defense Intelligence Agency  
Directorate for Scientific & Technical Intelligence  
Attn: DT1B  
Washington, DC 20340-6158

Secretary of the Air Force  
(SAFRD)  
Washington, DC 20330

AFTAC/CA  
(STINFO)  
Patrick AFB, FL 32925-6001

Office of the Secretary Defense  
DDR & E  
Washington, DC 20330

TACTEC  
Battelle Memorial Institute  
505 King Avenue  
Columbus, OH 43201 (Final Report Only)

HQ DNA  
Attn: Technical Library  
Washington, DC 20305

DARPA/RMO/RETRIEVAL  
1400 Wilson Boulevard  
Arlington, VA 22209

DARPA/RMO/Security Office  
1400 Wilson Boulevard  
Arlington, VA 22209

CONTRACTORS (Foreign)

Dr. Ramon Cabre, S.J.  
Observatorio San Calixto  
Casilla 5939  
La Paz, Bolivia

Prof. Hans-Peter Harjes  
Institute for Geophysik  
Ruhr University/Bochum  
P.O. Box 102148  
4630 Bochum 1, FRG

Prof. Eystein Husebye  
NTNF/NORSAR  
P.O. Box 51  
N-2007 Kjeller, NORWAY

Prof. Brian L.N. Kennett  
Research School of Earth Sciences  
Institute of Advanced Studies  
G.P.O. Box 4  
Canberra 2601, AUSTRALIA

Dr. Bernard Massinon  
Societe Radiomana  
27 rue Claude Bernard  
75005 Paris, FRANCE (2 Copies)

Dr. Pierre Mecheler  
Societe Radiomana  
27 rue Claude Bernard  
75005 Paris, FRANCE

Dr. Svein Mykkeltveit  
NTNF/NORSAR  
P.O. Box 51  
N-2007 Kjeller, NORWAY (3 copies)

FOREIGN (Others)

Dr. Peter Basham  
Earth Physics Branch  
Geological Survey of Canada  
1 Observatory Crescent  
Ottawa, Ontario, CANADA K1A 0Y3

Dr. Eduard Berg  
Institute of Geophysics  
University of Hawaii  
Honolulu, HI 96822

Dr. Michel Bouchon  
I.R.I.G.M.-B.P. 68  
38402 St. Martin D'Herès  
Cedex, FRANCE

Dr. Hilmar Bungum  
NTNF/NORSAR  
P.O. Box 51  
N-2007 Kjeller, NORWAY

Dr. Michel Campillo  
Observatoire de Grenoble  
I.R.I.G.M.-B.P. 53  
38041 Grenoble, FRANCE

Dr. Kin Yip Chun  
Geophysics Division  
Physics Department  
University of Toronto  
Ontario, CANADA M5S 1A7

Dr. Alan Douglas  
Ministry of Defense  
Blacknest, Brimpton  
Reading RG7-4RS, UNITED KINGDOM

Dr. Manfred Henger  
Federal Institute for Geosciences & Nat'l Res.  
Postfach 510153  
D-3000 Hanover 51, FRG

Ms. Eva Johannisson  
Senior Research Officer  
National Defense Research Inst.  
P.O. Box 27322  
S-102 54 Stockholm, SWEDEN

Dr. Fekadu Kebede  
Geophysical Observatory, Science Faculty  
Addis Ababa University  
P. O. Box 1176  
Addis Ababa, ETHIOPIA

Dr. Tormod Kvaerna  
NTNF/NORSAR  
P.O. Box 51  
N-2007 Kjeller, NORWAY

Dr. Peter Marshall  
Procurement Executive  
Ministry of Defense  
Blacknest, Brimpton  
Reading FG7-4RS, UNITED KINGDOM

Prof. Ari Ben-Menahem  
Department of Applied Mathematics  
Weizman Institute of Science  
Rehovot, ISRAEL 951729

Dr. Robert North  
Geophysics Division  
Geological Survey of Canada  
1 Observatory Crescent  
Ottawa, Ontario, CANADA K1A 0Y3

Dr. Frode Ringdal  
NTNF/NORSAR  
P.O. Box 51  
N-2007 Kjeller, NORWAY

Dr. Jorg Schlittenhardt  
Federal Institute for Geosciences & Nat'l Res.  
Postfach 510153  
D-3000 Hannover 51, FEDERAL REPUBLIC OF  
GERMANY

Universita Degli Studi Di Trieste  
Facolta Di Ingegneria  
Istituto Di Miniere E. Geofisica Applicata, Trieste,  
ITALY

Dr. John Woodhouse  
Oxford University  
Dept of Earth Sciences  
Parks Road  
Oxford OX13PR, ENGLAND